

Washington University in St. Louis
Washington University Open Scholarship

All Theses and Dissertations (ETDs)

Summer 9-1-2014

The Role of Hspa9 in Mouse Hematopoiesis and IL-7 Receptor Signaling

Kilannin Krysiak

Washington University in St. Louis

Follow this and additional works at: <https://openscholarship.wustl.edu/etd>

Recommended Citation

Krysiak, Kilannin, "The Role of Hspa9 in Mouse Hematopoiesis and IL-7 Receptor Signaling" (2014). *All Theses and Dissertations (ETDs)*. 1314.

<https://openscholarship.wustl.edu/etd/1314>

This Dissertation is brought to you for free and open access by Washington University Open Scholarship. It has been accepted for inclusion in All Theses and Dissertations (ETDs) by an authorized administrator of Washington University Open Scholarship. For more information, please contact digital@wumail.wustl.edu.

WASHINGTON UNIVERSITY IN ST. LOUIS
Division of Biology & Biomedical Sciences
Molecular Genetics & Genomics

Dissertation Examination Committee:
Matthew Walter, Chair
Deepta Bhattacharya
Kyunghee Choi
Timothy Ley
Daniel Link
David Ornitz

The Role of Hspa9 in Mouse Hematopoiesis and IL-7 Receptor Signaling

by

Kilannin Cathleen Krysiak

A dissertation presented to the
Graduate School of Arts and Sciences
of Washington University in
partial fulfillment of the
requirements for the degree
of Doctor of Philosophy

August 2014

St. Louis, Missouri

© 2014, Kilannin Cathleen Krysiak

TABLE OF CONTENTS

LIST OF FIGURES	iv
LIST OF TABLES	vii
ACKNOWLEDGEMENT	viii
ABSTRACT	xi
CHAPTER 1: INTRODUCTION.....	1
REFERENCES	39
CHAPTER 2: THE ROLE OF HSPA9 IN MOUSE HEMATOPOIESIS	50
ABSTRACT.....	51
INTRODUCTION	51
METHODS.....	53
RESULTS	64
DISCUSSION	71
FIGURES.....	75
TABLES.....	97
REFERENCES	103
CHAPTER 3: THE ROLE OF HSPA9 IN IL-7 RECEPTOR SIGNALING	106
ABSTRACT.....	107
INTRODUCTION	107

METHODS.....	109
RESULTS	115
DISCUSSION	121
FIGURES.....	127
TABLES.....	141
REFERENCES	142
CHAPTER 4: ONGOING WORK AND FUTURE DIRECTIONS	145
ONGOING WORK	146
FUTURE DIRECTIONS	148
REFERENCES	154
CURRICULUM VITAE.....	156

LIST OF FIGURES

CHAPTER 1:

FIGURE 1.1: Schematic of genes implicated in MDS and commonly deleted regions on chromosome 5	32
FIGURE 1.2: Schematic of canonical HSP70 family member proteins as well as the HSPA9 protein and locus	33
FIGURE 1.3: The ATP-dependent chaperone cycle of HSP70 proteins.....	34
FIGURE 1.4: Import of precursor proteins into the mitochondrial matrix	35

CHAPTER 2:

FIGURE 2.1: Southern blot confirmation and PCR genotyping of <i>Hspa9</i> ^{+^{Gt}(IST14901H6)TIGM} (<i>Hspa9</i> ^{+/-}) mice	81
FIGURE 2.2: Mouse <i>Hspa9</i> locus with gene trap insertion.....	82
FIGURE 2.3: <i>Hspa9</i> expression is 50% reduced at the protein and mRNA level.....	83
FIGURE 2.4: Organ cellularity, spleen size and CBCs are normal in <i>Hspa9</i> ^{+/-} mice ...	84
FIGURE 2.5: Immunophenotyping of bone marrow, peripheral blood and spleen cells up to 12 months of age	85
FIGURE 2.6: Progenitor and stem cell enriched populations are not altered in <i>Hspa9</i> ^{+/-} mice	86
FIGURE 2.7: Colony forming ability of erythroid and myeloid spleen and bone marrow progenitors from <i>Hspa9</i> ^{+/-} and <i>Hspa9</i> ^{+/+} mice are similar.....	87
FIGURE 2.8: <i>Hspa9</i> ^{+/-} and <i>Hspa9</i> ^{+/+} littermate mice respond similarly to hematopoietic stress	88
FIGURE 2.9: Colony forming ability of B-cell progenitors is significantly reduced in <i>Hspa9</i> ^{+/-} compared to <i>Hspa9</i> ^{+/+} mice.....	89

FIGURE 2.10: The gene trap insertion in <i>Hspa9</i> disrupts expression of both <i>Hspa9</i> and the snoRNA <i>Gm26109</i> located in intron 10 of <i>Hspa9</i>	90
FIGURE 2.11: Overexpression of HSPA9 in <i>Hspa9</i> ^{+/-} bone marrow partially rescues the reduction in CFU-PreB colonies.....	91
FIGURE 2.12: The reduction in CFU-PreB colony formation is hematopoietic cell-intrinsic.....	92
FIGURE 2.13: <i>Hspa9</i> ^{+/-} bone marrow does not have a competitive advantage over control marrow in primary or secondary transplants.....	93
FIGURE 2.14: B-cell recovery is similar from <i>Hspa9</i> ^{+/-} and <i>Hspa9</i> ^{+/+} bone marrow following GCSF treatment.....	94
FIGURE 2.15: Overall and leukemia-free survival of <i>Hspa9</i> ^{+/+} and <i>Hspa9</i> ^{+/-} mice are not different.....	95
FIGURE 2.16: <i>Hspa9</i> ^{+/-} mice are not more susceptible to leukemia induced by MOL4070LTR virus.....	96

CHAPTER 3:

FIGURE 3.1: <i>Hspa9</i> ^{+/-} B-cells isolated from CFU-PreB culture have an ~50% reduction in <i>Hspa9</i> mRNA expression.....	131
FIGURE 3.2: The cell cycle distributions of <i>Hspa9</i> ^{+/-} bone marrow and spleen B-cell fractions are not different than <i>Hspa9</i> ^{+/+} B-cell fractions.....	132
FIGURE 3.3: Exogenous IL-7, but not Flt3-ligand, partially rescues the reduction in <i>Hspa9</i> ^{+/-} CFU-PreB colony formation.....	133
FIGURE 3.4: Total bone marrow expression of <i>IL-7</i> , <i>IL-6</i> and <i>Flt3-ligand</i> are not different in <i>Hspa9</i> ^{+/-} mice.....	134
FIGURE 3.5: <i>Hspa9</i> expression levels are reduced more than 50% by shRNA-	

mediated knockdown	135
FIGURE 3.6: CFU-PreB colony numbers are significantly reduced in mice that received Fcpsi-shHspa9-transduced bone marrow	136
FIGURE 3.7: Significant reduction in B-cell progenitors in mice following lentviral-mediated knockdown of <i>Hspa9</i>	137
FIGURE 3.8: Reduction in IL-7 levels and knockdown of <i>Hspa9</i> in IL-7 dependent cells (B7) reduces cell counts in culture	138
FIGURE 3.9: Stat5 activation by IL-7 receptor signaling is reduced in B7 cells following knockdown of <i>Hspa9</i>	139
FIGURE 3.10: Prolonged survival of BCR-ABL induced leukemia in <i>Hspa9</i> ^{+/-} mice	140

LIST OF TABLES

CHAPTER 1:

Table 1.1: Hematopoietic phenotypes of genes on chromosome 5 implicated in MDS	36
Table 1.2: HSPA9 homologs.....	37
Table 1.3: Genetic models with knockdown or knockout of HSPA9 orthologs	38

CHAPTER 2:

Table 2.1: Western blot antibodies	97
Table 2.2: Flow cytometry antibodies	98
Table 2.3: Results of <i>Hspa9</i> ^{+/-} breeding indicate embryonic lethality.....	99
Table 2.4: No <i>Hspa9</i> ^{-/-} embryos are found following fetal liver formation	100
Table 2.5: Immunophenotypic markers.....	101

CHAPTER 3:

Table 3.1: Enriched pathways in genes significantly down-regulated in <i>Hspa9</i> ^{+/-} CFU-PreB colonies	141
---	-----

ACKNOWLEDGEMENTS

I have received a great deal of support during the pursuit of my doctorate and for that I am extremely grateful.

I would like to begin by thanking my thesis mentor, Dr. Matt Walter, who taught me how to be a better scientist, critical thinker and communicator. His patience and wisdom throughout this journey has been instrumental to my success and fundamentally changed me as a person. He pushed me to achieve things I never thought possible, not the least of which was mouse work. His interest in our personal and professional lives has seen us weather more ups and downs than I can count but his support has never wavered. I have been very privileged to be his first student.

Two former members of the Walter Lab made significant contributions to this work and my early graduate career. Justin Tibbitts, our Mr. Fix-it and an endless source of optimism, helped me keep up my humor even when the science was a disaster. He has been a colleague and a friend that always made early mornings more manageable. Tim Chen taught me the skills that I built my thesis on. He patiently taught me the basics of flow cytometry and primary cell culture, among other things for which I am extremely grateful. This work builds on his discoveries.

I would like to acknowledge the other members of the Walter Lab that have helped in the design and execution of so many of these experiments. I would like to thank Meagan for being both literally, and figuratively, in my corner all these years. Cara has been a great sounding board for both personal and scientific plans. Rigo and Jim consistently do a lot of little things around the lab that really add up but are also responsible for an array of lab hijinks that keep us on our toes. Jin has not only provided amazing PCR skills to this work, but also has been a constant and reliable force in the lab as long as I have been there. I would also like to thank Matthew,

Tueon, Eric and Sanghyun who have provided help with experiments, scientific discussion and day-to-day life in the lab.

The 6th floor provides an amazing amount of support with protocols, reagents, scientific discussion, camaraderie and cookies that have been a crucial part of my graduate work. I would also like to thank the staff of the Siteman Flow Cytometry Core for their help with this work and, particularly, Bill Eades for his guidance and friendship.

I would like to thank the members of my committee, Kyunghye Choi, David Ornitz, Dan Link, Tim Ley, and Deepta Bhattacharya, for their support and scientific guidance throughout this process. I would especially like to thank Tim and Dan for their discussions during lab meetings and for always having an open door. Dan has not only been my committee chair but a co-mentor on my grant, for which I am greatly appreciative.

On a more personal note, I would like to thank my parents and husband for their unending support and patience. The values my parents instilled in me have allowed me to reach levels of success I never knew I could achieve. I would like to thank my Mom for proofreading my thesis proposal, grant proposal and this work. I'm not sure how many graduate students can say their Mom read their thesis, but I'm proud to be one of them. I would also like to acknowledge my husband who met me while I was in graduate school and decided to marry me anyway. And to my in-laws, who welcomed me into the family with open arms like I was meant to be there all along. Their support (and home cooked meals) meant a lot to me during this process.

I would like to thank my friends who have been with me on this rollercoaster but never stopped believing in me.

This work was supported by:

National Cancer Institute of the National Institutes of Health Ruth L. Kirschstein

National Research Service Award Predoctoral Fellowship (F31CA165702)

Siteman Cancer Center Special Emphasis Pathway in Cancer Biology Predoctoral
Fellowship

and

National Heart Lung Blood Institute of the National Institutes of Health Research Project
Grant (R01HL109336, Matt Walter)

Howard Hughes Medical Institute Physician-Scientist Early Career Award (Matt Walter)

Technical assistance was provided by:

The Siteman Cancer Center Flow Cytometry Core and Tissue Procurement Core
(supported in part by an NCI Cancer Center Support Grant, P30 CA91842)

The HOPE Center Viral Vectors Core (supported in part by a Neuroscience Blueprint
Interdisciplinary Center Core award, P30 NS057105)

ABSTRACT OF THE DISSERTATION

The Role of Hspa9 in Mouse Hematopoiesis and IL-7 Receptor Signaling

by

Kilannin Cathleen Krysiak

Doctor of Philosophy in Biology and Biomedical Sciences, Molecular Genetics and Genomics

Washington University in St. Louis, 2014

Associate Professor Matthew J. Walter, Chair

HSPA9 was previously identified as a candidate gene in a commonly deleted region (CDR) associated with myelodysplastic syndrome (MDS), a clonal hematopoietic stem cell disorder. Cytogenetic abnormalities occur in ~50% of MDS patients and an interstitial deletion or loss of chromosome 5 containing *HSPA9* is the most common, occurring in up to 25% of patients. In order to understand the role of *HSPA9* in hematopoiesis and disease development, we created an *Hspa9* knockout mouse model. We characterized hematopoiesis of heterozygous mice (*Hspa9*^{+/-}), which have a 50% reduction in *Hspa9* expression, modeling the heterozygous loss of *HSPA9* and 50% reduction in mRNA observed in MDS patients. Homozygous knockout of *Hspa9* is embryonic lethal prior to fetal liver hematopoiesis, preventing further evaluation of hematopoiesis in *Hspa9*^{-/-} mice.

Analysis of stem, progenitor and mature stages of hematopoiesis up to 18 months of age identified no significant differences in *Hspa9*^{+/-} mice compared to *Hspa9*^{+/+} littermates *in vivo*. However, as early as 2 months of age, *Hspa9*^{+/-} mice have a significant reduction in CFU-PreB colony formation *in vitro*, indicating a B-cell progenitor defect. This reduction in colony formation is hematopoietic-cell intrinsic and likely due to a functional B-cell progenitor defect, since B-cell progenitor frequencies in *Hspa9*^{+/-} mice are normal. Gene expression array analysis revealed a reduction in gene expression pathways associated with proliferation and activation of B-

lymphocytes. Gene expression analysis of hematopoietic progenitor cells from MDS patients also identified B-cell signaling pathways as the most down-regulated pathways. IL-7 added exogenously to CFU-PreB cultures was able to partially rescue the reduction in *Hspa9*^{+/-} CFU-PreB colony formation, further indicating dysfunctional IL-7 signaling in *Hspa9*^{+/-} B-cells.

To explore the contribution of Hspa9 to altered IL-7R signaling, we interrogated an IL-7 dependent cell line treated with an *Hspa9* or non-targeting control siRNA. Knockdown of Hspa9 resulted in a significant growth defect in these cells and reduced Stat5 phosphorylation following IL-7 stimulation of cytokine-starved cells. Collectively, these data implicate *Hspa9* in IL-7R signaling in B-cells. Further work will determine whether *HSPA9* loss contributes to the reduction in B-cell progenitors and increased B-cell apoptosis observed in patients with MDS.

CHAPTER 1:

Introduction

1. Myelodysplastic Syndromes

1.1. Disease statistics

Patients with myelodysplastic syndromes (MDS) have a clonal hematopoietic stem cell (HSC) disorder that results in dysplastic hematopoietic cells in their bone marrow as well as peripheral blood cytopenias^{1,2}. Commonly occurring in older individuals (20-36/100,000 in >70 year olds), MDS is associated with an increased risk of transformation to acute myeloid leukemia (AML)³⁻⁵. Ultimately, 30% of MDS patients will progress to a highly-chemotherapy resistant form of AML⁵. The World Health Organization (WHO) and French-British American (FAB) classification systems are used for the diagnosis of MDS subtypes based on clinical, cytochemical, immunophenotypic, morphologic and genetic information⁶⁻⁸. These, in conjunction with the International Prognostic Scoring System (IPSS) or the recently released revised IPSS (IPSS-R), are used to predict an individual patient's prognosis^{9,10}. Despite the utility of such systems, we need a better understanding of MDS pathogenesis to improve treatment options and better predict patient outcomes.

1.2. Genetics

The genetic events leading to the development of MDS and the subsequent transformation to AML are poorly understood. However, approximately 50% of MDS patients have an acquired cytogenetic abnormality, highlighting the role of genetic alterations in disease pathogenesis². These cytogenetic abnormalities are a key prognostic factor in both MDS and AML transformation, and while prognostically important, they alone do not provide mechanisms of pathogenesis². With more recent applications of next-generation sequencing technology, additional mutations have been identified in patients both with and without a cytogenetic abnormality, greatly expanding our understanding of the genetics of MDS¹¹⁻¹⁴. One of these studies highlighted the complexity of MDS and its evolution by dissecting its clonal architecture in serial samples¹³. Deep sequencing of 15 secondary AML genomes, 8

of which were also analyzed at the MDS stage, were used to identify founder clones and subclones. Founder clones produce subclones as malignant cells undergo self-renewal and produce progeny. While some genes tend to occur in the founding clone, no commonly mutated genes were identified to always be associated with either the founding clone or subclones. Such heterogeneity in clonal architecture and evolution means mutations in MDS cannot be simply thought of in binary terms of absent or present. This greatly complicates how we interpret and treat the mutational spectrum of MDS patients. Deep sequencing studies also reveal a much higher percentage of bone marrow cells involved in the disease clone than described by the blast percentage that is currently used for diagnosis and prognosis. Taken together, these discoveries have greatly expanded our understanding of the complexity of MDS; however, the functional and clinical implications of these discoveries are still being investigated.

1.2.1. Gene level mutations

Recent advances in sequencing technology have reduced costs and increased sensitivity, allowing for genomic studies of large cohorts of MDS patients at the nucleotide level. These studies have revealed not only the clonal heterogeneity of MDS but also identified novel mutations associated with MDS¹¹⁻¹⁴. The largest category of recently identified mutations involves splicing machinery, effecting up to 50% of MDS patients¹⁵⁻¹⁸. Sequencing of candidate genes in large cohorts has been able to identify mutations or cytogenetic abnormalities in up to 90% of patients¹⁴. As we understand more about the genetics of MDS, we must understand how these mutations individually and in combination effect hematopoiesis and drive disease.

1.2.2. Chromosomal abnormalities

While recent technological advances have identified individual genes commonly mutated in MDS, the clinical application of this information is still being determined. However, cytogenetic analysis has been standard practice for diagnosis and prognosis of MDS for decades. Cytogenetic abnormalities are identified in approximately 50% of MDS patients². As part of the original IPSS, patients were given a score based on three cytogenetic categories that would factor into their overall prognosis and included several of the most common cytogenetic abnormalities⁹. The IPSS-R now stratifies patients into five cytogenetic categories and incorporates more rare cytogenetic abnormalities¹⁰. Regardless, having 3 or more cytogenetic abnormalities has been consistently associated with poor prognosis. Common cytogenetic abnormalities in MDS include del(5q), -7/del(7q), trisomy 8 and del(20q), all of which occur in both isolation and in complex karyotypes². Del(5q), the most common of these cytogenetic abnormalities, is our focus.

1.2.2.1. Del5q

Approximately 15-25% of MDS patients have an interstitial deletion or loss of the long arm of chromosome 5 (5q)^{2,13,19,20}. This frequency places it among the most frequently acquired mutations identified in MDS, indicating the importance of understanding its contribution to this disease^{11,13}. There are two commonly deleted regions (CDR) on 5q²⁰⁻²⁸. The distal CDR on 5q33.1 is associated with 5q minus syndrome, which has a good prognosis and a low risk of AML transformation^{20,22,29}. Alternatively, the proximal CDR on 5q31.2 is associated with a high risk of AML transformation^{20,24-27} (**FIGURE 1.1**).

1.2.2.1.1. Haploinsufficiency

The interstitial deletions on chromosome 5 are single copy losses, and no biallelic disruptions of genes in either the proximal or distal regions have been identified, implicating haploinsufficiency as the underlying genetic mechanism^{20,26,27,30,31} (**TABLE 1.1**). In both regions, genes that contribute to features of MDS have been successfully identified^{21,32-36}. However, none of them can fully explain the clinical phenotypes observed, suggesting that multiple genes on the interval contribute to pathogenesis³³.

1.2.2.1.2. Association with TP53

Recent next-generation sequencing has also identified the frequent co-occurrence of *TP53* mutations with del(5q)^{12,13,37-39}. Earlier studies had identified *TP53* mutations associated with del(5q) in patients with poor prognosis, specifically with either therapy-related MDS and AML or refractory MDS and AML^{38,40-42}. Loss of 5q clearly preceded mutations identified in *TP53* in one patient. This patient, as well as data supporting loss of 5q as an early event in MDS development, indicates *TP53* mutations may be a transforming event following establishment of a del(5q) MDS clone^{41,43,44}.

1.2.2.2. Genes implicated in the pathogenesis of del(5q) MDS

Genes on del(5q) that have been implicated in that pathogenesis of MDS, including the two CDRs, are illustrated in **FIGURE 1.1**, and the studies supporting their involvement are listed in **TABLE 1.1**. 5q deletions are often large, resulting in the CDRs being defined by a small number of patients, implicating additional genes that reside on 5q outside the two commonly described CDRs (including *NPM1* and *APC*)^{34,45-48}. As described above, the distal CDR is associated with 5q- syndrome, a

phenotypically defined subtype of MDS consisting of refractory macrocytic anemia, a normal or high platelet count, hypolobated megakaryocytes, and del(5q) as the only cytogenetic abnormality⁶. Reduced expression of *Rps14*, *miR-145/146A* and *Sparc* recapitulate phenotypes associated with 5q- syndrome as detailed in **TABLE 1.1**^{32,35,49,50}. Studies of genes in the proximal CDR, 5q31.2, associated with high-risk MDS have identified *EGR1* and *CTNNA1* as genes in this region that may contribute to hematopoietic dysfunction, also detailed in **TABLE 1.1**^{21,30}. Consistent with haploinsufficiency, *Graubert et. al.* identified 7 genes, including *CTNNA1* and *HSPA9*, whose mRNA were significantly reduced in CD34+ cells from MDS patients with del(5q) relative to normal CD34+ cells by microarray analysis, which are shown in red in **FIGURE 1.1**²⁶. Collectively, several genes on chromosome 5q impact hematopoiesis and suggest that more than one gene may contribute to the phenotypes associated with MDS.

1.2.2.2.1. Identification of a candidate gene on the proximal CDR

In order to investigate the impact of reduced expression of genes on the interval in hematopoiesis, we performed an shRNA screen of genes in this interval. Utilizing 3-5 independent shRNA constructs available for 22 of 28 protein coding genes on the interval, we reduced expression of each gene in primary human CD34+ cells in erythroid differentiation media and evaluated differentiation by flow cytometry (CD71/GpA). *HSPA9* was identified as the top-scoring gene of the 22 assayed that met the following criteria: targeted shRNAs in our erythroid differentiation assay resulted in a ≥ 1.5 fold reduction in mature erythroid cells relative to control shRNA (CD71+/GpA+)(8/22), the gene was normally expressed in CD34+ cells at the mRNA level (15/21), and it had ~50% expression in CD34+ cells from del(5q) MDS patients compared to normal control

marrow (7/22). For these reasons we chose to further investigate the role of *HSPA9* in hematopoiesis.

2. HSPA9

2.1. HSP70 family of proteins

HSPA9 is a member of the HSP70 (heat shock protein 70 kD) family of chaperone proteins. This highly conserved family of proteins plays an essential role in protein homeostasis and cellular stress response⁵¹. Members of this family are involved in protein transport, organelle import, folding, disaggregation and sequestration⁵²⁻⁵⁵. Although not all eukaryotic HSP70 proteins are heat-inducible, they respond to a variety of cellular stresses^{52,53,55,56}. The protein products of this multi-gene family are located in multiple compartments of the cell where they perform different functions. It is clear by their sequence differences that many of these family members were the result of gene duplication events that have been maintained throughout evolution^{54,57,58}.

2.1.1. Structure and mechanism

The highly conserved domains of HSP70 proteins serve different functions. The nucleotide binding domain (NBD) is the site of nucleotide exchange as well as the location of most co-chaperone interactions (**FIGURE 1.2**). The flexible linker region facilitates allosteric regulation and communication of the domains. The substrate binding domain (SBD) is the site of client protein binding and interacts with exposed hydrophobic residues on client proteins. Finally, the C-terminal lid domain is involved in client protein affinity. The functions of these domains work together to perform the substrate binding and nucleotide exchange necessary for HSP70 family functions^{53,59,60}.

Members of the HSP70 family of proteins are key regulators of protein homeostasis. They are involved in protein unfolding, disaggregation, stabilization, folding, membrane translocation, transport and targeting for degradation^{59,61}. They bind and release proteins through an ATP-dependent functional cycle common to this family and depicted in **FIGURE 1.3**. ATP hydrolysis of HSP70 proteins is extremely slow without the help of co-chaperones. J-domain proteins (also known as HSP40 proteins) bind to the nucleotide binding domain (NBD) of HSP70 proteins and assist in initial binding of client proteins⁶². When the HSP70 protein binds a client protein in the SBD, a global conformational change occurs, enhancing ATP hydrolysis at the NBD⁶³. ATP hydrolysis of the NBD enhances affinity for the substrate by closing the lid domain. Finally, another co-chaperone acts as a nucleotide exchange factor (NEF) and catalyzes the release of the substrate by ADP-ATP exchange.

While this functional cycle is common among all HSP70 family members, differences in cellular localization as well as client and co-chaperone specificity provide unique roles for the human HSP70 family members.

2.1.2. Human HSP70 genes

The human genome produces 8 proteins that fulfill the basic structural criteria for a conserved HSP70 family protein as described in **Section 2.1.1**. However, transcripts are generated from an additional 9 genes with either incomplete or highly divergent substrate binding domains, which will not be discussed here^{64,65}. The human genome produces 6 cytosolic (HSPA1A, HSPA1B, HSPA1L, HSPA2, HSPA6, HSPA8), 1 endoplasmic reticulum (HSPA5) and 1 mitochondrial (HSPA9) enriched HSP70 proteins^{53,64}.

While HSP70 family members are highly conserved, their functions are clearly not redundant. Murine knockout of *Hspa8* and *Hspa5* are known to be embryonic lethal, and loss of the testis-specific *Hspa2* results in male infertility^{60,66-68}. However, *Hspa1a*, *Hspa1b* and *Hspa2* knockout mice are all viable. *Hspa6* and *Hspa11* knockout mice have not yet been described⁶⁹⁻⁷¹. Lastly, *Hspa9* knockout mice have not been described prior to this work.

2.2. Cellular localization and expression

The ubiquitously expressed HSPA9 is present in a variety of subcellular locations including the mitochondrial matrix, endoplasmic reticulum, cytoplasmic vesicles and cytosol⁷²⁻⁷⁴.

Although HSPA9 has been shown to have cytoplasmic functions, its primary localization is in the mitochondria where it functions in mitochondrial protein import⁷⁵⁻⁷⁸. Unlike other HSP70 proteins, HSPA9 has an N-terminal 46-amino acid mitochondrial targeting sequence (MTS) that is required for mitochondrial import (**FIGURE 1.2**)^{73,76}. HSPA9 is the only mitochondrial HSP70 protein described in most eukaryotes, yeast being a notable exception, attributing to its highly conserved functions observed across species.

2.3. Homology/conservation

HSPA9 is highly conserved as illustrated by **TABLE 1.2**. Studies utilizing *S. cerevisiae* have provided many useful insights into the function of HSPA9. However, unlike most other eukaryotes that have one mitochondrial HSP70 protein, yeast have three HSP70 family proteins that localize to mitochondria (*Ssc1p*, *Ecm10p*, *Ssq1p*)⁷⁹. *Ssc1p* shares the greatest homology with human HSPA9, sharing 65.8% identity at the protein level. *Ssc1p* is involved in mitochondrial import, protein folding and protein degradation, functions that are described in **Sections 2.5.1** and **2.5.2**. *SSC1*, the gene encoding *Ssc1p*, is an essential gene in yeast. *ECM10* is a paralog of *SSC1* resulting from a whole genome duplication event. *Ecm10p* has

been implicated in mitochondrial import, shares 82% identity with Ssc1p and 63.4% identity with HSPA9 at the protein level, and when overexpressed can rescue *SSC1* mutants. However, *ECM10* is not an essential gene and has only been described to have overlapping function with *SSC1*. For these reasons *ECM10* will not be discussed further^{79,80}. The third protein, Ssq1p, only shares 48.8% identity with HSPA9 and has no closer mammalian homolog. Ssq1p is 1000-fold less abundant than Ssc1p but has a highly specified role in iron sulfur (Fe-S) cluster biosynthesis⁸¹. Overexpression Ssc1p can rescue Fe-S cluster biosynthesis, indicating Ssc1p (and possibly HSPA9) may be involved in this process⁷⁹. Functional evidence for HSPA9's role in Fe-S cluster biosynthesis is presented in **Section 2.6.2**.

2.4. Co-chaperone specificity

Even though HSPA9 is highly conserved, its function and specificity can be altered by its interactions with co-chaperones, indicating HSPA9 may not have entirely overlapping functions across all species. Just as different HSP70 family members have different co-chaperone specificity, HSPA9 utilizes different co-chaperones to mediate different functions within the same cell. As described in the following sections, HSPA9's role in mitochondrial import and mitochondrial protein folding are among its most well characterized functions. For these roles, HSPA9 utilizes the nucleotide exchange factor GRPEL1; however, different J proteins are utilized to aid in substrate binding and ATP hydrolysis. For mitochondrial import, J proteins DNAJC19 and DNLZ (better known as PAM18 and HEP1, respectively) are used, while for mitochondrial protein folding HSPA9 utilizes DNAJA3^{63,82-84}.

2.5. Mitochondrial protein import and homeostasis

2.5.1. Translocase of the inner membrane (TIM)/Translocase of the outer membrane (TOM)

HSPA9's role in mitochondrial import is highly conserved and well described. The majority of mitochondrial proteins are encoded in the nucleus and must be imported to the mitochondria. For mitochondrial import into the mitochondrial matrix to occur, proteins must pass through two highly regulated membranes. Multi-protein complexes known as the translocase of the outer membrane (TOM) and translocase of the inner membrane (TIM) regulate the translocation of proteins across these membranes^{85,86}. Proteins targeted to the mitochondria first pass through the TOM complex to reach the intermembrane space. Precursor proteins with N-terminal presequences are sorted and directed by additional protein complexes to the appropriate TIM complex, which will insert them into the inner mitochondrial membrane or translocate them into the mitochondrial matrix.

HSPA9 works in concert with the TIM23 translocon to facilitate translocation of proteins from the intermembrane space to the mitochondrial matrix^{87,88}. The process is depicted in **FIGURE 1.4**. A pH gradient between the matrix and intermembrane space starts this process by translocating the positively charged N-terminal presequence of the precursor protein^{89,90}. ATP-dependent binding of HSPA9 to the precursor protein is required to complete translocation^{78,91-93}. The membrane-spanning heterodimer PAM16/18 and matrix protein TIM44 tether HSPA9 to the TIM23 translocon, where it binds the incoming presequence of the matrix protein^{87,94}. For its mitochondrial import function, PAM18 is recognized as HSPA9's J protein and GRPEL1 acts as its nucleotide exchange factor. Together, these proteins are known as the presequence translocase-associated motor (PAM), of which HSPA9 is the core component. The PAM complex is required to complete the ATP-dependent translocation of these precursor proteins; however, the exact mechanism of how HSPA9 facilitates transfer of the incoming protein is a subject of much debate.

Two models were initially proposed for how HSPA9 interacts with incoming proteins. The first suggests that proteins can move in either direction through the TIM23 complex, but HSPA9 clamps down on the incoming preprotein, preventing it from sliding back into the intermembrane space. As additional HSPA9 molecules are recruited to the protein, it becomes trapped in the matrix^{95,96}. The other describes HSPA9 as pulling the preprotein into the matrix by acting as an active import motor^{97,98}. Regardless of its mechanism, HSPA9 is an essential component of inner mitochondrial membrane import and this process does not occur in its absence^{78,92,93}.

2.5.2. Protein folding, degradation and disaggregation

Studies of the *S. cerevisiae* Ssc1p, an ortholog of HSPA9, have yielded useful insights into the function of HSPA9. In addition to mitochondrial import, HSPA9 is involved in the process of folding and refolding proteins in the mitochondria. Transformation of a temperature-sensitive *SSC1* yeast mutant with plasmids expressing either wild-type or mutant Ssc1p was used to measure the ability of mutant Ssc1p to refold an engineered hybrid protein after translocation into the membrane⁹⁹. The previously described hybrid protein was shown to be resistant to proteinase K digestion when properly refolded¹⁰⁰. The mutant Ssc1p allowed translocation of the hybrid protein; however, the hybrid protein was sensitive to proteinase K digestion, indicating it was not refolded following translocation⁹⁹. Proper refolding of newly imported proteins requires HSPA9 to recruit the help of the J protein DNAJA3 (also known as hTid1), which is not involved in mitochondrial import, and GRPEL1 as a nucleotide exchange factor^{63,101}. Following ATP hydrolysis, HSPA9 releases the precursor protein to the HSP60/HSP10 complex to complete the folding process¹⁰²⁻¹⁰⁴.

Through additional studies of Ssc1p, HSPA9 has also been implicated in the degradation of misfolded proteins through its interactions with GRPEL1. By stabilizing misfolded or damaged proteins in an unfolded conformation, Ssc1p makes these proteins available to mitochondrial proteases¹⁰⁵⁻¹⁰⁷.

Denaturation and aggregation of proteins can occur following cellular stress. HSPA9 has been implicated in disaggregation of these proteins as one method of protecting cells from stress^{101,108}. Loss of Ssc1p was also shown to result in mitochondrial protein aggregation independent of its mitochondrial import and extra-mitochondrial functions¹⁰⁹.

2.6. Additional functions

2.6.1. Centrosome duplication

HSPA9 is a positive regulator of centrosome duplication⁷⁵. Overexpression of HSPA9 promotes centrosome re-duplication through its physical interactions with p53 and Mps1 kinase (also known as TTK). HSPA9 modulates cell cycle progression by superactivating an initiator of centrosome duplication, Mps1, and disassociating p53, an inhibitor of duplication. HSPA9 is a target of Mps1 phosphorylation at threonine 62 and serine 65, which is necessary for its ability to superactivate Mps1 and creates a feedback loop that promotes centrosome duplication. During mid-late G₁, HSPA9 associates with centrosomes in an Mps1-dependent manner and disassociates during mitosis¹¹⁰. As a cell cycle checkpoint mediator, p53 can induce G₁-arrest, potentially through its interactions with the centrosome¹¹¹. Through these interactions, HSPA9 has been implicated in the promotion of centrosome duplication.

2.6.2. Fe-S cluster transfer

HSPA9 is the nearest homolog of the yeast protein Ssq1p, which is required for Fe-S cluster biosynthesis^{81,112}. The highly homologous Ssc1p can rescue deficiencies of Ssq1p, indicating Ssc1p can play a role in Fe-S cluster biosynthesis, but is significantly less efficient than Ssq1p¹¹³. Ssq1p is thought to be responsible for the transfer of assembled Fe-S clusters to recipient apo-proteins¹¹⁴. *In vivo* function of Ssq1p was shown to be dependent on its ability to bind the LPPVK binding motif of the Fe-S cluster scaffold protein, Isu¹¹⁵. Biochemical assays have shown that HSPA9 can bind this LPPVK binding motif found on the human Fe-S cluster scaffold protein ISU1, providing additional evidence for a possible role of HSPA9 in Fe-S cluster biosynthesis¹¹⁶.

2.6.3. HSPA9 in endo- and exocytosis

Murine Hspa9 has been identified in lipid rafts of various mouse organs¹¹⁷. Investigating the heparan sulfate proteoglycan (HSPG)-dependent endocytic compartment confirmed the presence of Hspa9 in lipid rafts, as well as implicated it in the nonclathrin-, noncaveolin-dependent endocytic pathway⁷⁴. Endocytosis of magnetic nanoparticles conjugated to HSPG-specific antibodies was inhibited by knockdown of *HSPA9* by siRNA in HeLa cells.

It was shown that HSPA9 interacts with fibroblast growth factor (FGF)-1 during late G₁ of the cell cycle^{118,119}. When FGF-1 binds to cell surface receptors or heparan sulfate on the cell surface, it is internalized by an endocytic pathway and translocated through the cytosol into the nucleus. This interaction was shown to be dependent on previously described tyrosine phosphorylation of HSPA9, and the authors postulated that due to cellular localization, HSPA9 influences FGF-1 availability to FGF receptors¹¹⁹⁻¹²¹. Given

the more recent discovery of HSPA9 in HSPG-dependent endocytosis, it stands to reason that it may be involved in uptake of FGF-1.

Another study demonstrated the presence of HSPA9 on vesicles exocytosed from tumor cells exposed to the membrane attack complex (MAC), implicating a role for HSPA9 in protection from MAC-mediated lysis. The MAC consists of blood plasma proteins that induce lysis in invading pathogens by insertion into the plasma membrane, inducing intracellular signaling or physical damage¹²². It has been shown that some cells can escape MAC-induced lysis through exocytosis¹²³. HSPA9 was initially found in the exocytic vesicles that shed the MAC from K562 cells, protecting them from lysis induced by MAC insertion into the plasma membrane¹²⁴. Knockdown of HSPA9 in K562 cells led to the rapid lysis of these cells by induction of the MAC¹²⁵. In contrast, addition of purified HSPA9 protein to the media could protect rabbit erythrocytes from MAC-mediated lysis. The precise role of HSPA9 in this process is unknown; however, it has been shown to bind two key plasma membrane proteins involved in this process, C8 and C9, and may prevent the polymerization required for their function¹²⁴.

HSPA9 has also been observed to associate with the IL-1 receptor type I, independent of ligand binding. HSPA9 could be dissociated from the immunoprecipitated receptor complex by increasing concentrations of ATP, and loss of this interaction does not interfere with receptor activation of downstream kinases. For these reasons the authors speculated that HSPA9 might be involved in receptor internalization, rather than IL-1 signal transduction¹²⁶.

2.7. Additional HSPA9 protein interactions

Sections 2.5 and **2.6** describe known and putative functions of HSPA9 in various cellular pathways, which include interactions with a variety of proteins; however, HSPA9 has been shown to bind a variety of proteins by co-immunoprecipitation or yeast 2-hybrid that are not mentioned above. Further studies are needed to understand the functional impact of the interactions listed below.

2.7.1. p53

As described in **Section 2.6.1**, HSPA9 has been shown to bind and inhibit p53. HSPA9 binds to p53 in the C-terminal cytoplasmic sequestration domain of p53 (amino acid residues 312-352), and through this interaction p53 is sequestered in the cytoplasm, preventing its nuclear translocation¹²⁷. The pleiotropic effects of p53 have led to speculation about the role of HSPA9 in modulating p53 and regulating apoptosis¹²⁸. HSPA9 interacts with p53 through its ATPase domain (amino acid residues 253-282, see **FIGURE 1.2**)^{129,130}. One study identified that HSPA9 binds p53 as a substrate protein in a purified protein system. In this study, they were not able to recapitulate previous reports of the ATPase domain interaction, potentially due to the lack of other proteins that may be required for this interaction¹³¹. One protein that may mediate this interaction is HSPA9's J protein and cochaperone, DNAJA3, that was shown to bind p53 during hypoxia-induced cellular stress¹³².

2.7.2. VDAC1 voltage-dependent anion-selective channel & IP3R (inositol 1,4,5-trisphosphate receptor)

HSPA9 was initially shown to interact with VDAC by a yeast 2-hybrid assay¹³³. In order to enter or leave the mitochondria, most metabolites, including the ATP/ADP required for oxidative phosphorylation and cations such as K⁺ and Ca²⁺ that regulate mitochondrial

membrane potential, have to pass through a VDAC channel¹³⁴. VDAC1 interacts with an endoplasmic reticulum Ca²⁺ release channel IP3R, promoting the transfer of Ca²⁺ between these organelles⁷⁶. HSPA9 was shown to colocalize and coimmunoprecipitate with VDAC1 and the endoplasmic reticulum receptor IP3R. Furthermore, HSPA9 overexpression protected cells from Ca²⁺ overload, a key event in apoptosis that induces the opening of the permeability transition pore in mitochondria. It was postulated that HSPA9 protects the mitochondria from Ca²⁺ overload by connecting the IP3 receptor and VDAC and reducing the cationic selectivity of the VDAC^{76,135}.

2.7.3. p66shc

HSPA9 may protect cells from oxidative stress through its interaction with the key mediator of oxidative stress-induced apoptosis, p66shc (SHC1). p66shc was found in a protein complex with HSPA9 in the mitochondria by size exclusion chromatography and confirmed by co-immunoprecipitation. This interaction is disrupted when cells are treated with inducers of oxidative stress¹³⁶. When unbound in the intermembrane space of mitochondria, p66shc can oxidize cytochrome c to produce H₂O₂ and induce apoptosis through opening of the mitochondrial permeability transition pore (MTP)¹³⁷. Overexpression of p66shc enhances apoptotic response to oxidative stress and increases ROS levels in a variety of cell types. In contrast, loss of p66shc protects cells from oxidative stress, reducing apoptosis and ROS levels¹³⁸⁻¹⁴⁰.

2.7.4. Parkin, DJ-1 and α -synuclein

Three proteins associated with Parkinson's disease (PD) have been shown to physically interact with HSPA9, the functional consequences of which are not well understood. Hspa9 can be co-immunoprecipitated with DJ-1, a protein linked to autosomal recessive forms of PD, in multiple cell types¹⁴¹⁻¹⁴⁴. DJ-1 has a known role in protecting cells from

reactive oxygen species, and upon treatment of cells with H₂O₂, more DJ-1 can be found in association with HSPA9¹⁴⁵. HSPA9 has also been identified as a binding partner of α -synuclein and Parkin, other genes associated with PD, using isotope-coded affinity tags (ICAT) and mass spectrometry of cellular models of PD^{143,146-150}. Mutations in the gene encoding Parkin, PARK2, are the most common cause of autosomal recessive cases of PD¹⁵⁰. The interaction between HSPA9 and Parkin was confirmed using co-immunoprecipitation, and functional consequences of this interaction were further studied. In this study, knockdown of HSPA9 sensitized HeLa cells to oxidative stress-induced apoptosis, a phenotype that could be rescued by overexpression of Parkin¹⁵⁰. α -Synuclein protein aggregation is associated with neural degeneration, and missense mutations in the gene that encodes this protein, SNCA, have been associated with familial PD. Overexpression of HSPA9 protected rotenone-induced neurotoxicity and α -synuclein protein aggregation¹⁴⁶. HSPA9's role in PD will be further discussed in **Section 2.9.1**.

2.7.5. Additional HSPA9 binding partners and possible mechanisms of signaling regulation

As a chaperone protein, it is likely that HSPA9 binds many proteins without exerting functional consequences. The following studies have shown HSPA9 binds AKT and ERK2, as well as other proteins that influence signaling through these proteins. However, reports of these interactions vary between groups and are likely context-dependent. Additional studies are required to fully understand the functional consequences of these interactions.

2.7.5.1. AKT

Immunoprecipitation of proteins using activated or inhibited AKT as bait revealed an interaction between AKT and HSPA9 in K562 cells¹⁵¹. In PC12 cells overexpression of HSPA9 was protective against glucose deprivation-mediated apoptosis by maintaining pro-survival signals through increased phosphorylation of ERK1/2 and AKT. However, this group was unable to repeat the previously described co-immunoprecipitation of AKT and HSPA9 during glucose deprivation conditions in this cell type¹⁵².

2.7.5.2. ERK

In contrast to *Yang et. al.* (**Section 2.7.5.1**), another group observed a reduction in ERK2 phosphorylation in COS7 cells following HSPA9 overexpression¹⁵³. This observation stemmed from an unbiased yeast two-hybrid screen of proteins that interact with HSPA9. As expected, this screen identified components of the TIM-TOM complex that were already known to interact with HSPA9 for its mitochondrial matrix import function previously described in **Section 2.5.1**. Two novel HSPA9 binding partners identified in this screen included mevalonate pyrophosphate decarboxylase (MPD) and NADH dehydrogenase. The interaction between HSPA9 and MPD was confirmed by co-immunoprecipitation. Overexpression of HSPA9 resulted in a reduction in ERK2 phosphorylation that was rescued when MPD was also overexpressed. From this data, it was proposed that HSPA9 regulates ERK2 through its inhibition of the mevalonate pathway protein MPD. This study did not further characterize the interaction with NADH dehydrogenase¹²⁸.

Another protein associating ERK and HSPA9 is the receptor for hyaluronan mediated motility (RHAMM)¹⁵⁴. HSPA9 and HSPA5 were both co-immunoprecipitated and

shown to co-localize with RHAMM during interphase but not mitosis. RHAMM can bind ERK1/2 and is thought to regulate its activity¹⁵⁵. Additional studies are needed to confirm functional consequences of this interaction and whether the cytoplasmic staining pattern is truly specific to RHAMM localization. However, if this interaction is real, HSPA9 likely plays a role in microtubule stabilization and may alter ERK1/2 signaling through its interaction with RHAMM.

2.8. Overexpression of HSPA9

2.8.1. Disease associations

Overexpression of HSP70 family members is common in a variety of cancers and is often associated with poor prognosis⁵⁹. Overexpression of HSPA9 has been shown to provide a cytoprotective effect against glucose deprivation, hypoxia and ROS accumulation, and results in increased proliferation and survival in cells and worms¹⁵⁶⁻¹⁵⁹. Like other HSP70 family members, this protection from cellular stresses acts as an important survival function of the cell that is often utilized by cancer cells. Increased HSPA9 expression has been described in colon, liver, brain, skin, and breast cancers¹⁶⁰⁻¹⁶³. Retroviral overexpression of HSPA9 in MCF-7 cells injected into nude mice resulted in more rapid tumor formation than the control virus, as well as an increase in chemotactic invasive response in a transwell assay compared to control constructs¹⁶⁰. Additionally, HSPA9 overexpression is correlated with poor-survival in colorectal adenocarcinomas and melanoma tumor malignancy^{162,163}.

2.8.2. Genetic models

The number of population doublings by normal human lung fibroblasts was dramatically increased by overexpression of HSPA9¹⁶⁴. Expanding on this result, transgenic

overexpression of the *C. elegans* ortholog HSP-6 resulted in ~43% increase in worm life span¹⁵⁹.

2.9. Inactivation or loss of HSPA9

2.9.1. Disease associations

Although most commonly described as being overexpressed in various diseases, loss of HSPA9 is associated with neurodegenerative disorders.

2.9.1.1. Parkinson's Disease

Mitochondrial dysfunction and increased accumulation of reactive oxygen species have been implicated in the pathology of Parkinson's disease (PD), a neurodegenerative disorder^{142,165,166}. As an essential mitochondrial protein, HSPA9 expression, protein interactions, and sequence variants have been investigated in the context of PD. An unbiased comparison of mitochondrial proteins isolated from substantia nigra, an area of the brain affected by PD, revealed reduced levels of HSPA9 in samples from patients with PD compared to normal controls¹⁴⁴. Another study of proteins differentially expressed in post-mortem brain tissue from PD patients at different stages of disease progression identified an association between a reduction in cytosolic HSPA9 levels and PD progression¹⁶⁷. From these studies, it was not clear whether a reduction in HSPA9 levels was a marker for disease or a risk factor for disease development and progression.

Two groups sought to identify genetic variants in HSPA9 that may be risk factors for the development of disease^{142,165}. For each study, DNA was isolated from ~300 patients with PD and ~300 age matched controls and evaluated for mutations associated with disease. In both studies, 4 single nucleotide polymorphisms in

HSPA9 that are found with high frequency in the general population showed no association with disease risk. However, 4 heterozygous single nucleotide variants were identified between the two cohorts, each identified in a single patient with PD. The second study expanded their analysis and screened 1008 PD patients and 1342 population controls for 3 of these variants¹⁴². Only 1 of the variants was identified in additional patients at an allele frequency of 0.0069%, indicating HSPA9 variants are quite rare. However, further analysis of these disease-associated variants shows they occur in highly conserved regions with functional consequences. Two of the newly discovered variants, A476T and P509S, are located in the substrate-binding domain of HSPA9, while the R126W variant is in the ATPase domain. Functional studies of these variants utilized knockdown of HSPA9 in the dopaminergic cell line SH-SY5Y, which resulted in increased mitochondrial reactive oxygen species (ROS) production and reduced mitochondrial membrane potential. Overexpression of wild-type HSPA9 can rescue these mitochondrial changes. However, overexpression of these disease-associated variants could not rescue mitochondria in these cells, indicating these variants have reduced function. Additionally, fibroblasts isolated from a patient with the A476T variant had altered mitochondrial morphology compared to fibroblasts from a sibling without the variant. Collectively, these studies indicate that although these disease-associated variants are rare, they have functional consequences that may contribute to PD pathogenesis.

Other studies indicate that HSPA9 may also influence the development of PD through its interactions with three proteins associated with PD, Parkin, DJ-1 and α -synuclein as described in **Section 2.7.4**. Taken together, these data indicate that loss of HSPA9 expression or function may contribute to PD pathogenesis or risk.

2.9.1.2. Alzheimer's Disease

HSPA9 has also been implicated in another neurodegenerative disorder, Alzheimer's disease (AD). HSPA9 normally provides a cytoprotective effect in neuronal cells but may be functionally altered in AD patients.

HSPA9 is involved in disaggregation of proteins, as discussed in **Section 2.5.2**.

Aggregation of β -amyloid causes plaque formation and neurotoxicity in AD^{168,169}.

Hspa9 is up-regulated in response to β -amyloid in both PC12 cells overexpressing the amyloid precursor protein and in brains of P301L tau mice injected with β -amyloid^{170,171}. This upregulation may be a cytoprotective response to the β -amyloid accumulation since HSPA9 overexpression protected SH-SY5Y cells from β -amyloid induced toxicity¹⁷².

HSPA9 is also altered by another protein associated with AD, ApoE, which may affect its ability to protect neuronal cells. ApoE variants are associated with 90% of AD cases in individuals under the age of 65¹⁷³. Both HSPA9 isoform expression and phosphorylation were altered in an ApoE-driven mouse model of AD. These results were confirmed in AD patients with *APOE* variants, however, the significance of these changes are not well understood¹⁷⁴. Loss of ApoE also results in a 10-fold increase in Hspa9 oxidation, potentially altering its function¹⁷⁵.

In summary, HSPA9 has been shown to have a cytoprotective effect in neuronal cells and loss of its function, regardless of mechanism, may contribute to neurodegenerative disorder pathology or risk.

2.9.2. Genetic models

HSPA9 orthologs have been identified as essential genes in genetic models from yeast to zebrafish. **TABLE 1.3** lists genetic models involving knockout or knockdown of known *HSPA9* orthologs and their associated phenotypes. Collectively, unlike many HSP70 family members, HSPA9 has an essential role in organismal development.

2.10. Role in hematopoiesis

Several HSP70 family members have been shown to influence hematopoiesis (recently reviewed in *Mjahed et. al.*). Hsp70 regulates Stat5 and Bcl-xl signaling in hematopoietic cells transformed with the BCR-ABL fusion gene and regulates erythropoiesis by protecting GATA-1 from caspase-3 mediated cleavage^{52,176}. HSPA8 was previously shown to regulate the localization of cyclin D in hematopoietic stem cells, thereby controlling HSC quiescence¹⁷⁷. Another HSP70 family member, the ER-specific HSPA5, was shown to regulate glycolytic metabolism and HSC self-renewal¹⁷⁸. Collectively, the HSP70 family of proteins is involved in a wide variety of functions in hematopoiesis. It stands to reason that the highly expressed HSPA9 may also play a role in normal or malignant hematopoiesis.

2.10.1. Zebrafish

The earliest compelling data for HSPA9's role in hematopoiesis came from *Danio rerio*. Analysis of a blood development mutant known as crimsonless (*crs*), initially identified in an ENU mutagenesis screen, revealed a single point mutation in a highly conserved residue within the nucleotide-binding domain of Hspa9. **(FIGURE 1.2)**¹⁷⁹ In the homozygous state this mutation caused phenotypes characteristic of MDS: severe anemia, defects in erythroid differentiation, multilineage cytopenias, and increased apoptosis. Heterozygotes also showed increases in ROS accumulation. Evidence from other HSPA9 orthologs indicates that the point mutation observed in the zebrafish *crs*

mutant likely resulted in a hypomorphic allele. Mutations in the corresponding conserved amino acid of *E. coli*'s HSPA9 homolog, DnaK, results in a significant reduction in peptide binding^{61,180}. *In vitro* biochemical analysis of human HSPA9 carrying this mutation disrupted its chaperoning ability by significantly reducing its affinity for J-protein co-chaperones involved in client protein recognition as well as the rate of nucleotide exchange following client protein recognition. This group also created a mutation in the corresponding location of the *S. cerevisiae* ortholog Ssc1, which resulted in a lethal phenotype⁶³. Collectively, these data indicate that loss of normal Hspa9 function causes ineffective hematopoiesis in zebrafish and provide compelling evidence to study HSPA9 in hematopoiesis.

2.10.2. Erythropoietin signaling

Analysis of erythropoietin (EPO)-dependent PI3K/AKT signaling in purified human erythroid colony forming cells identified *HSPA9* as a target regulated by this pathway¹⁵⁸. Increasing *HSPA9* mRNA levels correlated with increasing levels of EPO. Investigation of signaling pathways downstream of EPO-R implicated that regulation of *HSPA9* mRNA was downstream of the PI3K, and not the MAPK, signaling pathway. Furthermore, knockdown of *HSPA9* by siRNA, like inhibition of PI3K signaling, inhibited cell growth in a human erythroid culture system. These results indicate that *HSPA9* is both regulated by this indispensable erythroid-specific signaling pathway and is also involved in promoting erythropoiesis.

2.10.3. CD34+ cell *in vitro* differentiation

Human cord blood derived CD34+ cells were used to further evaluate the effects of HSPA9 knockdown in human hematopoiesis³⁶. HSPA9 levels were reduced ~30-90% using 5 lentiviral shRNA knockdown constructs. These cells exhibited a dose-dependent

reduction in the percentage of cells in S-phase, decreased erythroid differentiation, and increased apoptosis; all common features observed in early-stage MDS. No disruption of megakaryocyte or myeloid differentiation was identified. Consistent with a reduction in erythroid differentiation, erythroid colonies grown in methylcellulose media were reduced in number and had reduced hemoglobin levels. The dose-dependent increase of apoptosis in *HSPA9* knockdown cells was accompanied by increased caspase-3 cleavage and increased mitochondrial depolarization, changes that were significant when *HSPA9* levels were reduced by ~50%³⁶. Collectively, these results support a role for *HSPA9* in human erythropoiesis, which may contribute to the clinical features of MDS.

2.10.4. Fe-S clusters in erythropoiesis

As described in **Section 2.6.2**, HSPA9 has been implicated in iron sulfur cluster biosynthesis. Disruption of Fe-S cluster biosynthesis has been shown to disrupt mitochondrial iron metabolism and result in ineffective erythropoiesis¹⁸¹. Erythroid maturation is highly dependent on iron homeostasis due to the high demands of heme biosynthesis. Mutations in Fe-S cluster biosynthesis proteins GLRX5 and ABCB7 have been shown to cause ineffective erythropoiesis in model organisms and are associated with congenital sideroblastic anemia in humans¹⁸²⁻¹⁸⁶. If HSPA9 performs the same role as one of two yeast homologs, Ssq1p, its loss may alter erythropoiesis through this mechanism.

2.10.5. Mouse knockdown

Two groups have utilized shRNA knockdown of *Hspa9* in murine bone marrow and described alterations of early hematopoietic cells in mice.

In 2010, *Chen et. al.* modeled Hspa9 loss in a murine bone marrow transduction/transplantation model. Mouse bone marrow cells were transduced with lentiviral vectors co-expressing a YFP reporter and an *Hspa9* shRNA or a control shRNA. These bone marrow cells were then transplanted into lethally irradiated congenic recipients. With this method ~50% knockdown was achieved in bone marrow and spleen cells. *Hspa9* shRNA recipient mice had reduced erythroid precursors and B cells with normal T cell, neutrophil, and monocyte populations in their bone marrow, spleen, and peripheral blood. A population of early progenitors (KLS cells) and megakaryocyte/erythrocyte progenitors (MEP) were also significantly reduced³⁶. Collectively, the data suggests that loss of Hspa9 alters hematopoietic progenitors, leading to ineffective hematopoiesis, particularly erythropoiesis and B-cells, in mice.

More recently, increased reactive oxygen species production was observed in hematopoietic stem cells (HSC) treated with a small molecule inhibitor of Hspa9 and other Hsp70 proteins, MKT-077¹⁸⁷. This increase coincided with a decrease in HSC number, but not hematopoietic progenitor number, that could be partially rescued with the antioxidant N-acetyl-L-cysteine. Since MKT-077 has been shown to target other members of the HSP70 family with described HSC function, follow-up studies utilized shRNA knockdown constructs to reduce Hspa9 expression¹⁸⁷. HSC numbers were greatly reduced after 10 days in culture compared to controls. Following this result, retrovirally transduced HSCs were sorted and 5000 GFP+ HSCs and 200,000 helper mononuclear cells were transplanted into lethally irradiated recipients to evaluate stem cell function *in vivo*. Bone marrow myeloid, T- and B-cell frequencies were normal 1 month after transplant; however, HSC and mononuclear numbers were reduced and KLS cells in G₀ were significantly reduced. Evaluation of mRNA expression of cell cycle and ROS-related genes identified alterations in cell cycle genes (increased c-myc and

decreased p21^{Cip1} and p57^{Kip2}), as well as decreased genes associated with oxidative stress (sestrin2, Sod2, Foxo1, Prdm16). In contrast, overexpression of Hspa9 resulted in increased donor-derived HSCs. Further investigation of Hspa9's role in modulating ROS in HSCs was performed in the context of a protein known to interact with Hspa9, DJ-1. DJ-1 was previously shown to interact with Hspa9 in neuronal cells and has a known role in protection from ROS generation as described in **Section 2.7.4**^{141,142,145}. This study confirmed that DJ-1 could be immunoprecipitated by Hspa9 in a murine hematopoietic progenitor cell line (EML cells) and co-localizes with Hspa9 in mitochondria following H₂O₂. DJ-1^{-/-} mice have a significant reduction in HSCs at 24 months of age and a significant increase in fluorescent ROS indicator, DCF-DA, in these cells. Overexpression of Hspa9 significantly increased the number of HSCs in culture, but could not reduce the ROS generation in DJ-1^{-/-} HSCs, collectively indicating that DJ-1 is required for Hspa9 to reduce ROS generation¹⁸⁷.

2.10.6. Association with AML

As described in **Section 1.2.2.2**, HSPA9 lies on chromosome 5 within a commonly deleted region associated with transformation from MDS to acute myeloid leukemia (AML). Hspa9 has also been associated with murine AML development. In two retroviral insertional mutagenesis screens, Hspa9 was identified as a common integration site in mice that develop AML^{188,189}. *Hspa9* mRNA levels were not increased in tumors containing insertions, consistent with inactivation and not overexpression of Hspa9.

3. Conclusions

HSPA9 is a member of the highly conserved HSP70 family of proteins. This nuclear-encoded mitochondrial HSP70 chaperone has a known role in mitochondrial protein import and folding, as well as a cytoplasmic role in centrosome duplication. However, due to its plethora of

identified protein interactions, it has a putative role in a variety of cellular functions including Ca^+ homeostasis in the mitochondria, mitochondrial iron-sulfur cluster biosynthesis, apoptosis inhibition, and cell signaling. As with many anti-apoptotic proteins, it is often associated with up-regulation in a variety of cancer cell types; however, loss of HSPA9 has also been associated with human disease. In humans, HSPA9 is located on the long arm of chromosome 5 in a commonly deleted region identified in myelodysplastic syndrome that is associated with transformation to acute myeloid leukemia. Supporting a role for HSPA9 in hematopoiesis, RNAi-mediated knockdown alters erythroid differentiation of human CD34+ cells and stem and progenitor cells in mice. Finally, zebrafish with a functionally relevant point mutation have severe anemia and other hematopoietic alterations. Further understanding of HSPA9's role in hematopoiesis is key to understanding if its loss contributes to myelodysplastic syndrome and acute myeloid leukemia. Generation of a murine Hspa9 knockout model will provide a valuable tool to understand and study HSPA9's functions *in vivo*.

Figure 1.1: Schematic of genes implicated in MDS and commonly deleted regions on chromosome 5

Chromosome 5 is depicted with delineations of the two commonly deleted regions (CDRs) associated with MDS. **TABLE 1.1** presents published data from genetic models supporting the role of candidate genes (*depicted in blue*) on 5q with MDS/AML. The proximal interval is associated with transformation to AML and all genes in this region are listed. This 2.5 megabase region contains 35 genes: 29 protein-coding genes, 5 non-coding RNAs (*denoted with a **) and 1 hypothetical gene (*denoted with #*). Genes in the proximal region are color coded based on a previously published gene expression array dataset of CD34+ cells from normal controls, MDS patients with del(5q) and non-del(5q) MDS patients²⁶. *Grey*: hypothetical/pseudogenes and genes not detected in >70% of normal and MDS samples. *Red*: candidate genes that have significantly reduced mRNA levels in MDS patients with del(5q) compared to normal controls. *Black*: expressed in CD34+ cells but not significantly reduced in MDS patients with del(5q).

Figure 1.2: Schematic of canonical HSP70 family member proteins as well as the HSPA9 protein and locus

A) Top: Predicted structure of HSP70 with ADP bound to the nucleotide binding domain (PDB code #2kho¹⁸⁰). **Bottom:** HSP70 proteins consist of a highly conserved substrate binding domain (SBD, *blue*), linker domain (*grey*) and nucleotide binding domain (NBD, *green*). **B)** Unlike other HSP70 proteins, HSPA9 also has mitochondrial targeting sequence (MTS, *red*). The p53 binding domain, known sites of phosphorylation (P, Thr62 and Ser65) and the homologous amino acid for the zebrafish point mutation (G498A) of HSPA9 are noted. **C)** HSPA9 has 17 exons. The C/D box snoRNA *SNORD63* lies within intron 10 of *HSPA9*.

Figure 1.3: The ATP-dependent chaperone cycle of HSP70 proteins

Top of figure: The substrate binding domain (SBD) of the HSP70 protein (*red*) exists in the open conformation when the nucleotide binding domain (NBD) is bound to ATP. **1)** A J protein co-chaperone (*green*) facilitates binding of the client protein (*purple*) to HSP70's SBD. **2)** Binding of the client protein causes a global conformational change, promoting hydrolysis of ATP. **3)** ATP hydrolysis increases affinity of the client protein by closing the lid domain. **4)** Binding of the nucleotide exchange factor (NEF; *blue*) promotes the exchange of ADP for ATP and release of the client protein.

Figure 1.4: Import of precursor proteins into the mitochondrial matrix

Precursor proteins (*pink*) are imported into the intermembrane space of mitochondria through the translocase of the outer membrane (TOM) complex. Precursor proteins with a positively charged N-terminal presequence (*purple*) are targeted to the presequence translocase of the inner membrane (TIM23 complex). Mitochondrial membrane potential begins precursor protein translocation by TIM23 but assembly of the presequence translocase-associated motor is required to complete precursor protein translocation. PAM16 recruits PAM18 and TIM44 is required for recruitment of HSPA9. PAM18 (*green*) acts as HSPA9's J protein co-chaperone to facilitate ATP hydrolysis, increasing HSPA9's (*red*) affinity for the incoming precursor protein. Finally, GRPEL1 (*blue*) acts as HSPA9's nucleotide exchange factor facilitating release of the precursor protein and the exchange of ADP for ATP, resetting HSPA9.

Figure 1.1: Schematic of genes implicated in MDS and commonly deleted regions on chromosome 5

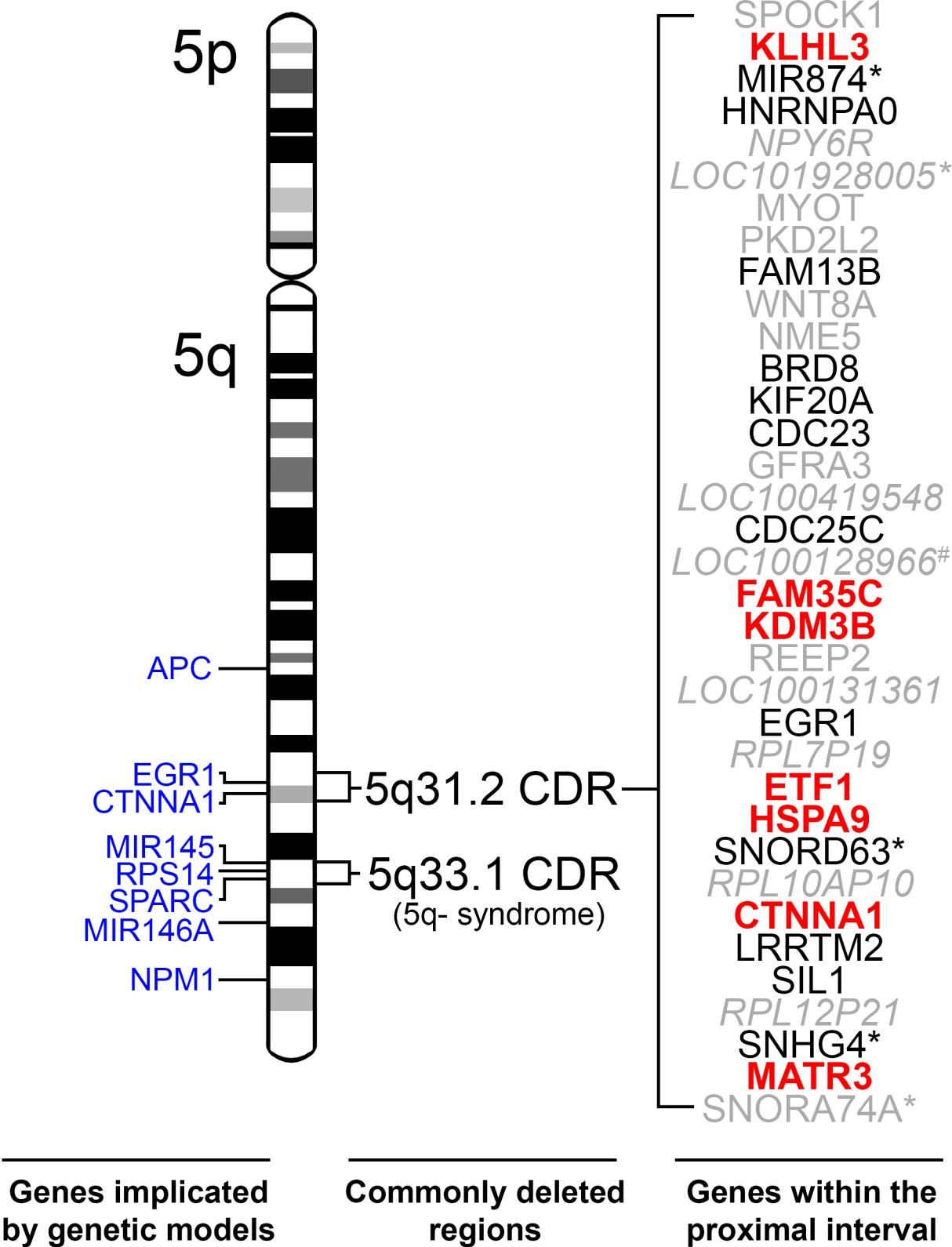


Figure 1.2: Schematic of canonical HSP70 family member proteins as well as the HSPA9 protein and locus

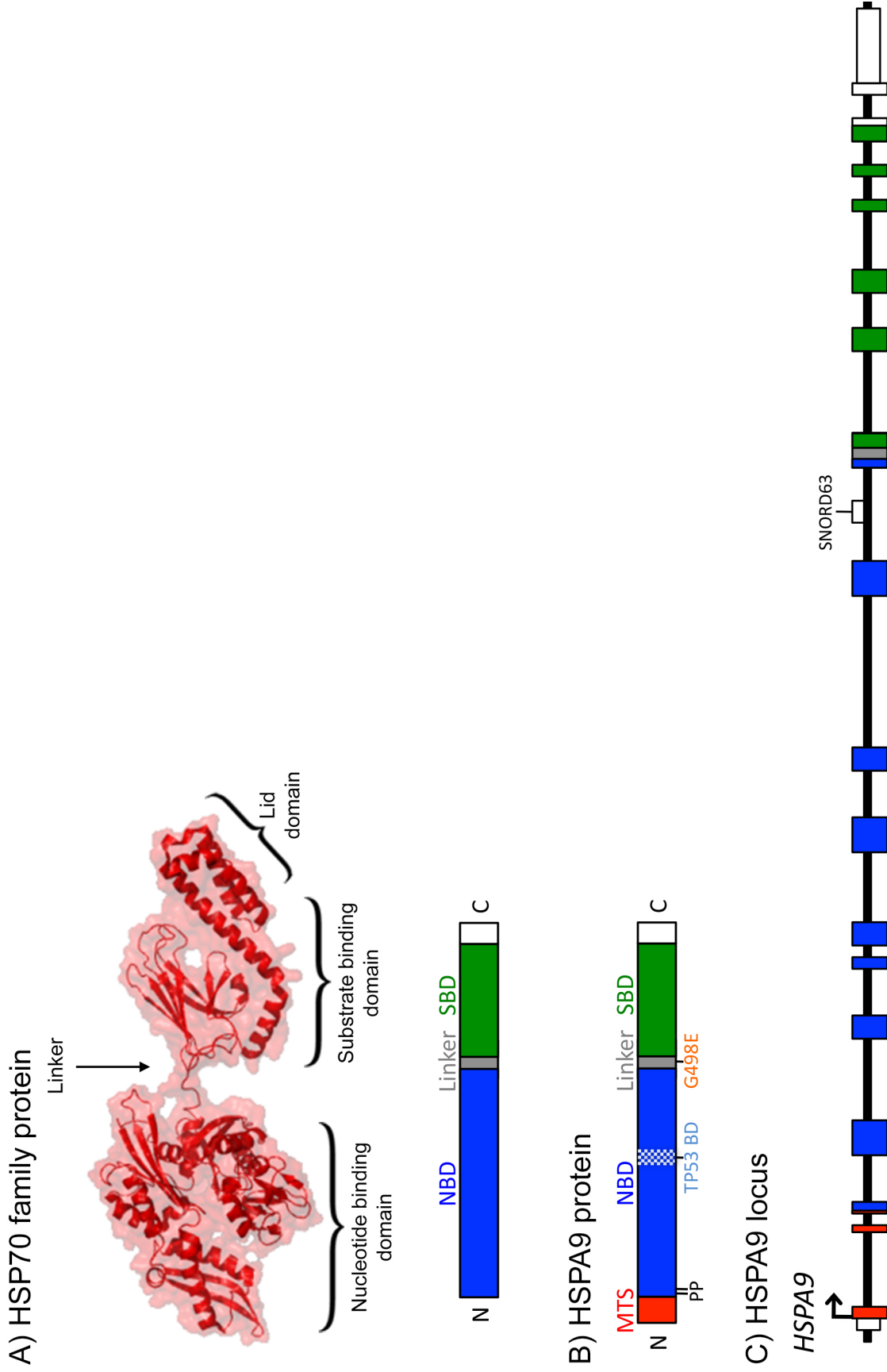


Figure 1.3: The ATP-dependent chaperone cycle of HSP70 proteins

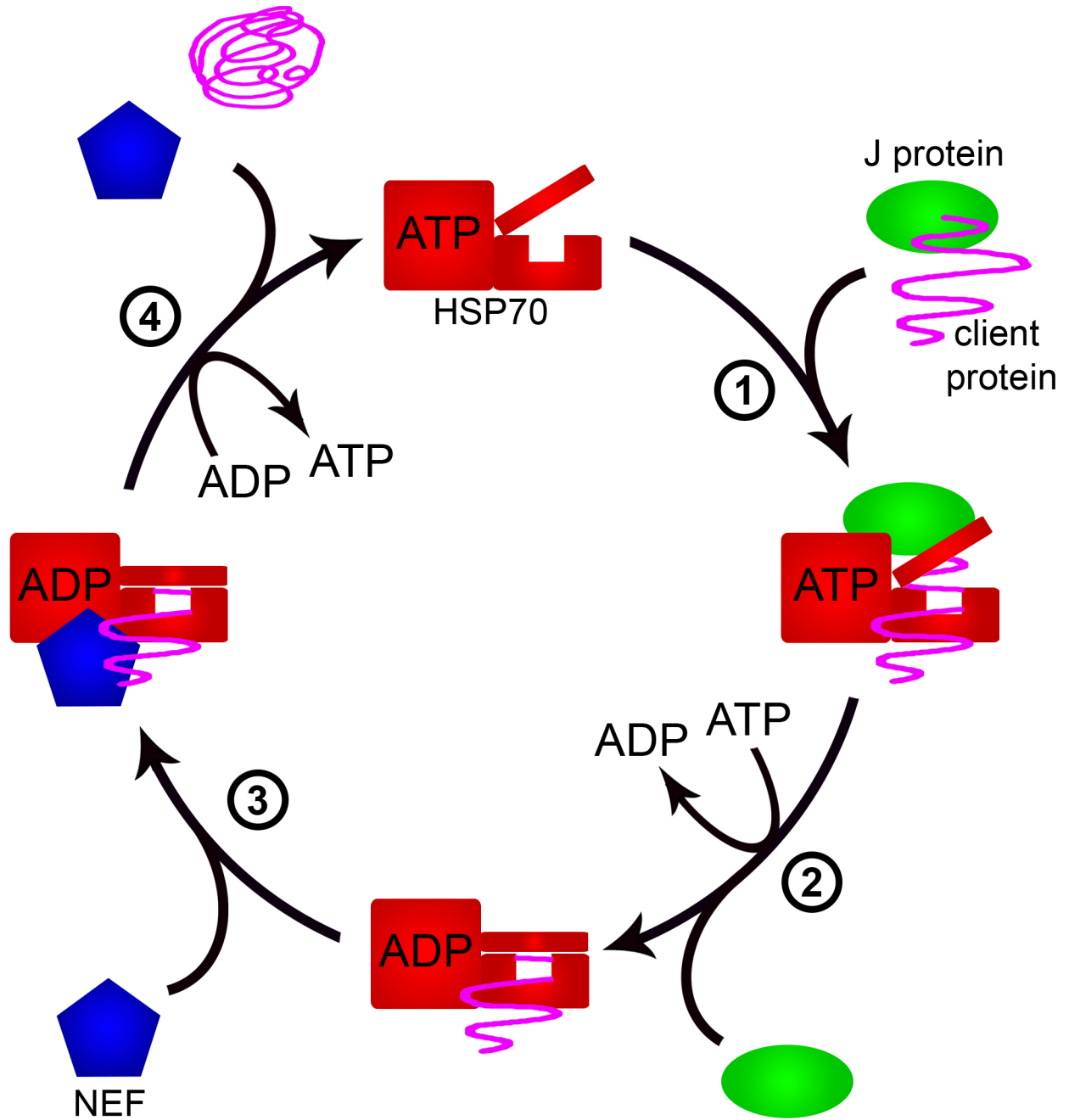


Figure 1.4: Import of precursor proteins into the mitochondrial matrix

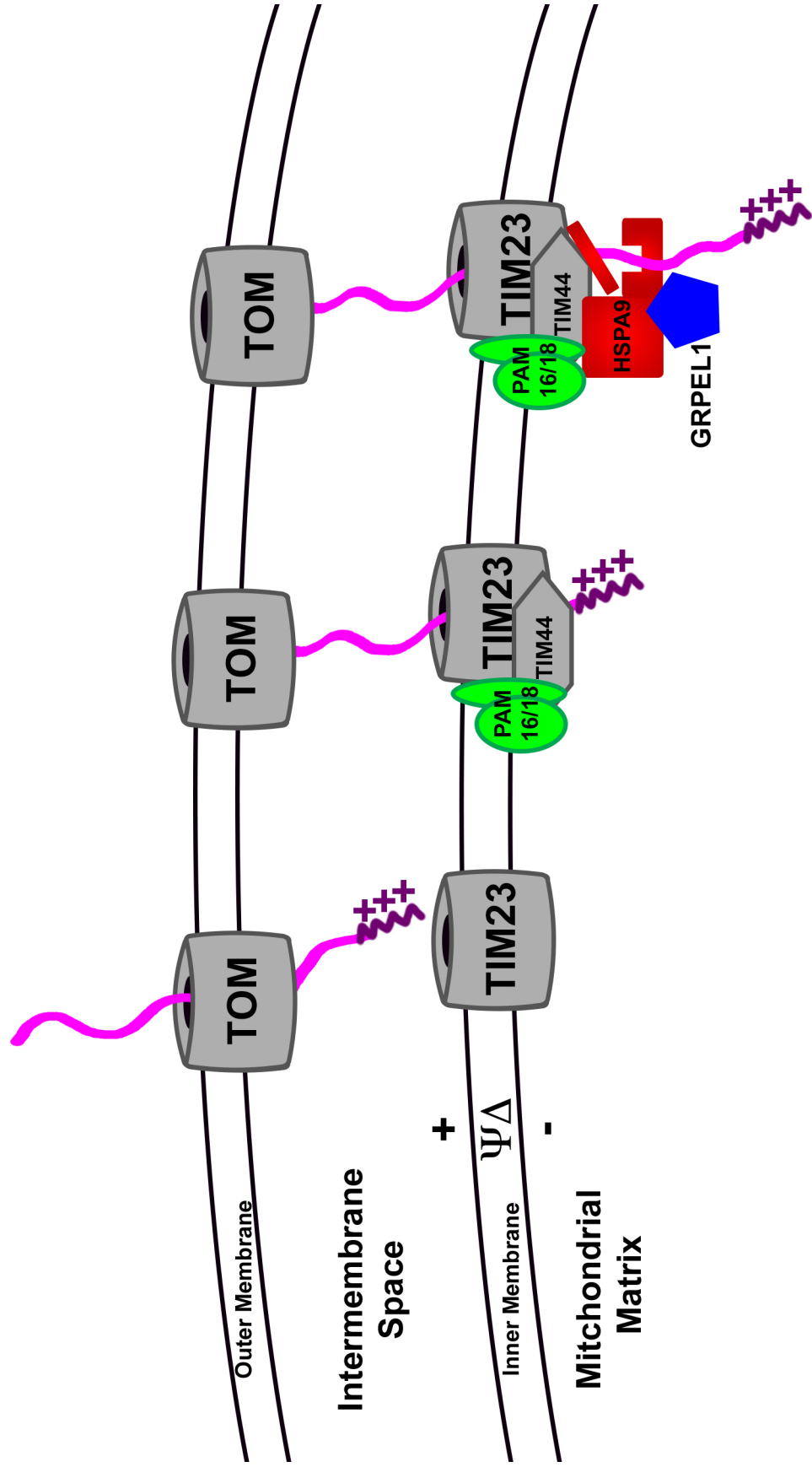


Table 1.1: Hematopoietic phenotypes of genes on chromosome 5 implicated in MDS

Distal CDR (5q33.1)	Phenotype	Citation
<i>RPS14</i>	Knockdown of RPS14 with shRNAs leads to a block in erythroid differentiation of human CD34+ hematopoietic progenitors	32
8 gene deletion, including <i>RPS14</i>	Heterozygous mice lacking a region spanning Rps14 and seven other genes in the distal region have macrocytic anemia, erythroid dysplasia and reduced colony forming capacity of hematopoietic progenitors. Loss of p53 in these mice restored the colony forming capacity of hematopoietic progenitors.	49
<i>miR-145/miR-146a</i>	Retroviral-mediated overexpression of target sequences causing knockdown of miR-145 and miR-146a in murine transduction/transplantation model resulted in thrombocytosis, mild neutropenia, and megakaryocytic dysplasia 8 weeks post transplant.	35
<i>SPARC</i>	Homozygous deletion in mice caused thrombocytopenia and impaired BFU-E formation.	50
Proximal CDR (5q31.2)	Phenotype	Citation
<i>EGR1</i>	<i>Egr1</i> ^{+/-} mice do not exhibit differences in basal hematopoiesis, but do develop increased rates of T cell lymphomas and a myeloproliferative disorder following N-ethyl-N-nitrosourea (ENU) mutagenesis	30
<i>CTNNA1</i>	Epigenetic silencing of the residual, non-deleted <i>CTNNA1</i> allele was identified in high-risk MDS patients and AML patients with del(5q). Overexpression of <i>CTNNA1</i> reduced proliferation and increased apoptosis of a human promyelocytic cell line that harbors del(5q).	21
Implicated genes not in a CDR	Phenotype	Citation
<i>APC</i>	Heterozygous knockout mice die of macrocytic anemia and have reduced myeloid colony forming ability and hematopoietic stem cells (HSCs) with reduced ability to reconstitute hematopoiesis. The APC ^{min} allele is the result of a point mutation that causes a premature stop codon and these mice develop a cell-extrinsic MDS/MPD. Homozygous knockout results in rapid bone marrow failure with increased apoptosis and cell cycle entry of HSCs.	34,47,48
<i>NPM1</i>	Heterozygous mice frequently develop myeloid and lymphoid malignancies. Knockout mice die embryonically with reduced hematopoietic precursors and severe anemia.	45,46

Table 1.2: HSPA9 homologs

Species	Common name	Symbol	Identity (%)	
			Protein	DNA
H.sapiens	Human	<i>HSPA9</i>		
vs. P.troglodytes	Chimpanzee	<i>HSPA9</i>	99.9	99.9
vs. M.mulatta	Rhesus monkey	<i>HSPA9</i>	99.6	98.3
vs. C.lupus	Dog	<i>HSPA9</i>	98.8	92.7
vs. B.taurus	Cow	<i>HSPA9</i>	98.5	92.7
vs. M.musculus	Mouse	<i>Hspa9</i>	98.4	90.3
vs. R.norvegicus	Rat	<i>Hspa9</i>	97.8	90.4
vs. G.gallus	Chicken	<i>HSPA9</i>	92.7	80.2
vs. D.rerio	Zebrafish	<i>hspa9</i>	86.4	75.2
vs. D.melanogaster	Fruit Fly	<i>Hsc70-5</i>	78.0	68.4
vs. A.gambiae	Mosquito	<i>AgaP_AGAP010876</i>	80.9	67.9
vs. C.elegans	Worm	<i>hsp-6</i>	77.3	67.2
vs. S.cerevisiae	Yeast	<i>SSC1</i>	65.6	62.5
vs. S.pombe	Fission yeast	<i>ssc1</i>	64.4	61.0
vs. M.oryzae	Rice blast fungus	<i>MGG_04191</i>	66.1	61.6
vs. N.crassa	Bread mold	<i>NCU08693</i>	67.7	61.3
vs. A.thaliana	Mouseear cress	<i>MTHSC70-2</i>	62.8	63.7
vs. O.sativa	Asian rice	<i>Os02g0774300</i>	63.5	64.0
vs. O.sativa	Asian rice	<i>Os03g0113700</i>	64.3	64.4

Table 1.3: Genetic models with knockdown or knockout of *HSPA9* orthologs

Species	Ortholog	Phenotype	Citation
<i>Saccharomyces cerevisiae</i> (yeast)	<i>SSC1</i>	Essential for growth	190,191
<i>Drosophila melanogaster</i> (fly)	<i>Hsc70-5</i>	Two large forward genetic screens observed lethality through RNAi-mediated knockdown or P-element mediated homozygous knockout.	192,193
<i>Dugesia japonica</i> (flatworm)	<i>Djmot</i>	siRNA-mediated knockdown results in loss of regenerative abilities and stem cell (neoblast) growth arrest leading to the death of the animal	194
<i>Caenorhabditis elegans</i> (nematode)	<i>hsp-6</i>	RNAi-mediated knockdown is embryonic lethal and in adult worms causes a progeria-like (early aging) phenotype with a reduction in ATP levels and abnormal mitochondrial morphology. Expression levels of HSP-6 also decreases with age.	195-197
<i>Danio rerio</i> (zebrafish)	<i>Hspa9b</i>	Homozygous point mutants are developmentally arrested before reaching the larvae stage, ~48 hpf. An independent retroviral insertional mutant resulted in developmental delays and death prior to 5dpf and exhibited reduce fin regeneration after being cut due to a severe reduction in cell proliferation.	179,198, 199

REFERENCES

1. Nolte F, Hofmann WK. Myelodysplastic syndromes: molecular pathogenesis and genomic changes. *Ann. Hematol.* 2008.
2. Haase D, Germing U, Schanz J, et al. New insights into the prognostic impact of the karyotype in MDS and correlation with subtypes: evidence from a core dataset of 2124 patients. *Blood.* 2007;110(13):4385–4395.
3. Aul C, Giagounidis A, Germing U. Epidemiological features of myelodysplastic syndromes: results from regional cancer surveys and hospital-based statistics. *Int. J. Hematol.* 2001;73(4):405–410.
4. Ma X, Does M, Raza A, Mayne ST. Myelodysplastic syndromes: incidence and survival in the United States. *Cancer.* 2007;109(8):1536–1542.
5. Rollison DE, Howlader N, Smith MT, et al. Epidemiology of myelodysplastic syndromes and chronic myeloproliferative disorders in the United States, 2001-2004, using data from the NAACCR and SEER programs. *Blood.* 2008;112(1):45–52.
6. Vardiman JW, Harris NL, Brunning RD. The World Health Organization (WHO) classification of the myeloid neoplasms. *Blood.* 2002;100(7):2292–2302.
7. Vardiman JW, Thiele J, Arber DA, et al. The 2008 revision of the World Health Organization (WHO) classification of myeloid neoplasms and acute leukemia: rationale and important changes. *Blood.* 2009;114(5):937–951.
8. Bennett JM, Catovsky D, Daniel M-T, et al. Proposals for the Classification of the Acute Leukaemias French-American-British (FAB) Co-operative Group. *Br. J. Haematol.* 1976;33(4):451–458.
9. Greenberg P, Cox C, LeBeau MM, et al. International scoring system for evaluating prognosis in myelodysplastic syndromes. *Blood.* 1997;89(6):2079–2088.
10. Greenberg PL, Tuechler H, Schanz J, et al. Revised international prognostic scoring system for myelodysplastic syndromes. *Blood.* 2012;120(12):2454–2465.
11. Papaemmanuil E, Gerstung M, Malcovati L, et al. Clinical and biological implications of driver mutations in myelodysplastic syndromes. *Blood.* 2013;122(22):3616–3627.
12. Bejar R, Stevenson K, Abdel-Wahab O, et al. Clinical effect of point mutations in myelodysplastic syndromes. *N. Engl. J. Med.* 2011;364(26):2496–2506.
13. Walter MJ, Shen D, Shao J, et al. Clonal diversity of recurrently mutated genes in myelodysplastic syndromes. *Leukemia.* 2013;27(6):1275–1282.
14. Haferlach T, Nagata Y, Grossmann V, et al. Landscape of genetic lesions in 944 patients with myelodysplastic syndromes. *Leukemia.* 2014;28(2):241–247.
15. Graubert TA, Shen D, Ding L, et al. Recurrent mutations in the U2AF1 splicing factor in myelodysplastic syndromes. *Nat. Genet.* 2011;44(1):53–57.
16. Yoshida K, Sanada M, Shiraishi Y, et al. Frequent pathway mutations of splicing machinery in myelodysplasia. *Nature.* 2011;478(7367):64–69.
17. Visconte V, Makishima H, Jankowska A, et al. SF3B1, a splicing factor is frequently mutated in refractory anemia with ring sideroblasts. *Leukemia.* 2012;26(3):542–545.
18. Papaemmanuil E, Cazzola M, Boulwood J, et al. Somatic SF3B1 mutation in myelodysplasia with ring sideroblasts. *N. Engl. J. Med.* 2011;365(15):1384–1395.
19. Mauritzson N, Albin M, Rylander L, et al. Pooled analysis of clinical and cytogenetic features in treatment-related and de novo adult acute myeloid leukemia and myelodysplastic syndromes based on a consecutive series of 761 patients analyzed 1976-1993 and on 5098 unselected cases reported in the literature 1974-2001. *Leukemia.* 2002;16(12):2366–2378.
20. Jerez A, Gondek LP, Jankowska AM, et al. Topography, clinical, and genomic correlates of 5q myeloid malignancies revisited. *J. Clin. Oncol.* 2012;30(12):1343–1349.
21. Liu TX, Becker MW, Jelinek J, et al. Chromosome 5q deletion and epigenetic suppression of the gene encoding α -catenin (CTNNA1) in myeloid cell transformation.

- Nat. Med.* 2006;13(1):78–83.
22. Boultwood J, Fidler C, Strickson AJ, et al. Narrowing and genomic annotation of the commonly deleted region of the 5q- syndrome. *Blood.* 2002;99(12):4638–4641.
 23. Le Beau MM, Espinosa R, Neuman WL, et al. Cytogenetic and molecular delineation of the smallest commonly deleted region of chromosome 5 in malignant myeloid diseases. *Proc. Natl. Acad. Sci. U.S.A.* 1993;90(12):5484–5488.
 24. Zhao N, Stoffel A, Wang PW, et al. Molecular delineation of the smallest commonly deleted region of chromosome 5 in malignant myeloid diseases to 1-1.5 Mb and preparation of a PAC-based physical map. *Proc. Natl. Acad. Sci. U.S.A.* 1997;94(13):6948–6953.
 25. Horrigan SK, Arbieva ZH, Xie HY, et al. Delineation of a minimal interval and identification of 9 candidates for a tumor suppressor gene in malignant myeloid disorders on 5q31. *Blood.* 2000;95(7):2372–2377.
 26. Graubert TA, Payton MA, Shao J, et al. Integrated Genomic Analysis Implicates Haploinsufficiency of Multiple Chromosome 5q31.2 Genes in De Novo Myelodysplastic Syndromes Pathogenesis. *PLoS ONE.* 2009;4(2):e4583.
 27. Lai F, Godley LA, Joslin J, et al. Transcript map and comparative analysis of the 1.5-Mb commonly deleted segment of human 5q31 in malignant myeloid diseases with a del(5q). *Genomics.* 2001;71(2):235–245.
 28. Liang JC, Ning Y, Wang RY, et al. Spectral karyotypic study of the HL-60 cell line: detection of complex rearrangements involving chromosomes 5, 7, and 16 and delineation of critical region of deletion on 5q31.1. *Cancer Genet. Cytogenet.* 1999;113(2):105–109.
 29. Patnaik MM, Lasho TL, Finke CM, et al. WHO-defined “myelodysplastic syndrome with isolated del (5q)” in 88 consecutive patients: survival data, leukemic transformation rates and prevalence of JAK2, MPL and IDH mutations. *Leukemia.* 2010;24(7):1283–1289.
 30. Joslin JM, Fernald AA, Tennant TR, et al. Haploinsufficiency of EGR1, a candidate gene in the del(5q), leads to the development of myeloid disorders. *Blood.* 2007;110(2):719–726.
 31. Dubourg C, Toutain B, Hélias C, et al. Evaluation of ETF1/eRF1, mapping to 5q31, as a candidate myeloid tumor suppressor gene. *Cancer Genet. Cytogenet.* 2002;134(1):33–37.
 32. Ebert BL, Pretz J, Bosco J, et al. Identification of RPS14 as a 5q- syndrome gene by RNA interference screen. *Nature.* 2008;451(7176):335–339.
 33. Ebert BL. Molecular dissection of the 5q deletion in myelodysplastic syndrome. *Semin. Oncol.* 2011;38(5):621–626.
 34. Wang J, Fernald AA, Anastasi J, Le Beau MM, Qian Z. Haploinsufficiency of Apc leads to ineffective hematopoiesis. *Blood.* 2010;115(17):3481–3488.
 35. Starczynowski DT, Kuchenbauer F, Argiropoulos B, et al. Identification of miR-145 and miR-146a as mediators of the 5q- syndrome phenotype. *Nat. Med.* 2009;16(1):49–58.
 36. Chen TH-P, Kambal A, Krysiak K, et al. Knockdown of Hspa9, a del(5q31.2) gene, results in a decrease in hematopoietic progenitors in mice. *Blood.* 2011;117(5):1530–1539.
 37. Kulasekararaj AG, Smith AE, Mian SA, et al. TP53 mutations in myelodysplastic syndrome are strongly correlated with aberrations of chromosome 5, and correlate with adverse prognosis. *Br. J. Haematol.* 2013;160(5):660–672.
 38. Jadersten M, Saft L, Smith A, et al. TP53 Mutations in Low-Risk Myelodysplastic Syndromes With del(5q) Predict Disease Progression. *J. Clin. Oncol.* 2011;29(15):1971–1979.
 39. Jadersten M, Saft L, Pellagatti A, et al. Clonal heterogeneity in the 5q- syndrome: p53 expressing progenitors prevail during lenalidomide treatment and expand at disease

- progression. *Haematologica*. 2009;94(12):1762–1766.
40. Christiansen DH, Andersen MK, Pedersen-Bjergaard J. Mutations With Loss of Heterozygosity of p53 Are Common in Therapy-Related Myelodysplasia and Acute Myeloid Leukemia After Exposure to Alkylating Agents and Significantly Associated With Deletion or Loss of 5q, a Complex Karyotype, and a Poor Prognosis. *J. Clin. Oncol.* 2001.
 41. Castro PD, Liang JC, Nagarajan L. Deletions of chromosome 5q13.3 and 17p loci cooperate in myeloid neoplasms. *Blood*. 2000;95(6):2138–2143.
 42. Jadersten M, Saft L, Pellagatti A, et al. Clonal heterogeneity in the 5q- syndrome: p53 expressing progenitors prevail during lenalidomide treatment and expand at disease progression. *Haematologica*. 2009;94(12):1762–1766.
 43. List A, Dewald G, Bennett J, et al. Lenalidomide in the Myelodysplastic Syndrome with Chromosome 5q Deletion. *N. Engl. J. Med.* 2006;355(14):1456–1465.
 44. Nilsson L, Astrand-Grundström I, Arvidsson I, et al. Isolation and characterization of hematopoietic progenitor/stem cells in 5q-deleted myelodysplastic syndromes: evidence for involvement at the hematopoietic stem cell level. *Blood*. 2000;96(6):2012–2021.
 45. Sportoletti P, Grisendi S, Majid SM, et al. Npm1 is a haploinsufficient suppressor of myeloid and lymphoid malignancies in the mouse. *Blood*. 2008;111(7):3859–3862.
 46. Grisendi S, Bernardi R, Rossi M, et al. Role of nucleophosmin in embryonic development and tumorigenesis. *Nature*. 2005;437(7055):147–153.
 47. Lane SW, Sykes SM, Al-Shahrour F, et al. The Apc(min) mouse has altered hematopoietic stem cell function and provides a model for MPD/MDS. *Blood*. 2010;115(17):3489–3497.
 48. Qian Z, Chen L, Fernald AA, Williams BO, Le Beau MM. A critical role for Apc in hematopoietic stem and progenitor cell survival. *J. Exp. Med.* 2008;205(9):2163–2175.
 49. Barlow JL, Drynan LF, Hewett DR, et al. A p53-dependent mechanism underlies macrocytic anemia in a mouse model of human 5q- syndrome. *Nat. Med.* 2009;16(1):59–66.
 50. Lehmann S, O'Kelly J, Raynaud S, et al. Common deleted genes in the 5q- syndrome: thrombocytopenia and reduced erythroid colony formation in SPARC null mice. *Leukemia*. 2007;21(9):1931–1936.
 51. Talaria M, Gabriele T, Kola I, Anderson RL. A hitchhiker's guide to the human Hsp70 family. *Cell Stress Chaperones*. 1996;1(1):23–28.
 52. Guo F, Sigua C, Bali P, et al. Mechanistic role of heat shock protein 70 in Bcr-Abl-mediated resistance to apoptosis in human acute leukemia cells. *Blood*. 2005;105(3):1246–1255.
 53. Daugaard M, Rohde M, Jäättelä M. The heat shock protein 70 family: Highly homologous proteins with overlapping and distinct functions. *FEBS Lett.* 2007;581(19):3702–3710.
 54. Lindquist S, Craig EA. The heat-shock proteins. *Annu. Rev. Genet.* 1988.
 55. Jäättelä M. Heat shock proteins as cellular lifeguards. *Ann. Med.* 1999.
 56. Hunt C, Morimoto RI. Conserved features of eukaryotic hsp70 genes revealed by comparison with the nucleotide sequence of human hsp70. *Proc. Natl. Acad. Sci. U.S.A.* 1985;82(19):6455–6459.
 57. Boorstein W, Ziegelhoffer T, Craig E. Molecular evolution of the HSP70 multigene family. *J. Mol. Evol.* 1994;38(1):1–17.
 58. Gupta RS, Singh B. Phylogenetic analysis of 70 kD heat shock protein sequences suggests a chimeric origin for the eukaryotic cell nucleus. *Curr. Biol.* 1994;4(12):1104–1114.
 59. Murphy ME. The HSP70 family and cancer. *Carcinogenesis*. 2013;34(6):1181–1188.
 60. Zhu D, Dix DJ, Eddy EM. HSP70-2 is required for CDC2 kinase activity in meiosis I of

- mouse spermatocytes. *Development*. 1997;124(15):3007–3014.
61. Zhu X, Zhao X, Burkholder WF, et al. Structural analysis of substrate binding by the molecular chaperone DnaK. *Science*. 1996;272(5268):1606–1614.
 62. Saibil H. Chaperone machines for protein folding, unfolding and disaggregation. *Nat. Rev. Mol. Cell Biol.* 2013;14(10):630–642.
 63. Goswami AV, Chittoor B, D'Silva P. Understanding the Functional Interplay between Mammalian Mitochondrial Hsp70 Chaperone Machine Components. *J. Biol. Chem.* 2010;285(25):19472–19482.
 64. Brocchieri L, Conway de Macario E, Macario AJL. hsp70 genes in the human genome: Conservation and differentiation patterns predict a wide array of overlapping and specialized functions. *BMC Evol. Biol.* 2008;8:19.
 65. Clerico EM, Gierasch LM. Inhibitors of Molecular Chaperones as Therapeutic Agents. *Inhibitors of Molecular Chaperones as Therapeutic Agents*. 2013.
 66. Florin L, Becker KA, Sapp C, et al. Nuclear translocation of papillomavirus minor capsid protein L2 requires Hsc70. *J. Virol.* 2004;78(11):5546–5553.
 67. Luo S, Mao C, Lee B, Lee AS. GRP78/BiP is required for cell proliferation and protecting the inner cell mass from apoptosis during early mouse embryonic development. *Mol. Cell. Biol.* 2006;26(15):5688–5697.
 68. Dix DJ, Allen JW, Collins BW, et al. Targeted gene disruption of Hsp70-2 results in failed meiosis, germ cell apoptosis, and male infertility. *Proc. Natl. Acad. Sci. U.S.A.* 1996;93(8):3264–3268.
 69. Lee SH, Kim M, Yoon BW, et al. Targeted hsp70.1 disruption increases infarction volume after focal cerebral ischemia in mice. *Stroke*. 2001;32(12):2905–2912.
 70. Huang L, Mivechi NF, Moskopidis D. Insights into Regulation and Function of the Major Stress-Induced hsp70 Molecular Chaperone In Vivo: Analysis of Mice with Targeted Gene Disruption of the hsp70.1 or hsp70.3 Gene. *Mol. Cell. Biol.* 2001;21(24):8575–8591.
 71. Hampton CR, Shimamoto A, Rothnie CL, et al. HSP70.1 and -70.3 are required for late-phase protection induced by ischemic preconditioning of mouse hearts. *Am. J. Physiol. Heart Circ. Physiol.* 2003;285(2):H866–74.
 72. Dahlseid JN, Lill R, Green JM, et al. PBP74, a new member of the mammalian 70-kDa heat shock protein family, is a mitochondrial protein. *Mol. Biol. Cell.* 1994;5(11):1265–1275.
 73. Singh B, Soltys BJ, Wu ZC, et al. Cloning and some novel characteristics of mitochondrial Hsp70 from Chinese hamster cells. *Exp. Cell Res.* 1997;234(2):205–216.
 74. Wittrup A, Zhang S-H, Svensson KJ, et al. Magnetic nanoparticle-based isolation of endocytic vesicles reveals a role of the heat shock protein GRP75 in macromolecular delivery. *Proc. Natl. Acad. Sci. U.S.A.* 2010;107(30):13342–13347.
 75. Ma Z, Izumi H, Kanai M, et al. Mortalin controls centrosome duplication via modulating centrosomal localization of p53. *Oncogene*. 2006;25(39):5377–5390.
 76. Szabadkai G, Bianchi K, Várnai P, et al. Chaperone-mediated coupling of endoplasmic reticulum and mitochondrial Ca²⁺ channels. *J. Cell Biol.* 2006;175(6):901–911.
 77. Wadhwa R, Taira K, Kaul SC. An Hsp70 family chaperone, mortalin/mthsp70/PBP74/Grp75: what, when, and where? *Cell Stress Chaperones*. 2002;7(3):309.
 78. Moro F, Okamoto K, Donzeau M, Neupert W, Brunner M. Mitochondrial protein import: molecular basis of the ATP-dependent interaction of MtHsp70 with Tim44. *J. Biol. Chem.* 2002;277(9):6874–6880.
 79. Schilke B, Williams B, Knieszner H, et al. Evolution of Mitochondrial Chaperones Utilized in Fe-S Cluster Biogenesis. *Curr. Biol.* 2006;16(16):1660–1665.
 80. Baumann F, Milisav I, Neupert W, Herrmann JM. Ecm10, a novel Hsp70 homolog in the

- mitochondrial matrix of the yeast *Saccharomyces cerevisiae*. *FEBS Lett.* 2000;487(2):307–312.
81. Knight SA, Sepuri NB, Pain D, Dancis A. Mt-Hsp70 homolog, Ssc2p, required for maturation of yeast frataxin and mitochondrial iron homeostasis. *J. Biol. Chem.* 1998;273(29):18389–18393.
 82. Choglay AA, Chapple JP, Blatch GL, Cheetham ME. Identification and characterization of a human mitochondrial homologue of the bacterial co-chaperone GrpE. *Gene.* 2001;267(1):125–134.
 83. Burri L, Vascotto K, Fredersdorf S, et al. Zim17, a novel zinc finger protein essential for protein import into mitochondria. *J. Biol. Chem.* 2004;279(48):50243–50249.
 84. Zhai P, Stanworth C, Liu S, Silberg JJ. The human escort protein Hep binds to the ATPase domain of mitochondrial hsp70 and regulates ATP hydrolysis. *J. Biol. Chem.* 2008;283(38):26098–26106.
 85. Künkele KP, Heins S, Dembowski M, Nargang FE. The Preprotein Translocation Channel of the Outer Membrane of Mitochondria. *Cell.* 1998.
 86. Endo T, Kohda D. Functions of outer membrane receptors in mitochondrial protein import. *Biochim. Biophys. Acta.* 2002;1592(1):3–14.
 87. Mokranjac D, Sichting M, Neupert W, Hell K. Tim14, a novel key component of the import motor of the TIM23 protein translocase of mitochondria. *EMBO J.* 2003;22(19):4945–4956.
 88. Mokranjac D, Paschen SA, Kozany C, et al. Tim50, a novel component of the TIM23 preprotein translocase of mitochondria. *EMBO J.* 2003;22(4):816–825.
 89. Zhang Y, Deng H, Zhao Q, Li SJ. Interaction of presequence peptides with human translocase of inner membrane of mitochondria Tim23. *Biochem. Biophys. Res. Commun.* 2013;437(2):292–299.
 90. Gevorkyan-Airapetov L, Zohary K, Popov-Celeketic D, et al. Interaction of Tim23 with Tim50 is essential for protein translocation by the mitochondrial TIM23 complex. *J. Biol. Chem.* 2009;284(8):4865–4872.
 91. Kronidou NG, Oppliger W, Bolliger L, et al. Dynamic interaction between Isp45 and mitochondrial hsp70 in the protein import system of the yeast mitochondrial inner membrane. *Proc. Natl. Acad. Sci. U.S.A.* 1994;91(26):12818–12822.
 92. Dekker PJT. The Tim core complex defines the number of mitochondrial translocation contact sites and can hold arrested preproteins in the absence of matrix Hsp70-Tim44. *EMBO J.* 1997;16(17):5408–5419.
 93. Bömer U, Meijer M, Maarse AC, et al. Multiple interactions of components mediating preprotein translocation across the inner mitochondrial membrane. *EMBO J.* 1997;16(9):2205–2216.
 94. Koehler CM. New developments in mitochondrial assembly. *Annu. Rev. Cell Dev. Biol.* 2004;20:309–335.
 95. Okamoto K. The protein import motor of mitochondria: a targeted molecular ratchet driving unfolding and translocation. *EMBO J.* 2002;21(14):3659–3671.
 96. Neupert W, Brunner M. The protein import motor of mitochondria. *Nat. Rev. Mol. Cell Biol.* 2002;3(8):555–565.
 97. Pfanner N, Geissler A. Versatility of the mitochondrial protein import machinery. *Nat. Rev. Mol. Cell Biol.* 2001;2(5):339–349.
 98. Geissler A, Rassow J, Pfanner N, Voos W. Mitochondrial import driving forces: enhanced trapping by matrix Hsp70 stimulates translocation and reduces the membrane potential dependence of loosely folded preproteins. *Mol. Cell. Biol.* 2001;21(20):7097–7104.
 99. Kang PJ, Ostermann J, Shilling J, et al. Requirement for hsp70 in the mitochondrial matrix for translocation and folding of precursor proteins. *Nature.* 1990;348(6297):137–

- 143.
100. Pfanner N, Tropschug M, Neupert W. Mitochondrial protein import: nucleoside triphosphates are involved in conferring import-competence to precursors. *Cell*. 1987;49(6):815–823.
 101. Rowley N, Prip-Buus C, Westermann B, et al. Mdj1p, a novel chaperone of the DnaJ family, is involved in mitochondrial biogenesis and protein folding. *Cell*. 1994;77(2):249–259.
 102. Ostermann J, Horwich AL, Neupert W, Hartl FU. Protein folding in mitochondria requires complex formation with hsp60 and ATP hydrolysis. *Nature*. 1989;341(6238):125–130.
 103. Manning-Krieg UC, Scherer PE, Schatz G. Sequential action of mitochondrial chaperones in protein import into the matrix. *EMBO J*. 1991;10(11):3273–3280.
 104. Wadhwa R, Takano S, Kaur K, et al. Identification and characterization of molecular interactions between mortalin/mtHsp70 and HSP60. *Biochem. J*. 2005;391(2):185.
 105. Saveliev AS, Kovaleva IE, Novikova LA, Isaeva LV, Luzikov VN. Can foreign proteins imported into yeast mitochondria interfere with PIM1p protease and/or chaperone function? *Arch. Biochem. Biophys*. 1999;363(2):373–376.
 106. Wagner I, van Dyck L, Savel'ev AS, Neupert W, Langer T. Autocatalytic processing of the ATP-dependent PIM1 protease: crucial function of a pro-region for sorting to mitochondria. *EMBO J*. 1997;16(24):7317–7325.
 107. Wagner I, Artl H, van Dyck L, Langer T, Neupert W. Molecular chaperones cooperate with PIM1 protease in the degradation of misfolded proteins in mitochondria. *EMBO J*. 1994;13(21):5135–5145.
 108. Lionaki E, Tavernarakis N. Oxidative stress and mitochondrial protein quality control in aging. *J. Proteomics*. 2013;92:181–194.
 109. Kawai A, Nishikawa S, Hirata A, Endo T. Loss of the mitochondrial Hsp70 functions causes aggregation of mitochondria in yeast cells. *J. Cell. Sci*. 2001;114(Pt 19):3565–3574.
 110. Kanai M, Ma Z, Izumi H, et al. Physical and functional interaction between mortalin and Mps1 kinase. *Genes Cells*. 2007;12(6):797–810.
 111. Löffler H, Lukas J, Bartek J, Krämer A. Structure meets function—centrosomes, genome maintenance and the DNA damage response. *Exp. Cell Res*. 2006.
 112. Lutz T, Westermann B, Neupert W, Herrmann JM. The mitochondrial proteins Ssq1 and Jac1 are required for the assembly of iron sulfur clusters in mitochondria. *J. Mol. Biol*. 2001;307(3):815–825.
 113. Voisine C, Schilke B, Ohlson M, et al. Role of the mitochondrial Hsp70s, Ssc1 and Ssq1, in the maturation of Yfh1. *Mol. Cell. Biol*. 2000;20(10):3677–3684.
 114. Dutkiewicz R, Marszalek J, Schilke B, et al. The Hsp70 chaperone Ssq1p is dispensable for iron-sulfur cluster formation on the scaffold protein Isu1p. *J. Biol. Chem*. 2006;281(12):7801–7808.
 115. Dutkiewicz R. Sequence-specific Interaction between Mitochondrial Fe-S Scaffold Protein Isu and Hsp70 Ssq1 Is Essential for Their in Vivo Function. *J. Biol. Chem*. 2004;279(28):29167–29174.
 116. Luo W-I, Dizin E, Yoon T, Cowan JA. Kinetic and structural characterization of human mortalin. *Protein Expr. Purif*. 2010;72(1):75–81.
 117. Kim K-B, Lee J-W, Lee CS, et al. Oxidation-reduction respiratory chains and ATP synthase complex are localized in detergent-resistant lipid rafts. *Proteomics*. 2006;6(8):2444–2453.
 118. Mizukoshi E, Suzuki M, Loupatov A, et al. Fibroblast growth factor-1 interacts with the glucose-regulated protein GRP75/mortalin. *Biochem. J*. 1999;343:461–466.
 119. Mizukoshi E, Suzuki M, Misono T, et al. Cell-cycle dependent tyrosine phosphorylation on mortalin regulates its interaction with fibroblast growth factor-1. *Biochem. Biophys*.

- Res. Commun.* 2001;280(4):1203–1209.
120. Hadari YR, Haring HU, Zick Y. p75, a member of the heat shock protein family, undergoes tyrosine phosphorylation in response to oxidative stress. *J. Biol. Chem.* 1997;272(1):657–662.
 121. Egerton M, Moritz RL, Druker B, Kelso A, Simpson RJ. Identification of the 70kD heat shock cognate protein (Hsc70) and alpha-actinin-1 as novel phosphotyrosine-containing proteins in T lymphocytes. *Biochem. Biophys. Res. Commun.* 1996;224(3):666–674.
 122. Bohana-Kashtan O, Ziporen L, Donin N, Kraus S. Cell signals transduced by complement. *Mol. Immunol.* 2004.
 123. Morgan BP, Dankert JR, Esser AF. Recovery of human neutrophils from complement attack: removal of the membrane attack complex by endocytosis and exocytosis. *J. Immunol.* 1987;138(1):246–253.
 124. Pilzer D. Mortalin/GRP75 promotes release of membrane vesicles from immune attacked cells and protection from complement-mediated lysis. *Int. Immunol.* 2005;17(9):1239–1248.
 125. Pilzer D, Saar M, Koya K, Fishelson Z. Mortalin inhibitors sensitize K562 leukemia cells to complement-dependent cytotoxicity. *Int. J. Cancer.* 2010;126(6):1428–1435.
 126. Sacht G, Brigelius-Flohé R, Kiess M, Sztajer H, Flohé L. ATP-sensitive association of mortalin with the IL-1 receptor type I. *BioFactors.* 1999;9(1):49–60.
 127. Kaul S, Reddel RR, Mitsui Y, Wadhwa R. An N-terminal region of mot-2 binds to p53 in vitro. *Neoplasia.* 2001;3(2):110–114.
 128. Wadhwa R, Taira K, KAUL SC. Can mortalin be a candidate target for cancer therapy. *Cancer Ther.* 2003.
 129. Wadhwa R, Yaguchi T, Hasan MK, et al. Hsp70 family member, mot-2/mthsp70/GRP75, binds to the cytoplasmic sequestration domain of the p53 protein. *Exp. Cell Res.* 2002;274(2):246–253.
 130. Wadhwa R, Takano S, Robert M, et al. Inactivation of tumor suppressor p53 by mot-2, a hsp70 family member. *J. Biol. Chem.* 1998;273(45):29586–29591.
 131. Iosefson O, Azem A. Reconstitution of the mitochondrial Hsp70 (mortalin)-p53 interaction using purified proteins—identification of additional interacting regions. *FEBS Lett.* 2010;584(6):1080–1084.
 132. Ahn BY, Trinh DLN, Zajchowski LD, et al. Tid1 is a new regulator of p53 mitochondrial translocation and apoptosis in cancer. *Oncogene.* 2010;29(8):1155–1166.
 133. Schwarzer C, Barnikol-Watanabe S, Thinnies FP, Hilschmann N. Voltage-dependent anion-selective channel (VDAC) interacts with the dynein light chain Tctex1 and the heat-shock protein PBP74. *Int. J. Biochem. Cell Biol.* 2002;34(9):1059–1070.
 134. Lemasters JJ, Holmuhamedov E. Voltage-dependent anion channel (VDAC) as mitochondrial governor—Thinking outside the box. ... *Acta (BBA)-Molecular Basis of Disease.* 2006.
 135. Söti C, Csermely P. Aging cellular networks: Chaperones as major participants. *Exp. Gerontol.* 2007;42(1-2):113–119.
 136. Orsini F, Migliaccio E, Moroni M, et al. The life span determinant p66Shc localizes to mitochondria where it associates with mitochondrial heat shock protein 70 and regulates trans-membrane potential. *J. Biol. Chem.* 2004;279(24):25689–25695.
 137. Giorgio M, Migliaccio E, Orsini F, et al. Electron transfer between cytochrome c and p66Shc generates reactive oxygen species that trigger mitochondrial apoptosis. *Cell.* 2005;122(2):221–233.
 138. Sun L, Xiao L, Nie J, et al. p66Shc mediates high-glucose and angiotensin II-induced oxidative stress renal tubular injury via mitochondrial-dependent apoptotic pathway. *Am. J. Physiol. Renal Physiol.* 2010;299(5):F1014–25.
 139. Graiani G, Lagrasta C, Migliaccio E, et al. Genetic deletion of the p66Shc adaptor

- protein protects from angiotensin II-induced myocardial damage. *Hypertension*. 2005;46(2):433–440.
140. Migliaccio E, Giorgio M, Mele S, et al. The p66shc adaptor protein controls oxidative stress response and life span in mammals. *Nature*. 1999;402(6759):309–313.
 141. Bonifati V, Rizzu P, Squitieri F, et al. DJ-1(PARK7), a novel gene for autosomal recessive, early onset parkinsonism. *Neurol. Sci.* 2003;24(3):159–160.
 142. Burbulla LF, Schelling C, Kato H, et al. Dissecting the role of the mitochondrial chaperone mortalin in Parkinson's disease: functional impact of disease-related variants on mitochondrial homeostasis. *Hum. Mol. Genet.* 2010;19(22):4437–4452.
 143. Jin J, Li GJ, Davis J, et al. Identification of novel proteins associated with both alpha-synuclein and DJ-1. *Mol. Cell Proteomics*. 2007;6(5):845–859.
 144. Jin J, Hulette C, Wang Y, et al. Proteomic Identification of a Stress Protein, Mortalin/mthsp70/GRP75 Relevance To Parkinson Disease. *Mol. Cell Proteomics*. 2006;5(7):1193–1204.
 145. Li HM, Niki T, Taira T, Iguchi-Arigo SMM, Ariga H. Association of DJ-1 with chaperones and enhanced association and colocalization with mitochondrial Hsp70 by oxidative stress. *Free Radic. Res.* 2005;39(10):1091–1099.
 146. Zhou Y, Gu G, Goodlett DR, et al. Analysis of alpha-synuclein-associated proteins by quantitative proteomics. *J. Biol. Chem.* 2004;279(37):39155–39164.
 147. Fuchs J, Nilsson C, Kachergus J, et al. Phenotypic variation in a large Swedish pedigree due to SNCA duplication and triplication. *Neurology*. 2007;68(12):916–922.
 148. Chartier-Harlin M-C, Kachergus J, Roumier C, et al. Alpha-synuclein locus duplication as a cause of familial Parkinson's disease. *Lancet*. 2004;364(9440):1167–1169.
 149. Zarranz JJ, Alegre J, Gomez-Esteban JC, et al. The new mutation, E46K, of alpha-synuclein causes parkinson and Lewy body dementia. *Ann. Neurol.* 2004;55(2):164–173.
 150. Yang H, Zhou X, Liu X, et al. Mitochondrial dysfunction induced by knockdown of mortalin is rescued by Parkin. *Biochem. Biophys. Res. Commun.* 2011;410(1):114–120.
 151. Vandermoere F, Yazidi-Belkoura EI, Demont Y, et al. Proteomics exploration reveals that actin is a signaling target of the kinase Akt. *Mol. Cell Proteomics*. 2007;6(1):114–124.
 152. Yang L, Guo W, Zhang Q, et al. Crosstalk between Raf/MEK/ERK and PI3K/AKT in Suppression of Bax Conformational Change by Grp75 under Glucose Deprivation Conditions. *J. Mol. Biol.* 2011;414(5):654–666.
 153. Wadhwa R, Yaguchi T, Hasan MK, Taira K, Kaul SC. Mortalin–MPD (mevalonate pyrophosphate decarboxylase) interactions and their role in control of cellular proliferation. *Biochem. Biophys. Res. Commun.* 2003;302(4):735–742.
 154. Kuwabara H, Yoneda M, Hayasaki H, Nakamura T, Mori H. Glucose regulated proteins 78 and 75 bind to the receptor for hyaluronan mediated motility in interphase microtubules. *Biochem. Biophys. Res. Commun.* 2006;339(3):971–976.
 155. Zhang S, Chang MC, Zylka D, et al. The hyaluronan receptor RHAMM regulates extracellular-regulated kinase. *J. Biol. Chem.* 1998;273(18):11342–11348.
 156. Liu Y, Liu W, Song X-D, Zuo J. Effect of GRP75/mthsp70/PBP74/mortalin overexpression on intracellular ATP level, mitochondrial membrane potential and ROS accumulation following glucose deprivation in PC12 cells. *Mol. Cell. Biochem.* 2005;268(1-2):45–51.
 157. Williamson CL, Dabkowski ER, Dillmann WH, Hollander JM. Mitochondria protection from hypoxia/reoxygenation injury with mitochondria heat shock protein 70 overexpression. *Am. J. Physiol. Heart Circ. Physiol.* 2008;294(1):H249–56.
 158. Ohtsuka R, Abe Y, Fujii T, et al. Mortalin is a novel mediator of erythropoietin signaling. *Eur. J. Haematol.* 2007;79(2):114–125.
 159. Yokoyama K, Fukumoto K, Murakami T, et al. Extended longevity of *Caenorhabditis*

- elegans by knocking in extra copies of hsp70F, a homolog of mot-2 (mortalin)/mthsp70/Grp75. *FEBS Lett.* 2002;516(1-3):53–57.
160. Wadhwa R, Takano S, Kaur K, et al. Upregulation of mortalin/mthsp70/Grp75 contributes to human carcinogenesis. *Int. J. Cancer.* 2006;118(12):2973–2980.
 161. Yi X, Luk JM, Lee NP, et al. Association of Mortalin (HSPA9) with Liver Cancer Metastasis and Prediction for Early Tumor Recurrence. *Mol. Cell Proteomics.* 2007;7(2):315–325.
 162. Dundas SR, Lawrie LC, Rooney PH, Murray GI. Mortalin is over-expressed by colorectal adenocarcinomas and correlates with poor survival. *J. Pathol.* 2005;205(1):74–81.
 163. Wu PK, Hong SK, Veeranki S, et al. A Mortalin/HSPA9-Mediated Switch in Tumor-Suppressive Signaling of Raf/MEK/Extracellular Signal-Regulated Kinase. *Mol. Cell Biol.* 2013;33(20):4051–4067.
 164. Kaul S, Reddel RR, Sugihara T, Mitsui Y, Wadhwa R. Inactivation of p53 and life span extension of human diploid fibroblasts by mot-2. *FEBS Lett.* 2000;474(2-3):159–164.
 165. De Mena L, Coto E, Sánchez-Ferrero E, et al. Mutational screening of the mortalin gene (HSPA9) in Parkinson's disease. *J. Neural Transm.* 2009;116(10):1289–1293.
 166. Schapira AHV. Mitochondria in the aetiology and pathogenesis of Parkinson's disease. *Lancet Neurol.* 2008;7(1):97–109.
 167. Shi M, Jin J, Wang Y, et al. Mortalin: a protein associated with progression of Parkinson disease? *J. Neuropathol. Exp. Neurol.* 2008;67(2):117–124.
 168. Selkoe DJ. Alzheimer's disease: genes, proteins, and therapy. *Physiol. Rev.* 2001;81(2):741–766.
 169. Ferrari A, Hoerndli F, Baechi T, Nitsch RM, Götz J. beta-Amyloid induces paired helical filament-like tau filaments in tissue culture. *J. Biol. Chem.* 2003;278(41):40162–40168.
 170. Kögel D, Schomburg R, Copanaki E, Prehn JHM. Regulation of gene expression by the amyloid precursor protein: inhibition of the JNK/c-Jun pathway. *Cell Death Differ.* 2005;12(1):1–9.
 171. David DC, Ittner LM, Gehrig P, et al. Beta-amyloid treatment of two complementary P301L tau-expressing Alzheimer's disease models reveals similar deregulated cellular processes. *Proteomics.* 2006;6(24):6566–6577.
 172. Qu M, Zhou Z, Xu S, et al. Mortalin overexpression attenuates beta-amyloid-induced neurotoxicity in SH-SY5Y cells. *Brain Res.* 2011;1368:336–345.
 173. Rubinsztein DC, Easton DF. Apolipoprotein E Genetic Variation and Alzheimer's Disease. *Dement Geriatr Cogn Disord.* 1999;10(3):199–209.
 174. Osorio C, Sullivan PM, He DN, et al. Mortalin is regulated by APOE in hippocampus of AD patients and by human APOE in TR mice. *Neurobiol. Aging.* 2007;28(12):1853–1862.
 175. Choi J, Forster MJ, McDonald SR, et al. Proteomic identification of specific oxidized proteins in ApoE-knockout mice: relevance to Alzheimer's disease. *Free Radical Biology and Medicine.* 2004;36(9):1155–1162.
 176. Ribeil J-A, Zermati Y, Vandekerckhove J, et al. Hsp70 regulates erythropoiesis by preventing caspase-3-mediated cleavage of GATA-1. *Nature.* 2007;445(7123):102–105.
 177. Zou P, Yoshihara H, Hosokawa K, et al. p57(Kip2) and p27(Kip1) cooperate to maintain hematopoietic stem cell quiescence through interactions with Hsc70. *Cell Stem Cell.* 2011;9(3):247–261.
 178. Miharada K, Karlsson G, Rehn M, et al. Cripto Regulates Hematopoietic Stem Cells as a Hypoxic-Niche-Related Factor through Cell Surface Receptor GRP78. *Cell Stem Cell.* 2011;9(4):330–344.
 179. Craven SE, French D, Ye W, de Sauvage F, Rosenthal A. Loss of Hspa9b in zebrafish recapitulates the ineffective hematopoiesis of the myelodysplastic syndrome. *Blood.*

- 2005;105(9):3528–3534.
180. Bertelsen EB, Chang L, Gestwicki JE, Zuiderweg ERP. Solution conformation of wild-type E. coli Hsp70 (DnaK) chaperone complexed with ADP and substrate. *Proc. Natl. Acad. Sci. U.S.A.* 2009;106(21):8471–8476.
 181. Ye H, Rouault TA. Erythropoiesis and iron sulfur cluster biogenesis. *Adv. Hematol.* 2010;2010:.
 182. Wingert RA, Galloway JL, Barut B, et al. Deficiency of glutaredoxin 5 reveals Fe-S clusters are required for vertebrate haem synthesis. *Nature.* 2005;436(7053):1035–1039.
 183. Ponderre C, Campagna DR, Antiochos B, et al. Abcb7, the gene responsible for X-linked sideroblastic anemia with ataxia, is essential for hematopoiesis. *Blood.* 2007;109(8):3567–3569.
 184. Ponderre C, Antiochos BB, Campagna DR, et al. The mitochondrial ATP-binding cassette transporter Abcb7 is essential in mice and participates in cytosolic iron-sulfur cluster biogenesis. *Hum. Mol. Genet.* 2006;15(6):953–964.
 185. Ye H, Rouault TA. Human Iron–Sulfur Cluster Assembly, Cellular Iron Homeostasis, and Disease. *Biochemistry.* 2010;49(24):4945–4956.
 186. Camaschella C. Recent advances in the understanding of inherited sideroblastic anaemia. *Br. J. Haematol.* 2008;143(1):27–38.
 187. Tai-Nagara I, Matsuoka S, Ariga H, Suda T. Mortalin and DJ-1 coordinately regulate hematopoietic stem cell function through the control of oxidative stress. *Blood.* 2014;123(1):41–50.
 188. Suzuki T, Shen H, Akagi K, et al. New genes involved in cancer identified by retroviral tagging. *Nat. Genet.* 2002;32(1):166–174.
 189. Du Y, Spence SE, Jenkins NA, Copeland NG. Cooperating cancer-gene identification through oncogenic-retrovirus-induced insertional mutagenesis. *Blood.* 2005;106(7):2498–2505.
 190. Craig EA, Kramer J, Kasic-Smithers J. SSC1, a member of the 70-kDa heat shock protein multigene family of *Saccharomyces cerevisiae*, is essential for growth. *Proc. Natl. Acad. Sci. U.S.A.* 1987;84(12):4156–4160.
 191. Strub A, Zufall N, Voos W. The putative helical lid of the Hsp70 peptide-binding domain is required for efficient preprotein translocation into mitochondria. *J. Mol. Biol.* 2003;334(5):1087–1099.
 192. Dietzl G, Chen D, Schnorrer F, et al. A genome-wide transgenic RNAi library for conditional gene inactivation in *Drosophila*. *Nature.* 2007;448(7150):151–156.
 193. Spradling AC, Stern D, Beaton A, et al. The Berkeley *Drosophila* Genome Project gene disruption project: Single P-element insertions mutating 25% of vital *Drosophila* genes. *Genetics.* 1999;153(1):135–177.
 194. Conte M, Deri P, Isolani ME, Mannini L, Batistoni R. A mortalin-like gene is crucial for planarian stem cell viability. *Dev. Biol.* 2009;334(1):109–118.
 195. Kamath RS, Fraser AG, Dong Y, et al. Systematic functional analysis of the *Caenorhabditis elegans* genome using RNAi. *Nature.* 2003;421(6920):231–237.
 196. Simmer F, Moorman C, van der Linden AM, et al. Genome-wide RNAi of *C. elegans* using the hypersensitive rrf-3 strain reveals novel gene functions. *PLoS Biol.* 2003;1(1):E12.
 197. Kimura K, Tanaka N, Nakamura N, Takano S, Ohkuma S. Knockdown of mitochondrial heat shock protein 70 promotes progeria-like phenotypes in *caenorhabditis elegans*. *J. Biol. Chem.* 2007;282(8):5910–5918.
 198. Amsterdam A, Nissen RM, Sun Z, et al. Identification of 315 genes essential for early zebrafish development. *Proc. Natl. Acad. Sci. U.S.A.* 2004;101(35):12792–12797.
 199. Yoshinari N, Ishida T, Kudo A, Kawakami A. Gene expression and functional analysis of

zebrafish larval fin fold regeneration. *Dev. Biol.* 2009.

CHAPTER 2:

The Role of Hspa9 in Mouse Hematopoiesis

1. Abstract

HSPA9 is a gene located in a commonly deleted region of chromosome 5 that is associated with myelodysplastic syndromes. To investigate the role of *Hspa9* in mouse hematopoiesis, we created an *Hspa9* knockout mouse model that reduces mRNA and protein levels of *Hspa9* to 50% of normal. Analysis of hematopoietic stem, progenitor and mature populations of heterozygous knockout mice revealed no significant differences when compared to wild-type littermates *in vivo*. However, an *in vitro* colony-forming assay revealed that *Hspa9* heterozygous mice have a significant reduction in bone marrow B-cell progenitor colony forming ability. This reduction is hematopoietic cell-intrinsic. Enumeration of B-cell progenitor populations *in vivo* revealed no significant difference in *Hspa9*^{+/-} mice compared to *Hspa9*^{+/+} littermates, suggesting a functional defect exists for *Hspa9*^{+/-} B-cell progenitors *in vitro*. Homozygous knockout of *Hspa9* is embryonic lethal prior to fetal liver development, preventing further studies of the effects of complete loss of *Hspa9* on hematopoiesis. Collectively, these data indicate that heterozygous loss of *Hspa9* in mice does not affect hematopoiesis *in vivo*, however, does cause a functional defect in B-cell progenitors *in vitro*.

2. Introduction

Myelodysplastic syndromes (MDS) are a heterogeneous group of clonal hematopoietic stem cell disorders characterized by ineffective hematopoiesis and accelerated apoptosis^{1,2}. Approximately 30% of MDS patients will develop a highly chemotherapy-resistant form of acute myeloid leukemia (AML)³. Understanding initiating steps and the underlying mechanism of transformation may provide an avenue for therapeutic intervention.

Heterozygous, interstitial deletions or loss of the long arm of chromosome 5 (5q) are among the most common acquired genetic abnormalities found in MDS^{2,4-6}. Two commonly deleted regions (CDR) on chromosome 5 have been identified. Loss of the distal region, 5q33.1, is associated

with 5q minus syndrome, which carries a low risk for transformation to AML⁷⁻⁹. Loss of the proximal 5q31.2 region is correlated with a high-risk form of MDS and is associated with AML progression^{6,10-13}. No mutations resulting in loss of both copies of genes in either CDR have been identified, implicating gene haploinsufficiency as a driver of disease^{6,12-15}. In accordance with this, 7 of 28 genes in 5q31.2 were observed to have ~50% reduced mRNA levels in CD34+ cells from del(5q) MDS patients when compared to control samples¹². One of these genes encodes for the chaperone protein HSPA9. An unbiased screen of the protein coding genes on this interval in a primary human erythroid culture system identified HSPA9 as the top candidate gene on this interval that likely contributes to disruption of erythroid maturation, a hallmark of MDS.

The role of *HSPA9* in hematopoiesis has been studied in multiple systems. *Hspa9*^{-/-} zebrafish suffer from severe anemia and have defects in erythroid differentiation with increased apoptosis characteristic of MDS¹⁶. HSPA9 has also been implicated as a downstream mediator of erythropoietin signaling in a primary human CD34+ cell culture system¹⁷. Utilizing RNAi knockdown of *HSPA9* in primary human CD34+ cells and a murine bone marrow transplant model, *Chen et. al.* showed that ~50% knockdown of this gene results in cell cycle alterations, disruption of erythroid differentiation, reduced proliferation, and increased apoptosis—all characteristics of MDS. A more recent study utilizing RNAi knockdown of *Hspa9* in a murine bone marrow transplant model further characterized the consequences of *Hspa9* reduction in hematopoietic stem cells (HSCs), including increased reactive oxygen species and a reduction in quiescent HSCs, both of which are associated with altered HSC function¹⁸⁻²¹. Several members of the highly conserved family of HSP70 proteins have been shown to be involved in hematopoiesis. These chaperone proteins have been shown to influence hematopoiesis through their roles in cell signaling, cell cycle and glycolytic metabolism²²⁻²⁶. The diverse known and putative roles of HSPA9 indicate that it is likely involved in many cellular processes, all which

could contribute to alterations in hematopoiesis. In addition to its putative role in MDS, Hspa9 has been implicated in AML transformation. *Hspa9* is associated with mouse AML in retroviral insertional mutagenesis screens and as a cooperating mutation in tumor suppressor-deficient mice that develop cancer (insertion leading to inactivation)²⁷⁻²⁹. These data support *HSPA9* as a candidate gene that may contribute to abnormal hematopoiesis in MDS and development of AML.

Previous studies have utilized RNAi-mediated methods to study HSPA9 in primary human and mouse cells. These methods are transient and while they lead to global knockdown, there is a high degree of variability for the level of knockdown on a per cell basis, and do not accurately model single copy loss of Hspa9 as seen in patients. Previous studies have also illustrated how sensitive cells are to Hspa9 levels, showing phenotypes of increasing severity inversely correlated with Hspa9 levels³⁰. In order to improve upon existing models of Hspa9 loss of function and precisely model haploinsufficiency in a mammalian system, we created a heterozygous *Hspa9* knockout mouse model. This model results in 50% loss of Hspa9 protein in all cells and was used to evaluate the effects of Hspa9 haploinsufficiency in murine hematopoiesis.

3. Materials and Methods

3.1. Embryonic stem cell clones

Hspa9^{+Gt(IST14901H6)TIGM} mice (referred to as *Hspa9*^{+/-}) were generated using C57Bl/6N *Hspa9*^{Gt(IST14901H6)TIGM} embryonic stem (ES) cell clones provided by the Texas A&M Institute for Genomic Medicine. The ES cell clone library was created by random insertion of a retroviral gene trap vector containing a splice acceptor, a β -galactosidase/neomycin fusion reporter gene, and a poly-A tail, as previously described³¹. We identified an ES cell clone with a normal karyotype that harbored an insertion of the gene trap into intron 3 of *Hspa9*.

Confirmation of a single integration site was performed by Texas A&M using quantitative PCR for neomycin and inverse PCR for DNA adjacent to the insertion site, as previously described^{31,32}.

3.2. Mouse generation and colony maintenance

C57Bl/6N-Hspa9^{Gt(IST14901H6)TIGM} ES cells were injected into albino C57Bl/6J (C57BL/6J-*Tyr*^{2J/J}) blastocysts. Resulting chimeric progeny were bred to C57Bl/6N and produced viable *Hspa9*^{+/-} pups. Mice were maintained on a C57Bl/6N background with the following exceptions, as noted in the text: C57Bl/6N x 129x1/SvJ F₁ progeny for MOL4070LTR leukemogenesis studies, C57Bl/6N x FVB F₁ progeny for BCR-ABL leukemogenesis studies, and C57Bl/6N x 129x1/SvJ mixed strain mice for embryonic lethality studies. Mouse procedures were performed according to protocols approved by the Washington University Animal Studies Committee.

3.3. DNA extraction

Tail DNA was extracted by phenol/chloroform extraction. Briefly, tails were incubated at 55°C overnight in extraction buffer (25mM Tris pH 8.0, 25mM EDTA, 100mM NaCl, 1% Triton X-100) with 2mg/mL proteinase K (Sigma #2308). Protein and contaminants were removed by collection of the aqueous phase following the addition of phenol followed by the addition of chloroform. DNA was precipitated on ice by the addition of 100% ethanol and NaOAc (0.1M) followed by centrifugation. DNA pellets were washed with 100% ethanol to remove residual salt and left to dry. DNA was resuspended in TE buffer and used for southern blot or PCR genotyping.

3.4. Southern Blot

Southern blots were performed using standard methods. Briefly, 20µg tail DNA was digested overnight with XbaI. Digested DNA was precipitated by phenol-chloroform extraction as described above and resuspended 30µL TE followed by incubation at 37°C >1 hour to dissolve DNA. DNA was electrophoresed into 1% agarose gel overnight at 40V. The gel was

stained with ethidium bromide and photographed. DNA was depurinated by incubation with 0.12M HCl for 10 minutes and denatured by incubation with 0.4M NaOH for 20 minutes. DNA was transferred to Hybond-XL membrane by capillary action overnight and rinsed with 2xSSC buffer before drying. The membrane was exposed to ³²P-labeled probe overnight at 42°C. Following removal of the probe, the membrane was washed twice with 2xSSC buffer for 10 minutes at room temperature, twice with 2xSSC + 1% SDS at 65°C for 30 minutes and lastly 0.1xSSC for 30 minutes at room temperature. Finally, the bound probe was detected by autoradiography. The 300bp hybridization probe resulted in 4817bp fragment for a wild-type allele and 3303bp for a gene trap-containing allele (**FIGURE 2.1** and **2.2**)(Probe sequence: TTTTCCCCCAGGATGGCTGGAATGGCCTTAGCCATGAGGCTT TTAGATTTGTTTCAAGAAGAGATTATGCGTAAGTACAACCTCAGTTTCTCTGAGAAAAA AAAAAAACACTTATTGAACCTCAAAGCTTGGATGGGTTGGGTGCGTTATACATTTGTA CTTGTAGTTTATTCAATATGCCACTGGTAACACCAACATAAAACACAGTTCTTCGTATTG GAGACCACTGTTTCAGATGACCATGGAATTTCAATTTCTTACAGATCAGAAGCAATCAAGG GTGCAGTGGTTGGTATTG).

3.5. PCR genotyping

Genotyping was performed as described by Zambrowicz 2003³¹. An oligonucleotide primer for the LTR of the gene trap (V76R, 5'-CCA ATA AAC CCT CTT GCA GTT GC-3') and primers for regions flanking the gene trap insertion site (Forward, 5'-AGA CCA CTG TTC AGA TGA CCA TGG-3'; Reverse, 5'- TTA GAA GTC TGG AGC GGT CAA TGC-3') as depicted in **FIGURE 2.1** were used (synthesized by Sigma). This triple primer system results in a 453bp wild-type band and a 307bp band from the gene trap targeted allele. 50µL PCR reactions contained 50-100ng of tail DNA, 1.25 units of One Taq polymerase (NEB: M0480G), 1X One Taq standard reaction buffer with MgCl₂, 0.3µM of each primer and 200µM dNTPs. PCR was performed as follows: initial denaturation at 95°C for 5 minutes, 40 cycles (95°C for 15 seconds, 64°C for 1 minute, 72°C for 1 minute), and final extension at 72°C for 10 minutes.

PCR products (10 μ L) were electrophoresed on 2% agarose gel containing ethidium bromide using 100bp Ladder (NEB: N0467S) and 6x gel loading blue dye (NEB: B7021S). Typical results are shown in **FIGURE 2.2**.

3.6. Western blot analysis

3.6.1. Western blots

Western blots were performed as previously described³⁰. Cells were washed with PBS and pelleted before being resuspended in radioimmunoprecipitation (RIPA) buffer (150 mM NaCl, 50 mM Tris [pH 8], 1 mM EDTA, 0.1%SDS, 0.5% sodium deoxycholate, 1% NP-40, 1 mM PMSF) with proteinase and phosphatase inhibitors (10mM NaF, 20mM NaPP, 1.25mM Na₃VO₄). Protein lysates were quantified using a standard BCA Protein Assay Kit (Pierce). Equal amounts of protein were loaded onto 4-12% gradient or 10% Tris-HCL gels and transferred to PVDF membranes according to standard protocols. Antibody detection was performed using SuperSignal West Pico Substrate (Thermo Scientific: 34077).

3.6.2. Antibodies

See **TABLE 2.1**.

3.7. RT-PCR

3.7.1. RNA preparation

For preparation of whole bone marrow RNA, femurs were flushed with 1mL TRIzol Reagent (Invitrogen: 15596-018) using a 27 ½ gauge needle directly into microcentrifuge tubes. Alternatively, cells were sorted directly into TRIzol LS Reagent (Invitrogen: 10296-028) or cell pellets were resuspended in 250 μ L molecular grade water and 750 μ L TRIzol LS Reagent was added, mixed well and stored at -80°C. RNA was processed according to manufacturer's protocols. Briefly, 200 μ L chloroform was added, shaken vigorously, centrifuged at 12,000xg, and incubated at 4°C for 15 minutes. The aqueous phase was transferred to a fresh tube. 1 μ L of 15mg/mL RNase-free Glycogen (Invitrogen: AM9510)

was added as carrier followed by the addition of 500µL isopropanol. Samples were centrifuged at 12,000xg for 30 minutes at 4°C. Pellet was washed with 1000ul 75% ethanol and allowed to dry. RNA was resuspended in RNase-free water and incubated for 10 minutes at 55°C prior to storage at -80°C.

3.7.2. Protein coding genes

Genomic DNA was removed using TURBO DNA-free kit (Ambion AM#1907). cDNA was produced using SuperScript III First-Strand Synthesis System (Invitrogen: 18080-051) according to manufacturer's protocols using oligo(dT)₂₀ and random hexamer primers included in the kit. No reverse transcriptase (No RT) controls were processed in parallel. FAM-MGB primer/probe mixes for *IL-6* (Mm00446190_m1), *Flt-3L* (Mm00442801_m1) and *β-Actin* (Mm00607939_s1) were used for RT-PCR TaqMan gene expression assays (Applied Biosystems, 4331182). Assays were performed as singleplex reactions according to manufacturer's protocols using 60ng cDNA in 20µL reactions on a StepOne Plus Real time PCR System (Applied Biosystems). *IL-7* and *Gapdh* RT-PCR assays were performed with SYBR Green using previously reported primers (*IL-7* forward: 5'-TCT GCT GCC TGT CAC ATC ATC-3', *IL-7* reverse: 5'-GGA CAT TGA ATT CTT CAC TGA TAT TCA-3'; *Gapdh* forward: 5'-TGC ACC ACC AAC TGC TTA G-3', *Gapdh* reverse: 5'-GAT GCA GGG ATG ATG TTC-3')³³. *IL-7* and *Gapdh* assays were performed as singleplex reactions according to manufacturer's protocols using 40ng cDNA in 25µL reactions on a StepOne Plus Real time PCR System (Applied Biosystems).

For analysis of *Hspa9* mRNA expression, FAM-MGB *Hspa9* (Mm00477716_g1) and *Gapdh* (Mm99999915_g1) were used. The RT-PCR was performed with Taqman Universal PCR master Mix No AmpErase UNG (AB#4324018, Applied Biosystems). The cycling conditions consist of incubation for 2 min at 50°C, followed by 95°C for 10 min,

for denaturation followed by 40 cycles at 95°C for 15 sec and combined annealing and extension at 60°C for 1 min.

All RT-PCR reactions were performed in duplicate with no-RT control on a StepOne Plus Real time PCR System (Applied Biosystems). Individual cDNA samples were normalized according to their levels of *Gapdh* transcript. The relative standard curve method was used for analysis.

3.7.3. snoRNA

Amplification of snoRNAs from total RNA preparation was performed using TaqMan MicroRNA Reverse Transcription Kit (Applied Biosystems, 4366596) according to manufacturer's protocols utilizing the included stem-loop primers. Custom ordered FAM-NFQ primer/probe mixes were used for control *snoRNA-202* (Context sequence: 5'-GCT GTA CTG ACT TGA TGA AAG TAC TTT TGA ACC CTT TTC CAT CTG ATG-3'), *Gm26109* (Assay ID: CS5IOYS, context sequence: 5'-GCA TTT TAT TCA ACA CAT CAT TCT GAA AAT AGA TGT GTA GAG AAA TGA TAA CTG AGC ACA-3') and *Gm22200* (Assay ID: CS6RM40, context sequence: 5'-GAT GTA TTT GTC ACA TCA TTC TGA AGG AAA GTT TGT GGT GAC TTG TTA TTA CTG AGC ACA-3') for RT-PCR TaqMan Small RNA Assay (Applied Biosystems, 4427975). The RT-PCR was performed with Taqman Universal PCR master Mix No AmpErase UNG (AB#4324018, Applied Biosystems). The cycling conditions consist of incubation for 2 min at 50°C, followed by 95°C for 10 min, for denaturation followed by 40 cycles at 95°C for 15 sec and combined annealing and extension at 60°C for 1 min.

All RT-PCR reactions were performed in duplicate with no-RT control on a StepOne Plus Real time PCR System (Applied Biosystems). Individual cDNA samples were normalized

according to their levels of *snoRNA-202*. The comparative Ct method was used for analysis.

3.8. Cell counts

Complete blood counts were performed by a Hemavet 950 hematology system (Drew Scientific). Enumeration of cell numbers for both primary cells and cell lines was performed by trypan blue exclusion with a hemocytometer by standard protocols or acridine orange/propidium iodide staining with a Cellometer Auto 2000 (Nexcelom) per manufacturer's instructions. Red blood cell lysis was performed prior to enumeration of nucleated cells by incubation with 3% glacial acetic acid.

3.9. Flow cytometry

3.9.1. Cell preparation

Bone marrow, spleen or peripheral blood cells were isolated by standard methods and red cells were lysed with ACK (Ammonium chloride potassium) lysis buffer (0.15M ammonium chloride, 10mM potassium bicarbonate, 0.1M EDTA).

3.9.2. Antibodies

See **TABLE 2.2**.

3.10. Colony forming assays

Bone marrow cells or splenocytes were harvested, red cell lysed with ACK buffer prior to being counted and plated in methylcellulose media per standard protocols. All methylcellulose media was purchased from Stem Cell Technologies (MethoCult Media). Bone marrow cells were plated as follows: 10,000 cells/plate for CFU-C/CFU-E/BFU-E formation (M3434), 100,000 cells/plate for mature BFU-E formation (M3234 supplemented with 3 or 6U/mL hEPO), 100,000 cells/plate for CFU-PreB (M3630). Splenocytes were plated in the same media as follows: 100,000 cells/plate for CFU-C/CFU-E/BFU-E formation, 300,000 cells/plate for mature BFU-E formation. CFU-C and CFU-PreB colonies were scored on Day 7-10. BFU-E/mature BFU-E colonies were scored on Day 10-11. CFU-E

colonies were scored on Day 3. Benzidine staining of erythroid colonies was performed as follows: benzidine working solution was freshly prepared by mixing benzidine stock solution (30mg/mL benzidine in 90% glacial acetic acid) 1:1 with 21% H₂O₂, 400uL of working solution was added dropwise to methylcellulose plates, incubated 1-2 minutes and dark blue colonies were scored.

3.11. Hematopoietic stress experiments

3.11.1. 5-Fluorouracil

A working stock of 10mg/mL 5-fluorouracil (5-FU, Sigma F6627) was prepared in sterile PBS and placed on a room temperature rocker overnight to fully dissolve in solution. The working stock of 5-FU was filtered through a 0.22µm filter prior to injection. Mice were weighed and injected with 150mg/kg 5-FU intraperitoneally weekly.

3.11.2. Phenylhydrazine

A working stock of 12mg/mL phenylhydrazine hydrochloride (PHZ, Sigma P6926) was prepared in sterile PBS and the pH of the solution was brought to an appropriate physiologic range (pH=7.4). The working stock of PHZ was protected from light prior to injection to prevent degradation. Mice were weighed and injected with 30mg/kg PHZ subcutaneously on Day 0 and Day 1. Mice were bled prior to first injection and every 2-3 days during recovery.

3.11.3. Sublethal irradiation

Mice were bled prior to radiation for baseline measurements. On Day 0, mice were irradiated with 500 Rads and serial bleeds were performed weekly for 7 weeks to follow peripheral blood cell count recovery.

3.12. HSPA9 overexpression

3.12.1. Cloning

HSPA9 cDNA was cloned from the previously described FLAG-Mortalin-WT vector into MSCV-IRES-GFP vector³⁴. Briefly, primers (Forward: 5'-GTC ATG TAG GCT CGA GAT

CGA TTA CAA GGA TGA CGA TGA C-3' and Reverse: 5'-GTC ATG TAG GCT CGA GTC TTC ACT CCT AAG CTT CAT ATG TTG TC-3'; synthesized by Sigma) were used to add XhoI restriction digest sites to the end of PCR fragments amplified from the FLAG-Mortalin-WT vector using iProof DNA polymerase kit (BioRad: 172-5301). PCR fragments were purified using the Wizard SV PCR Clean-up system (Promega: A9282). PCR fragments and MSCV-IRES-GFP were digested with XhoI at 37°C for two hours. Digested fragments were purified by Wizard SV PCR Clean-up system and gel quantified prior to ligation. Ligation of the PCR fragment and MSCV backbone was performed using the Takara DNA Ligation Kit V2.1 (Takara: Cat No 6022), transformed into DH5 α cells using standard protocols and cultured overnight on Luria agar plates in the presence of 100 μ g/mL ampicillin. Individual colonies were picked and cultured in Luria broth for 8 hours before plasmid DNA was prepared using a QIAprep Spin Miniprep Kit (Qiagen: 27106). Plasmids were screened for the presence of *HSPA9* cDNA by XhoI restriction digest and orientation of the insert by EcoRI. Clones containing the *HSPA9* cDNA insert in the correct orientation were sequence verified using standard Sanger sequencing.

3.12.2. Viral preparation

MSCV-IRES-GFP, MSCV-HSPA9-IRES-GFP and packaging plasmids were prepared by EndoFree Plasmid Maxi Kit (Qiagen: 12362). 60% confluent 150mm dishes of HEK293T cells were transfected with MSCV and EcoPack packaging plasmids by calcium phosphate transfection using CalPhos Mammalian Transfection Kit (Clontech: 631312) and viral supernatant was collected. Viral titer was evaluated by flow cytometry analysis of GFP expression in NIH3T3 cells 2 days after being spininfected with serial dilutions of each virus.

3.12.3. Bone marrow transduction/transplantation

Bone marrow pools from either 3 *Hspa9*^{-/-} or 3 *Hspa9*^{+/+} mice were transduced with either MSCV-IRES-GFP control or MSCV-HSPA9-IRES-GFP at an MOI of 1 in RPMI media containing 20% FBS, 50ng/mL mFlt3L, 100ng/mL mSCF, 60ng/mL mIL-3 and 10ng/mL mTPO. Media was replaced following transduction and cells were cultured overnight. Cells were transduced again the following morning as described above, collected, and transplanted by injection of 100µL of cells in HBSS into the retro-orbital sinus of lethally irradiated recipients (1100Rads, 1 million cells/mouse). Remaining cells were cultured an additional day before transduction efficiency was evaluated by flow cytometry for GFP expression.

3.13. Bone marrow transplantation

Bone marrow was harvested from donor mice (Ly5.2), enumerated and pooled as necessary. Congenic recipients (Ly5.1) were lethally irradiated (1100Rads) 16-24 hours prior to transplant. 2 million non-RBC lysed cells were transplanted in 100uL DMEM with 20% FBS or HBSS into the retro-orbital sinus. Transplanted mice were given 5mL antibiotics (200mg Sulfamethoxazole/40mg Trimethoprim) in a 400mL water supply for 2 weeks following transplant to prevent bacterial infection. For competitive repopulation studies, equal numbers of non-RBC lysed test (Ly5.2) and competitor (Ly5.1/5.2) marrow were mixed and 2 million cells per mouse were transplanted into lethally irradiated recipients (Ly5.1).

3.14. GCSF treatment

Anesthetized mice were subcutaneously injected with twice daily 125µg/kg doses of GCSF (Amgen) for 5 days. Mice were weighed immediately prior to first treatment. Mice were euthanized immediately following the last injection (Day 5) or at 2-day intervals thereafter. Competitive transplant mice were treated after establishment of long-term engraftment (>6 months).

3.15. MOL4070LTR

3.15.1. Virus production and titering

MOL4070LTR infected NIH 3T3 cells (provided by Linda Wolff, NCI) were mixed at a 1:1 ratio with uninfected NIH 3T3 cells, seeded on 100mm plates and allowed to grow to confluence in D10 media (DMEM containing 10% FBS, 2mM L-Glutamine, 100U/mL penicillin and 100ug/mL streptomycin). Media containing virus was collected the following day, filtered, and stored at -80°C until use. Viral titer was established using the XC cell assay, as previously described³⁵.

3.15.2. Viral injection and leukemic evaluation

Hspa9^{+/-} and wild-type littermate B6129F1 neonate pups (1-2 days old) were injected with 4×10^4 infectious particles in 0.1mL of D10 medium intraperitoneally. Mice were routinely observed for evidence of disease and sacrificed when moribund. CBCs were performed on peripheral blood using a Hemavet. Spleen and bone marrow cells were cryopreserved in 10% DMSO (20×10^6 cells/vial). Leukemias were classified according to Bethesda proposal methods^{36,37}. Bone marrow or spleen cells were analyzed by flow cytometry for leukemic populations. For myeloid leukemias, cells were analyzed for the co-expression of immature (CD34, Sca, or c-kit) and mature (Gr-1 or CD11b) myeloid markers. For lymphoid leukemias, cells were analyzed for abnormal expression of B or T cell markers (B220, CD3, CD4 or CD8). Sections of spleen and liver, as well as thymus and lymph nodes when available, were fixed in 10% buffered formalin and sent for pathologic review by the Washington University Division of Comparative Medicine Research Animal Diagnostic Lab. Peripheral blood smears and cytopspins of bone marrow and spleen cells were stained with Wright-Giemsa for morphologic analysis.

4. Results

4.1. Generation of *Hspa9*^{+/-} mice

In order to evaluate *Hspa9* haploinsufficiency *in vivo*, we created a mouse model with a heterozygous inactivation of *Hspa9* (*Hspa9*^{+/-}) using ES cells containing a gene trap inserted in intron 3 of *Hspa9*. Gene trap insertion was confirmed by Southern blot (**FIGURE 2.2**).

Hspa9 protein levels were confirmed to be ~50% reduced in bone marrow and spleen cells by Western blot using both C-terminal and N-terminal antibodies (**FIGURE 2.3**). RT-PCR showed ~50% reduction in the mRNA level of *Hspa9*^{+/-} compared to *Hspa9*^{+/+} littermates (**FIGURE 2.3**).

Hspa9^{+/-} mice are born at normal Mendelian ratios from *Hspa9*^{+/-} x *Hspa9*^{+/+} matings (N>100) (**TABLE 2.3**). Intercrossing of *Hspa9*^{+/-} mice did not result in the generation of homozygous mice (*Hspa9*^{-/-}), suggesting that homozygous inactivation of *Hspa9* is embryonic lethal (N=73) (**TABLE 2.3**). Background genetic differences due to mouse strain have previously been described to alter penetrance of embryonic lethality in some knockout mice³⁸. In order to test whether the C57Bl/6 background of *Hspa9*^{+/-} mice influenced lethality in *Hspa9*^{-/-}, we crossed our C57Bl/6N *Hspa9*^{+/-} mice with wild-type 129X1/SvJ mice (Jax: 000691) to generate *Hspa9*^{+/-} B6129F1 mice. These heterozygous F₁ mice were intercrossed and pups were genotyped (N=139) (**TABLE 2.3**). No *Hspa9*^{-/-} pups were observed. Timed matings from *Hspa9*^{+/-} x *Hspa9*^{+/-} crosses failed to identify *Hspa9*^{-/-} pups after 9.5dpc, preventing analysis of *Hspa9*^{-/-} fetal livers (**TABLE 2.4**).

4.2. Basal hematopoiesis is largely normal in *Hspa9*^{+/-} mice up to 18 months of age

Hspa9^{+/-} mice and *Hspa9*^{+/+} littermates were evaluated at 2, 6, 9, 12 and 18 months of age. *Hspa9*^{+/-} mice have normal complete blood counts, bone marrow and spleen cellularity, body weight and spleen size at all time points evaluated (**FIGURE 2.4**). Wright-Giemsa stained

peripheral blood smears as well as bone marrow and spleen cytopspins evaluated for morphology appeared normal in *Hspa9*^{+/-} mice (data not shown). Immunophenotyping of mature myeloid (neutrophils and monocytes), precursor and mature B-cells, mature T-cells, and mature and precursor erythroid cells (proerythroblasts, polychromatic erythroblasts, basophilic erythroblasts, reticulocytes) in the blood, bone marrow and spleen were normal (See **TABLE 2.5** for immunophenotypic markers used) (**FIGURE 2.5**). The frequency of bone marrow hematopoietic progenitor (CMP, MEP, GMP) and stem-cell enriched (KLS, SLAM) populations were not significantly different up to 12 months of age (**FIGURE 2.6**). Consistent with our immunophenotypic analysis, bone marrow and spleen myeloid (CFU-C) and erythroid progenitors (mature BFU-E/BFU-E/CFU-E) evaluated by methylcellulose colony-forming assays were normal up to 18 months of age (**FIGURE 2.7**).

4.3. *Hspa9*^{+/-} mice did not exhibit altered recovery from hematopoietic stress

Hspa9 has previously been shown to be up-regulated in response to a number of cellular stresses and provide a cytoprotective effect^{17,39-41}. Although no overt phenotype was observed in hematopoietic stem and progenitor cells to affect myeloid and erythroid development in *Hspa9*^{+/-} mice, these mice may be more sensitive to hematopoietic stress. To test this possibility, we induced hematopoietic stress in *Hspa9*^{+/-} mice and their wild-type littermates with three methods: 5-fluorouracil, phenylhydrazine and sublethal irradiation. We utilized older mice (>5 months old) for these tests because they may be more susceptible to hematopoietic stress as evidenced by the late onset of MDS-like phenotypes in a variety of other mouse models⁴²⁻⁴⁴.

4.3.1. 5-Fluorouracil

5-fluorouracil (5-FU) is toxic to dividing cells and significantly reduces progenitor cell numbers in mice⁴⁵. To evaluate survival following 5-FU treatment, we treated mice with

150mg/kg 5-FU weekly and sacrificed them when they become moribund. Mean survival was not significantly different between cohorts (15 days for *Hspa9*^{+/-} and 17 days for *Hspa9*^{+/+}, N=6/genotype, 6-8 months old) (**FIGURE 2.8**).

4.3.2. Phenylhydrazine

Phenylhydrazine induces hemolytic anemia in mice. In order to evaluate recovery of erythroid progenitors and precursors in mice >11 months of age, 30mg/kg phenylhydrazine was administered to *Hspa9*^{+/-} and *Hspa9*^{+/+} littermate control mice. No difference in erythroid recovery was observed (**FIGURE 2.8**).

4.3.3. Sublethal irradiation

Finally, HSPA9 protein is highly up-regulated in several cellular stress inducing conditions, including following treatment with radiation⁴⁶. To evaluate whether Hspa9 was involved in recovery of hematopoietic cells following radiation, we irradiated 5-6 month old mice with 500 Rads and monitored recovery of peripheral blood cell counts. There was no significant difference in standard complete blood count parameters following a single dose of sublethal radiation (N=5/genotype) (**FIGURE 2.8**).

In summary, hematopoietic stress responses in *Hspa9*^{+/-} and *Hspa9*^{+/+} littermates are not significantly different in response to 5-fluorouracil, phenylhydrazine and sublethal irradiation.

4.4. CFU-PreB colonies are significantly reduced in *Hspa9*^{+/-} mice

As early as 2 months of age, the number of bone marrow CFU-preB methylcellulose colonies are significantly reduced in *Hspa9*^{+/-} mice compared to *Hspa9*^{+/+} littermates (14 vs 48 colonies/100,000 bone marrow cells plated, respectively, N=10 mice/genotype,

p<0.0001) (**FIGURE 2.9**). Splenic CFU-PreB colonies could not be evaluated due to the low frequency of B-cell progenitors in the spleen.

To determine whether the CFU-PreB colony reduction was due to fewer progenitors added to the media, we used flow cytometry to evaluate the frequency of B-cell progenitors and precursors. There was no significant difference in number or frequency of common lymphoid progenitors (lin-/CD27+/flk2+/IL7R α +/Ly6D-) or Hardy fractions A, B/C, D, E, or F in *Hspa9*^{+/-} mice (N=5-10/genotype) (**FIGURE 2.9**). Ig light chain rearrangement is an essential process of normal B-cell differentiation. However, if normal B-cell differentiation is perturbed, the ratio of Igk to Ig λ chain usage could be altered⁴⁷⁻⁴⁹. No significant difference in Igk or Ig λ expression in 9-month old mice was detected (N=5/genotype) (**FIGURE 2.9**).

4.5. The reduction in CFU-PreB colonies is partially rescued by HSPA9

Two putative snoRNAs exist within introns 10 and 11 of *Hspa9* that may contribute to the reduction in CFU-PreB colonies (**FIGURE 2.1**). Here we show that the gene trap insertion disrupts expression of the putative snoRNA, *Gm26109*, contained in intron 10 (**FIGURE 2.10**). This snoRNA shares 83% identity with human *SNORD63* located in intron 10 of *HSPA9*. The putative snoRNA *Gm22200* contained within intron 11 could not be detected in whole bone marrow or B-cell progenitor subsets (CLP, Hardy fractions A-E) isolated from wild-type mice (data not shown).

In order to show that loss of *Hspa9* is responsible for the CFU-PreB colony reduction observed in these mice, we attempted to rescue this phenotype using an MSCV vector to overexpress *HSPA9* in *Hspa9*^{+/-} mouse bone marrow. Human *HSPA9* cDNA was cloned into the MSCV-IRES-GFP expression vector (MSCV-IRES-HSPA9-GFP) and we achieved ~1.5 fold *HSPA9* protein overexpression in GFP+ NIH3T3 cells measured by densitometry

relative to MSCV-IRES-GFP vector (**FIGURE 2.11**). Bone marrow was harvested from *Hspa9^{+/+}* or *Hspa9^{+/-}* mice and transduced with MSCV-IRES-GFP or MSCV-HSPA9-IRES-GFP and transplanted into lethally irradiated recipients. GFP⁺ and GFP⁻ cells were sorted from 8-10 week old mice and cultured separately in CFU-PreB methylcellulose medium (N=7-8mice/genotype, representative of 2 independent experiments). Colonies were scored 7-days after plating. Untransduced (GFP⁻) cells from recipient mice yielded significantly fewer CFU-PreB colonies in recipients that received *Hspa9^{+/-}* marrow than those that received *Hspa9^{+/+}* marrow, as expected. Transduction of *Hspa9^{+/+}* marrow with either the *HSPA9* overexpression or control vector (GFP⁺ cells) did not significantly change the number of CFU-PreB colonies. However, *Hspa9^{+/-}* bone marrow transduced with the *HSPA9* overexpression vector (GFP⁺ cells) significantly increased the number of CFU-PreB colonies produced by *Hspa9^{+/-}* cells, while transduction of the control vector did not alter the number of colonies ($p=0.015$, *Students t-test*, N=7-8 mice/group) (**FIGURE 2.11**).

Collectively, the data suggest that loss of Hspa9 expression contributes to the reduction in CFU-PreB colonies.

4.6. The reduction of CFU-PreB colonies is hematopoietic-cell intrinsic

In *Hspa9^{+/-}* mice, one allele of *Hspa9* is disrupted in all cells of the body, which could result in the contribution of non-hematopoietic cells to hematopoietic phenotypes. Stromal cells not derived from hematopoietic stem cells (HSCs) provide support to HSCs and hematopoietic progenitors and can specifically alter hematopoiesis when disrupted⁵⁰⁻⁵². We tested whether the reduction in CFU-PreB colonies was a hematopoietic cell-intrinsic phenotype or due to a defect in non-hematopoietic stromal cells. We performed non-competitive bone marrow transplants of *Hspa9^{+/-}* and *Hspa9^{+/+}* cells into wild-type or *Hspa9^{+/-}* recipients. After long-term engraftment was established (>6 months), we harvested bone marrow from recipient mice and performed the CFU-PreB assay. Results show that the reduction in B-cell

progenitors in $Hspa9^{+/-}$ mice is a transplantable, hematopoietic cell-intrinsic effect. The number of CFU-PreB colonies from mice that received $Hspa9^{+/-}$ bone marrow is significantly reduced compared to mice that received $Hspa9^{+/+}$ bone marrow (N=7-9 mice/genotype, $p=0.002$). As expected, there was no reduction in CFU-PreB colonies following transplantation of wild-type donor bone marrow cells into $Hspa9^{+/-}$ recipients (N=5) (**FIGURE 2.12**). Consistent with results from untransplanted mice, CLP frequencies were not significantly different between mice that received $Hspa9^{+/-}$ or $Hspa9^{+/+}$ bone marrow following a non-competitive transplant (data not shown).

4.7. $Hspa9^{+/-}$ B-cells do not have a competitive disadvantage at baseline or following stress

Next, we tested whether $Hspa9^{+/-}$ lymphoid progenitors are at a functional disadvantage compared to progenitors from control mice *in vivo* by performing competitive repopulation studies. Pools of donor bone marrow from C57Bl/6 (Ly5.2) $Hspa9^{+/-}$ or $Hspa9^{+/+}$ mice were mixed at a 1:1 ratio with a competitor bone marrow pool from age- and sex-matched wild-type C57Bl/6 (Ly5.1) mice. There was no competitive advantage/disadvantage of $Hspa9^{+/-}$ cells compared to $Hspa9^{+/+}$ cells in recipient mice at >6 months of age in 2 independent cohorts (N=3-8 mice) following primary or secondary transplants (**FIGURE 2.13**). Analysis of donor-derived B-cell precursors and progenitors following competitive transplant revealed no significant difference in the number or frequency of mature B-cells, CLPs, or Hardy fractions (**FIGURE 2.14**).

We extended these studies to test whether $Hspa9^{+/-}$ B-cell progenitor recovery is abnormal following an acute, transient, decrease in bone marrow B-cells induced by granulocyte colony stimulating factor (GCSF). There was no detectable difference in recovery of B-cells progenitors or precursors following GCSF treatment in $Hspa9^{+/-}$ (N=2-5 mice/genotype) or

competitively transplanted mice (N=4-7/genotype) compared to wild-type controls (**FIGURE 2.14**).

4.8. *Hspa9* haploinsufficiency alone does not induce MDS or leukemia in mice

To determine whether heterozygous knockout of *Hspa9* alone promotes AML, we monitored 35 *Hspa9*^{+/-} and 35 wild-type littermate mice for development of AML for 18 months. *Hspa9*^{+/-} and control mice did not differ in overall or leukemia-free survival (**FIGURE 2.15**).

4.9. *Hspa9*^{+/-} mice are not more susceptible to leukemia induced by retroviral insertional mutagenesis

In order to determine whether *Hspa9* haploinsufficiency cooperates with additional mutations to cause leukemia, we used a well-established insertional mutagenesis model to induce leukemias³⁵. Pure C57Bl/6 mice are less susceptible to virus-induced leukemias than B6129F1 hybrid mice. Therefore, *Hspa9*^{+/-} mice were intercrossed with 129SvJ mice to create a cohort of B6129F1 mice, as previously described^{53,54}. By injecting 45 mice/genotype, we had 80% power to detect an increase in AML prevalence at one year from 20% in control to 50% in *Hspa9*^{+/-} mice with a significance level (alpha) of 0.05 (two-tailed) (GraphPad StatMate2). We injected 103 newborn mice (59 *Hspa9*^{+/-}, 44 *Hspa9*^{+/+}) with a Moloney murine leukemia-based virus (MOL4070LTR) and monitored mice for development of leukemia. MOL4070LTR induces both myeloid and T-cell leukemias that we characterized as described in the Methods (**Section 3.15**). We observed no difference in leukemia-free survival (all leukemias) (396 vs. 416 days, respectively, p=0.98) or AML-specific leukemia-free survival (p=0.82). (**FIGURE 2.16**)

5. Discussion

To evaluate the effects of *Hspa9* haploinsufficiency on murine hematopoiesis, we generated a heterozygous knockout mouse from ES cells produced by Texas A&M with a gene trap insertion. Heterozygous mice have 50% less Hspa9 protein and mRNA than their wild-type counterparts and are born at normal Mendelian ratios. Consistent with other genetic models with homozygous knockout of *Hspa9*, *Hspa9*^{-/-} mice are embryonic lethal. Lethality was prior to establishment of hematopoiesis in the fetal liver, preventing the use of *Hspa9*^{-/-} fetal livers to study hematopoiesis in transplantation studies. Since genetic background has been shown to influence knockout phenotypes, including embryonic lethality as in the case of *TGF-β1* mice⁵⁵, we attempted to rescue this lethality by creating a mixed strain background of C57Bl/6N and 129X1/SvJ. No *Hspa9*^{-/-} mice were born as a result of this cross, indicating the C57Bl/6N genetic background is not required for embryonic lethality of *Hspa9* homozygous knockout mice.

We evaluated hematopoiesis in *Hspa9*^{+/-} mice up to 18 months of age and identified a significant reduction in CFU-PreB colony formation as early as 2 months of age. We show this reduction is transplantable and a hematopoietic cell-intrinsic defect. This B-cell specific effect is consistent with our previous findings that lentiviral-mediated knockdown of *Hspa9* resulted in a significant reduction in B220+ B-cells in bone marrow, peripheral blood and spleen of recipient mice.

Unlike this model, however, we did not observe a reduction in the frequency of B220+ cells in *Hspa9*^{+/-} mice compared to *Hspa9*^{+/+} mice. Further analysis of B-cell progenitor and precursor populations revealed no differences in frequencies between *Hspa9*^{+/-} and *Hspa9*^{+/+} littermates. This indicates the reduction in CFU-PreB colonies is a functional defect and not a difference in the number of B-cell progenitors plated at the start of the assay. We also did not observe a reduction in B-cells derived from *Hspa9*^{+/-} mice following competitive transplants, indicating that there is *in vivo* compensation for the cell-intrinsic defect in B-cell progenitors, which is further addressed in **Chapter 3**. Although not well studied, defects in B-cell progenitors have been

described in association with MDS. Reduced frequency and increased apoptosis of B-cell progenitors have been described and will be discussed in more detail in **Chapter 3**^{56,57}. Of note, the del(5q) abnormality has been described in CD19+ cells from patients with MDS, indicating haploinsufficiency of *HSPA9* and other del(5q) genes could contribute to B-cell alterations.

In addition to reducing *Hspa9* expression levels, we have confirmed that the gene trap insertion disrupts expression of the snoRNA *Gm26109*, resulting in an ~30% reduction in expression (70% residual expression level). To our knowledge, this is the first time expression of this snoRNA has been measured in mice. However, we were unable to measure the expression of another putative snoRNA, *Gm22200*, located in intron 11 of *Hspa9*. The 70bp *Gm26109* shares 83% identity with the 68bp human C/D box small nucleolar RNA, *SNORD63*. The function of *SNORD63* has not been experimentally demonstrated; however, one study predicted that *SNORD63* was involved in the 2'-O-methylation of A4531 in 28S rRNA because of a 12-nt complementarity between these RNAs⁵⁸. It is unclear what effect the reduced expression of this snoRNA has or whether it contributes to the reduction in CFU-PreB colonies. We were able to partially rescue the CFU-PreB phenotype by mild overexpression of human *HSPA9* cDNA in mouse bone marrow by retroviral transduction; however, complete rescue was not observed. We chose mild overexpression (~2 fold in wild-type cells) in order to recapitulate wild-type levels to minimize bone marrow alterations, because overexpression of *HSPA9* has been shown to provide a proliferative advantage in multiple cell types, including murine HSCs^{18,39,59}. This incomplete rescue may be because *HSPA9* expression was not high enough. However, additional lines of evidence indicate *Gm26109* does not contribute to the CFU-PreB phenotype. In **Chapter 3**, shRNA-mediated knockdown of *Hspa9* in mouse bone marrow results in significant reduction in B-cell progenitors without perturbation of *Gm26109* expression. It is also very unlikely that the loss of *SNORD63* is involved in hematopoietic defects described in zebrafish harboring mutations in *hspa9b*, the zebrafish homolog of *HSPA9*, because the only

predicted zebrafish homolog of *SNORD63* (gene ID ENSDARG00000084148) is 56bp and only shares 54% identity with the human snoRNA. Additionally, this homolog is not located within *hspa9b* and is a predicted and not yet confirmed snoRNA. Therefore, it is unlikely to be effected in zebrafish knockout models of *HSPA9*.

Heterozygous *Hspa9* loss in zebrafish, and murine transduction/transplantation models evaluated by us and others, support a role for *Hspa9* in erythroid development as well as stem and progenitor cell function^{16,18,30}. Unexpectedly, we did not observe alterations in erythropoiesis or HSCs in *Hspa9*^{+/-} mice. We propose three possible explanations. First, genetic loss of *Hspa9* throughout the entire lifespan of the animal may cause compensation in these mice, allowing for normal development. It remains to be seen whether acute heterozygous loss of *Hspa9* in adult mice, as is seen in the context of human MDS, would results in additional hematopoietic defects. Second, heterozygous loss of *Hspa9* may not be enough of a reduction to cause defects in mice. The alterations in HSCs, including increased cycling, increased reactive oxygen species and reduced number described by *Tai-Nagara et. al.*, utilized 2 shRNA constructs that reduced *Hspa9* expression to ~20% and ~35% of control constructs¹⁸. *Chen et. al.* utilized different shRNA constructs that reduced *Hspa9* expression at the protein level to ~50% and ~30% of controls³⁰. We present data in **Chapter 3** that indicates the previously described 50% reduction was likely closer to 40% the expression of controls. However, in both studies, these knockdown levels are the average of the entire cell population and the actual knockdown per cell is highly variable. A third explanation is that *Hspa9* is not involved in murine erythropoiesis or HSC development, which is unlikely given the knockdown models utilizing 4 different shRNA constructs in assays performed by 2 independent groups.

Patients with a deletion of the proximal 5q31.2 CDR are at a high risk of transformation to AML, indicating that del(5q) may be an initiating step in this process. Murine retroviral insertional

mutagenesis screens have identified *Hspa9* as a common insertion site (CIS) in mice that develop AML and as a cooperating mutation in tumor suppressor-deficient mice that develop lymphomas²⁷⁻²⁹. Murine MDS and AML models often present hematopoietic alterations at 6-12 months of age. Therefore, we evaluated murine hematopoiesis up to 18 months of age. However, no MDS or AML-like phenotypes were observed^{42-44,60}. Leukemic development requires an accumulation of genetic and epigenetic alterations that provide a survival advantage for a cell. Del(5q) is thought to be an early event in MDS development and 5q31.2 is associated with increased transformation to AML^{61,62}. In order to identify if loss of *Hspa9* is an initiating step in this process, we induced additional mutations using retroviral insertional mutagenesis. The type and latency of leukemic development was not different in *Hspa9*^{+/-} mice compared to *Hspa9*^{+/+} littermates, indicating *Hspa9* may not be a gene on this interval associated with transformation. Conversely, a stronger cooperating gene, like *TP53* mutations that are associated with del(5q)(Chapter 1, **Section 1.2.2.1**), may need to be used to sensitize this model. It is also likely that multiple genes on this interval cooperate to cause MDS as well as sensitize cells to leukemic transformation. Loss of *Hspa9* may work in concert with loss of *Egr1* for this process. Mutagenesis induced by N-ethyl-N-nitrosourea showed heterozygous loss of *Egr1* sensitized mice to T-cell lymphomas and myeloproliferative disorders. Therefore, future experiments designed to address the role of *Hspa9* loss in the development of leukemia should focus on combinatorial approaches.

In conclusion, we have generated a novel murine model with haploinsufficiency of the 5q31.2 gene, *Hspa9*. These mice have a functional defect in B-cell progenitors but no other overt hematopoietic defects. Additional studies are needed to better understand how loss of *Hspa9* affects B-cells and whether this functional defect contributes to phenotypes observed in human MDS.

Figure 2.1: Southern blot confirmation and PCR genotyping of *Hspa9*^{+Gt(IST14901H6)TIGM}

(*Hspa9*^{+/-}) mice

A) Southern blot of tail DNA digested with XbaI from 2 *Hspa9*^{+/+} and 2 *Hspa9*^{+/-} mice showing a DNA fragment from a wild-type allele (*white arrow*, 4817 bp) and gene trap-disrupted allele (*black arrow*, 3303 bp). A Southern blot probe recognizing intron 1-exon 3, as depicted in **Figure 2.2**, was used. **B)** Results of 3 primer PCR amplification of tail DNA from 4 *Hspa9*^{+/+} and 4 *Hspa9*^{+/-} mice showing a band from the wild-type allele (*white arrow*, 453bp) and gene trap-disrupted allele (*black arrow*, 307bp).

Figure 2.2: Mouse *Hspa9* locus with gene trap insertion

A) 17 exons of the *Hspa9* mouse locus on chromosome 18 with the location of the gene trap insertion depicted. Location of two putative snoRNAs, *Gm26109* and *Gm22200*, in introns 10 and 11 are indicated. *Inset*: Exons 1-4 of the *Hspa9* locus with gene trap insertion. Locations of PCR genotyping primers (*blue*) and Southern blot probe (*red*) are indicated. **B)** Diagram of *Hspa9* protein with regions targeted by N- and C-terminal Western blot antibodies indicated (*black*), p53 binding domain (*light blue*), known sites of phosphorylation (P), mitochondrial localization sequence (MTS, *red*) and canonical HSP70 domains (nucleotide binding domain, NBD; linker; substrate binding domain, SBD).

Figure 2.3: *Hspa9* expression is 50% reduced at the protein and mRNA level

Western blots were used to evaluate *Hspa9* protein expression in hematopoietic tissues from *Hspa9*^{+/+} and *Hspa9*^{+/-} littermates. **A)** Expression of *Hspa9* in bone marrow and spleen of littermates by C-terminal antibody and β -Actin loading control. **B)** Expression of *Hspa9* in bone marrow of littermates by N-terminal antibody and β -Actin loading control. **C)** RT-PCR expression of *Hspa9* mRNA in bone marrow of littermates (N=3/genotype). Statistical analysis by two tailed Student's t-test. Error bars represent mean \pm SD.

Figure 2.4: Organ cellularity, spleen size and CBCs are normal in *Hspa9*^{+/-} mice

A) No difference in total cellularity of bone marrow (*left panel*; 2 femurs, 2 tibias) and spleens (*right panel*) of *Hspa9*^{+/-} (*open circles*) and *Hspa9*^{+/+} littermates (*filled circles*) at 2, 6, 9 and 12 months of age. **B)** No difference in body weight (*right panel*), spleen weight (*left panel*) were observed. **C)** Peripheral blood complete blood counts were evaluated by Hemavet at 2, 6, 9, 12, and 18 months of age with no difference between genotypes. (PLT, platelets; MCV, mean corpuscular volume; Hb, hemoglobin; WBC, white blood cells)

Figure 2.5: Immunophenotyping of bone marrow, peripheral blood and spleen cells up to 12 months of age

A) No difference was observed in red blood cell lysed bone marrow (*left panel*), peripheral blood (*middle panel*) and spleen (*right panel*) of *Hspa9*^{+/-} and *Hspa9*^{+/+} littermates analyzed by flow cytometry for immunophenotypic markers for neutrophils (Gr1⁺/CD115⁻, *red bars*), monocytes (Gr1^{lo}/CD115⁺, *orange bars*), B-cells (B220⁺, *green bars*) and T-cells (CD3e⁺, *blue bars*)(N=3-6/genotype at each time point). **B)** Red blood cell precursors in bone marrow (*left panel*), peripheral blood (*middle panel*), and spleen (*right panel*) of *Hspa9*^{+/-} (*open circles*) and *Hspa9*^{+/+} littermates (*closed circles*) at 12 months of age showing no difference in precursor frequencies between genotypes. Error bars represent mean ± SD.

Figure 2.6: Progenitor and stem cell enriched populations are not altered in *Hspa9*^{+/-} mice

Bone marrow cells from *Hspa9*^{+/-} (*open circles*) and wild-type littermates (*filled circles*) were collected, red blood cells lysed, and stained with immunophenotypic markers for **A)** KLS (cKit⁺, Lin⁻, Sca⁺), megakaryocyte-erythrocyte progenitors (MEP, Lin⁻Sca⁻cKit⁺FcγR^{lo}CD34⁻), granulocyte-monocyte progenitors (GMP, Lin⁻Sca⁻cKit⁺FcγR^{hi}CD34⁺), common myeloid

progenitors (CMP, Lin⁻Sca⁻cKit⁺FcyR^{lo}CD34⁺) and **B**) SLAM (Lin⁻Sca⁺cKit⁺CD150⁺CD48⁻) cells (N=3-8 mice/genotype). Data from 12 month old mice is shown.

Figure 2.7: Colony forming ability of erythroid and myeloid spleen and bone marrow progenitors from *Hspa9*^{+/-} and *Hspa9*^{+/+} mice are similar

Bone marrow or spleen cells were isolated from *Hspa9*^{+/-} (filled circles) and *Hspa9*^{+/+} (open circles) littermates at 2-18 months of age. **A**) 10,000 bone marrow (left panel) or 100,000 spleen cells (right panel) were plated in CFU-C media and total colonies/plate were counted on day 7. **B**) 100,000 bone marrow (left panel) or 250,000 spleen cells (right panel) were plated in media containing only erythropoietin and mature BFU-E colonies were counted at 10-11 days. **C**) Cells from 18-month old mice were tested with different concentrations of erythropoietin added to the media (3 U/mL or 6 U/mL, as indicated). **D**) Bone marrow (left panel) or spleen cells (right panel) from 12-month old mice were plated in CFU-C media containing erythropoietin. BFU-E colonies were counted on day 10-11 and CFU-E colonies were counted on day 3 by benzidine staining. Statistical analysis by two tailed Student's t-test. Error bars represent mean ± SD. (BM, bone marrow; Spl, spleen)

Figure 2.8: *Hspa9*^{+/-} and *Hspa9*^{+/+} littermate mice respond similarly to hematopoietic stress

A) Kaplan-Meier curve of overall survival for *Hspa9*^{+/-} (solid line) and *Hspa9*^{+/+} (dotted line) mice given weekly doses of 150mg/kg 5-fluorouracil (5-FU) is not different (mice aged 6-8 months, N=6 mice/genotype). **B**) Two doses of 30mg/kg phenylhydrazine (PHZ) was used to induce hemolytic anemia in *Hspa9*^{+/+} (black line) and *Hspa9*^{+/-} (red line) mice. Mice were bled at indicated intervals to monitor for red blood cell recovery (N=5 mice/genotype) (hemoglobin (Hb), left; mean corpuscular volume (MCV), right). **C**) A single, sublethal dose of radiation (500 rads) was given to 5-6 month old *Hspa9*^{+/-} (black line) and *Hspa9*^{+/+} (red line) mice and hematopoietic

recovery was monitored by complete blood counts at indicated time intervals (N=5 mice/genotype) (white blood cell count (WBC), *left*; hemoglobin (Hb), *right*).

Figure 2.9: Colony forming ability of B-cell progenitors is significantly reduced in *Hspa9*^{+/-} compared to *Hspa9*^{+/+} mice

A) CFU-PreB colonies were significantly reduced in *Hspa9*^{+/-} (*open circles*) compared to *Hspa9*^{+/+} (*filled circles*) littermates at all times evaluated. Frequencies of **B)** Hardy fractions and **C)** common lymphoid progenitors (CLP) were not significantly different in *Hspa9*^{+/-} mice at 4-5 months of age. **D)** The distribution of Igk and Igl chain expression in 9-month old *Hspa9*^{+/-} mice is normal.

Figure 2.10: The gene trap insertion in *Hspa9* disrupts expression of both *Hspa9* and the snoRNA *Gm26109* located in intron 10 of *Hspa9*

RNA was harvested from bone marrow of 2-month old *Hspa9*^{+/+} (*filled circles*) and *Hspa9*^{+/-} (*open circles*) littermates. qRT-PCR was performed on *Hspa9* (*left panel*) and the putative snoRNA *Gm26109* located in intron 10 of *Hspa9* (*right*). Expression was calculated relative to *Gapdh* and *sno202*, respectively. Fold change was normalized to *Hspa9*^{+/+} control. Statistical analysis by two tailed Student's t-test. Error bars represent mean ± SD.

Figure 2.11: Overexpression of HSPA9 in *Hspa9*^{+/-} bone marrow partially rescues the reduction in CFU-PreB colonies

A) Western blot showing overexpression of HSPA9 cDNA in GFP+ sorted 293T cells transduced with MSCV-IRES-GFP control or HSPA9 overexpression vector (MSCV-HSPA9-IRES-GFP). **B)** Bone marrow harvested from *Hspa9*^{+/+} or *Hspa9*^{+/-} mice was transduced with MSCV-IRES-GFP control or MSCV-HSPA9-IRES-GFP and transplanted into lethally irradiated recipients. Bone marrow was harvested 8-10 weeks after transplant. GFP- (*white bars*) and

GFP+ (*green bars*) cells from each mouse were sorted and plated in CFU-PreB methylcellulose media. CFU-PreB colonies were counted on day 7. GFP+ and GFP- groups were analyzed by one-way ANOVA and a * indicates significantly different groups by post-hoc Tukey's multiple comparison test, except for *Students' t-test* for GFP+ versus GFP- in MSCV-HSPA9-IRES-GFP transduced *Hspa9*^{+/-} colonies. Data includes two independently transduced and transplanted cohorts (N=7-8 mice/group).

Figure 2.12: The reduction in CFU-PreB colony formation is hematopoietic cell-intrinsic

A) Donor bone marrow from *Hspa9*^{+/-} or wild-type mice was transplanted into lethally irradiated wild-type or *Hspa9*^{+/-} recipients. Bone marrow was harvested 6 months after transplant and plated in CFU-PreB promoting methylcellulose (N=4-9 mice/genotype). **B)** Representative images of CFU-PreB colonies and individual cells following cytopsin and Wright-Giemsa staining. (WT, wild-type, *Hspa9*^{+/+}; HET, heterozygous, *Hspa9*^{+/-})

Figure 2.13: *Hspa9*^{+/-} bone marrow does not have a competitive advantage over control marrow in primary or secondary transplants

A ratio of 1:1 *Hspa9*^{+/+} (*blue lines*) or *Hspa9*^{+/-} (*red lines*) test cells (Ly5.2) and competitor bone marrow (Ly5.1/5.2) were transplanted into lethally irradiated recipients (Ly5.1). Mice were bled at intervals indicated after transplant and relative chimerism of peripheral blood (**Panel A**, *solid lines*) or B220+ cells (**Panel B**, *dashed lines*) were evaluated in primary recipients (*left*).

Following long-term engraftment, bone marrow from recipients were pooled and transplanted into lethally irradiated secondary recipients (*right*). Secondary recipients were bled and evaluated for chimerism and times indicated. Bone marrow from secondary recipients was pooled and transplanted into tertiary recipients but showed no difference in chimerism between *Hspa9*^{+/+} and *Hspa9*^{+/-} test marrow (data not shown). Data represents pooled results from two independently transplanted cohorts (N=10-15 mice/genotype). (Txp, transplant)

Figure 2.14: B-cell recovery is similar from $Hspa9^{+/-}$ and $Hspa9^{+/+}$ bone marrow following GCSF treatment

A) B-cell recovery in mice treated with GCSF twice daily for 5 days. Mice were sacrificed on days indicated and bone marrow B-cells were evaluated. No difference was observed in recovery of Hardy fractions A-F (data not shown). Representative results from B220+ cells are shown. **B)** $Hspa9^{+/-}$ (white bars) or $Hspa9^{+/+}$ (grey bars) bone marrow (Ly5.2) was mixed at a 1:1 ratio with competitor bone marrow (Ly5.1). Following long-term engraftment, frequencies of B-cell progenitors from donor test marrow (Ly5.2) were measured. No differences were observed. **C)** A second cohort of competitively transplanted mice was treated with GCSF twice daily for 5 days. Relative chimerism of B-cell progenitors was evaluated on day 11 and no differences were observed between genotypes.

Figure 2.15: Overall and leukemia-free survival of $Hspa9^{+/+}$ and $Hspa9^{+/-}$ mice are not different

Kaplan-Meier plots showing no difference in **A)** overall and **B)** leukemia-free survival of $Hspa9^{+/+}$ and $Hspa9^{+/-}$ littermates up to 18 months (N=35 mice/genotype). No difference was observed in mice followed up to 750 days (data not shown).

Figure 2.16: $Hspa9^{+/-}$ mice are not more susceptible to leukemia induced by MOL4070LTR virus

A) Overall survival of $Hspa9^{+/+}$ and $Hspa9^{+/-}$ neonates injected with MOL4070LTR. **B)** The distribution of leukemia types evaluated in $Hspa9^{+/+}$ and $Hspa9^{+/-}$ mice (mice sacrificed at 18 months of age were excluded). **C)** AML-free survival of mice following MOL4070LTR injection. **D)** Representative peripheral blood smears showing AML (*top*) and ALL (*bottom*) blasts from $Hspa9^{+/+}$ (*left*) and $Hspa9^{+/-}$ mice (*right*).

Figure 2.1: Southern blot confirmation and PCR genotyping of *Hspa9*^{+Gt(IST14901H6)TIGM} (*Hspa9*^{+/-}) mice

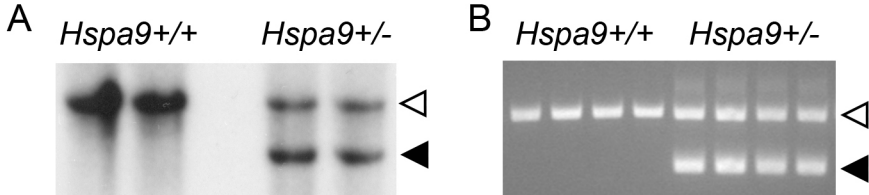


Figure 2.2: Mouse *Hspa9* locus with gene trap insertion

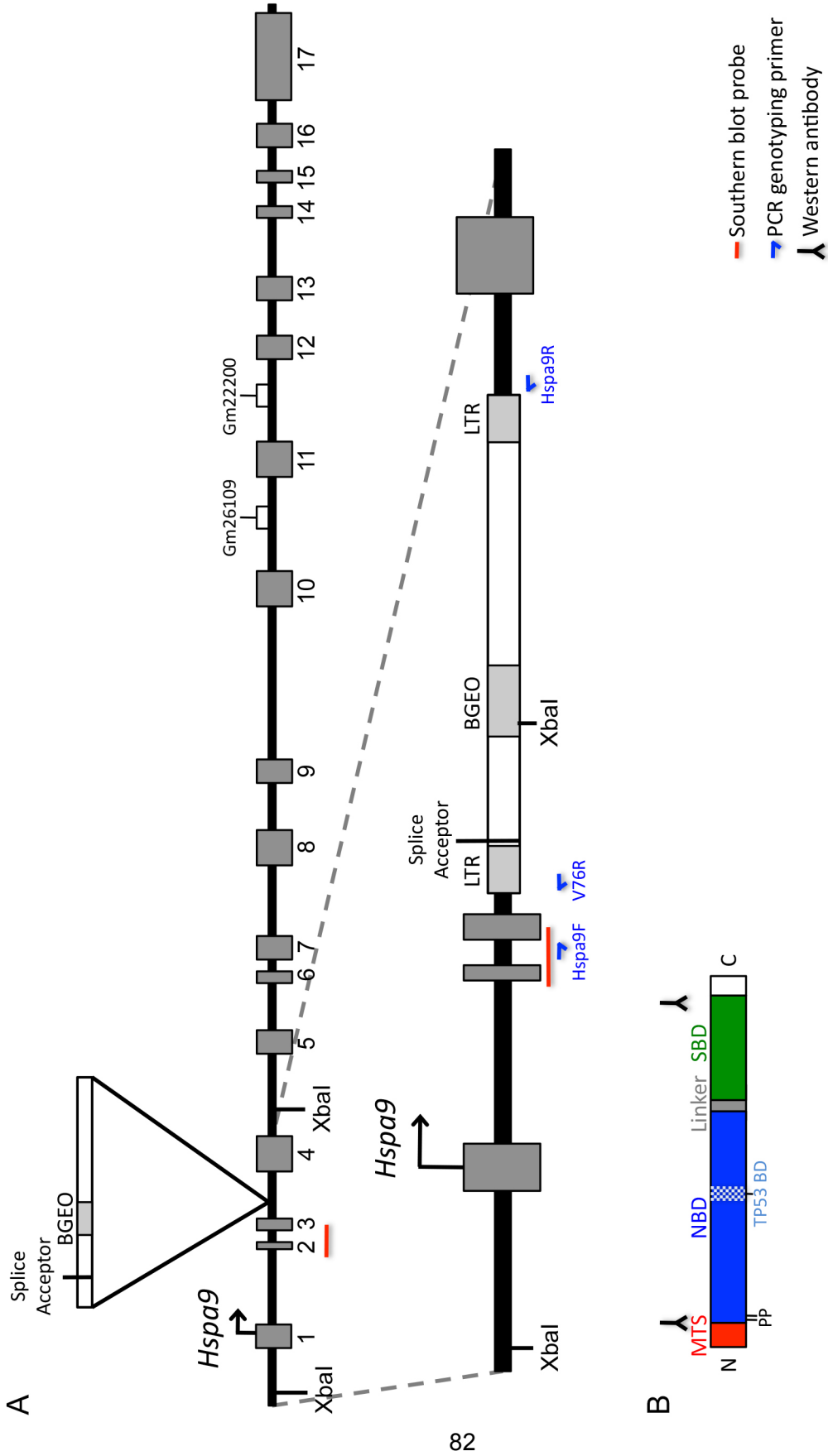


Figure 2.3: Hspa9 expression is 50% reduced at the protein and mRNA level

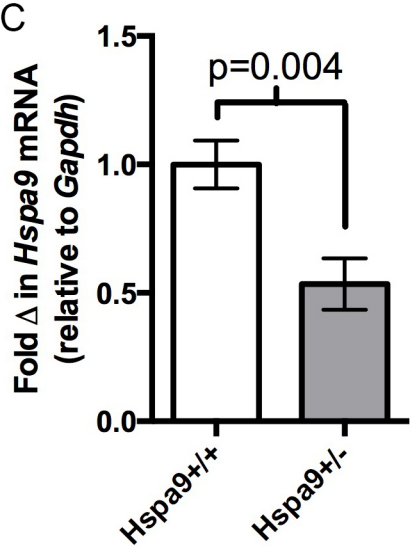
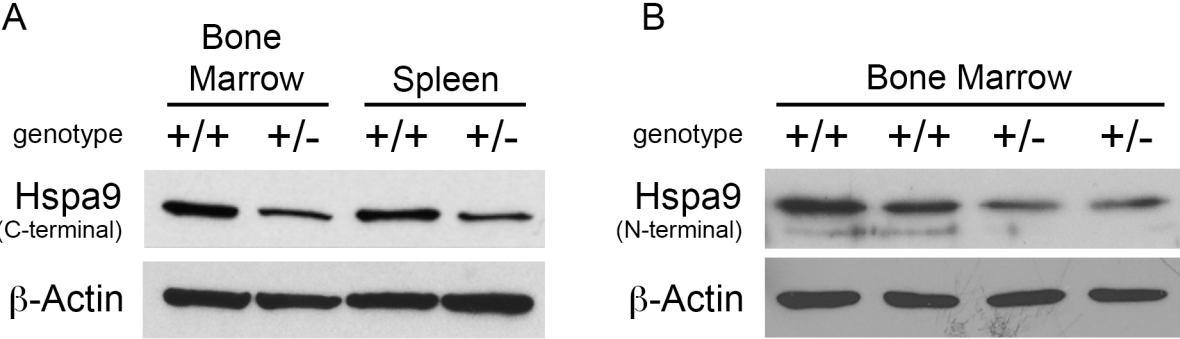


Figure 2.4: Organ cellularity, spleen size and CBCs are normal in *Hspa9*^{+/-} mice

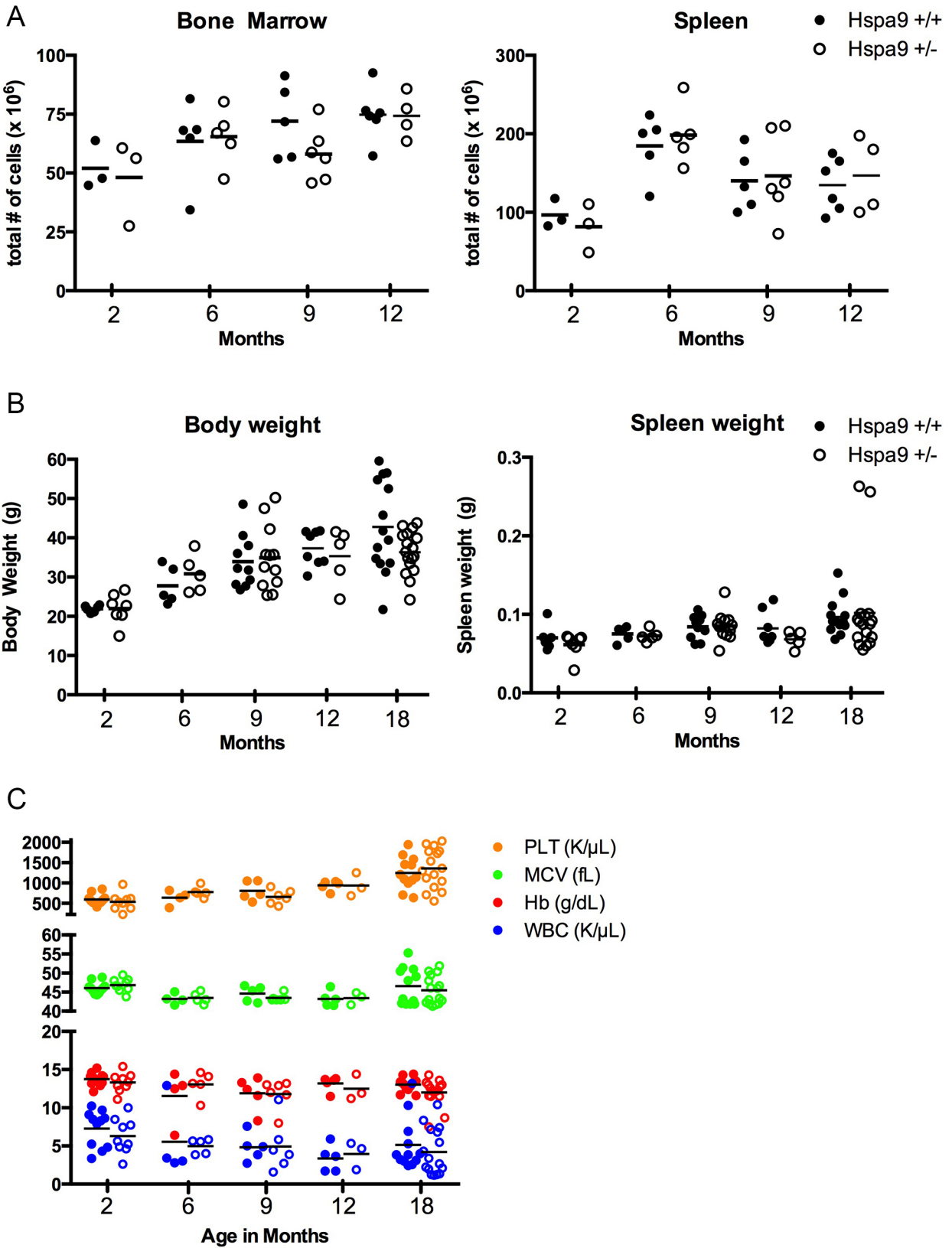


Figure 2.5: Immunophenotyping of bone marrow, peripheral blood and spleen cells up to 12 months of age

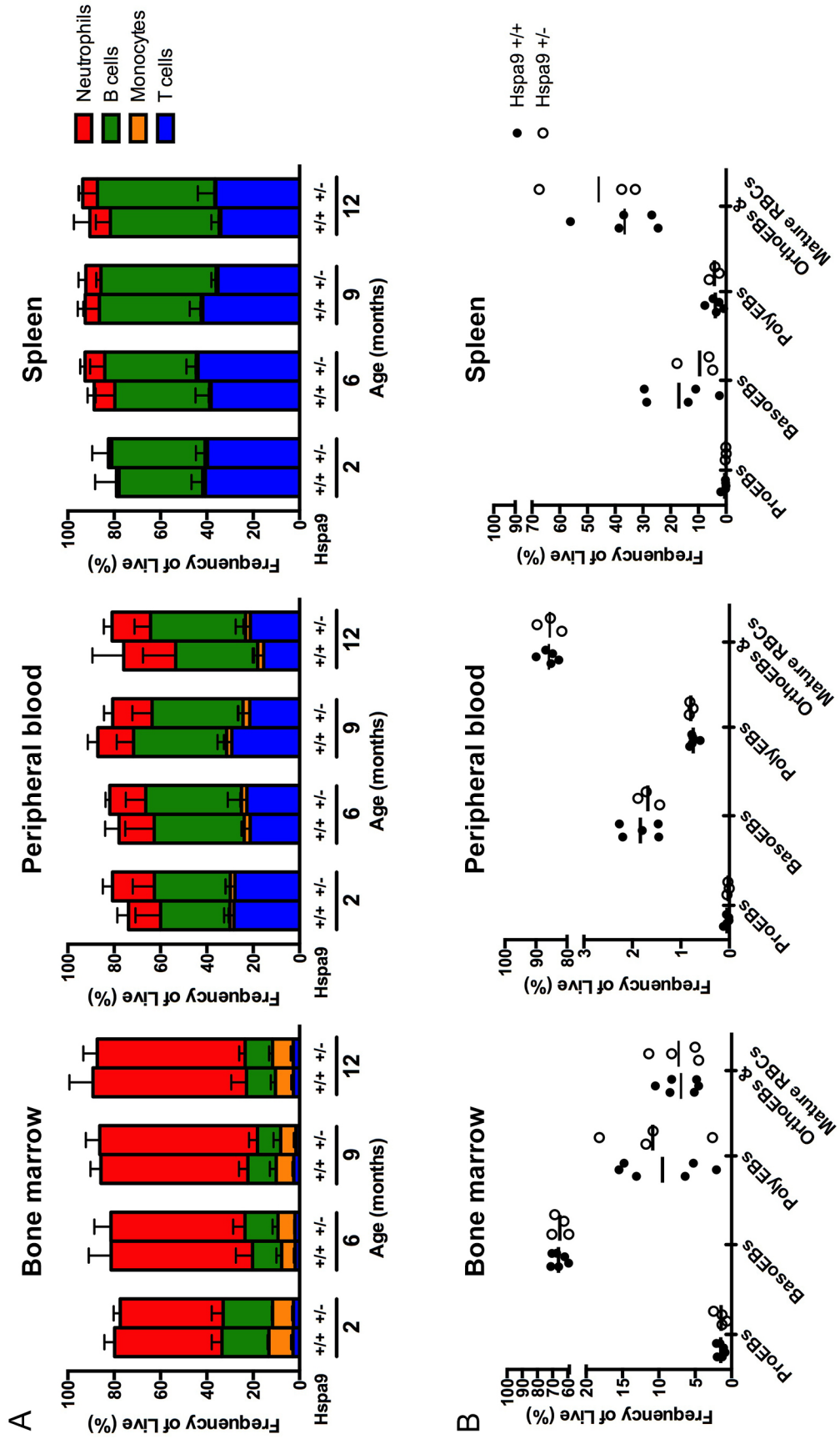


Figure 2.6: Progenitor and stem cell enriched populations are not altered in *Hspa9*^{+/-} mice

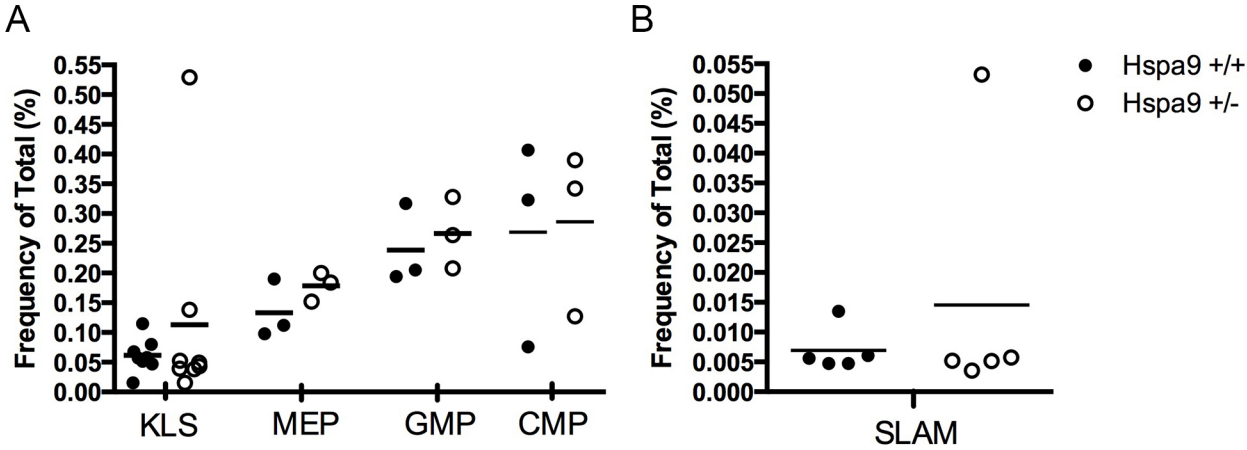


Figure 2.7: Colony forming ability of erythroid and myeloid spleen and bone marrow progenitors from *Hspa9*^{+/-} and *Hspa9*^{+/+} mice are similar

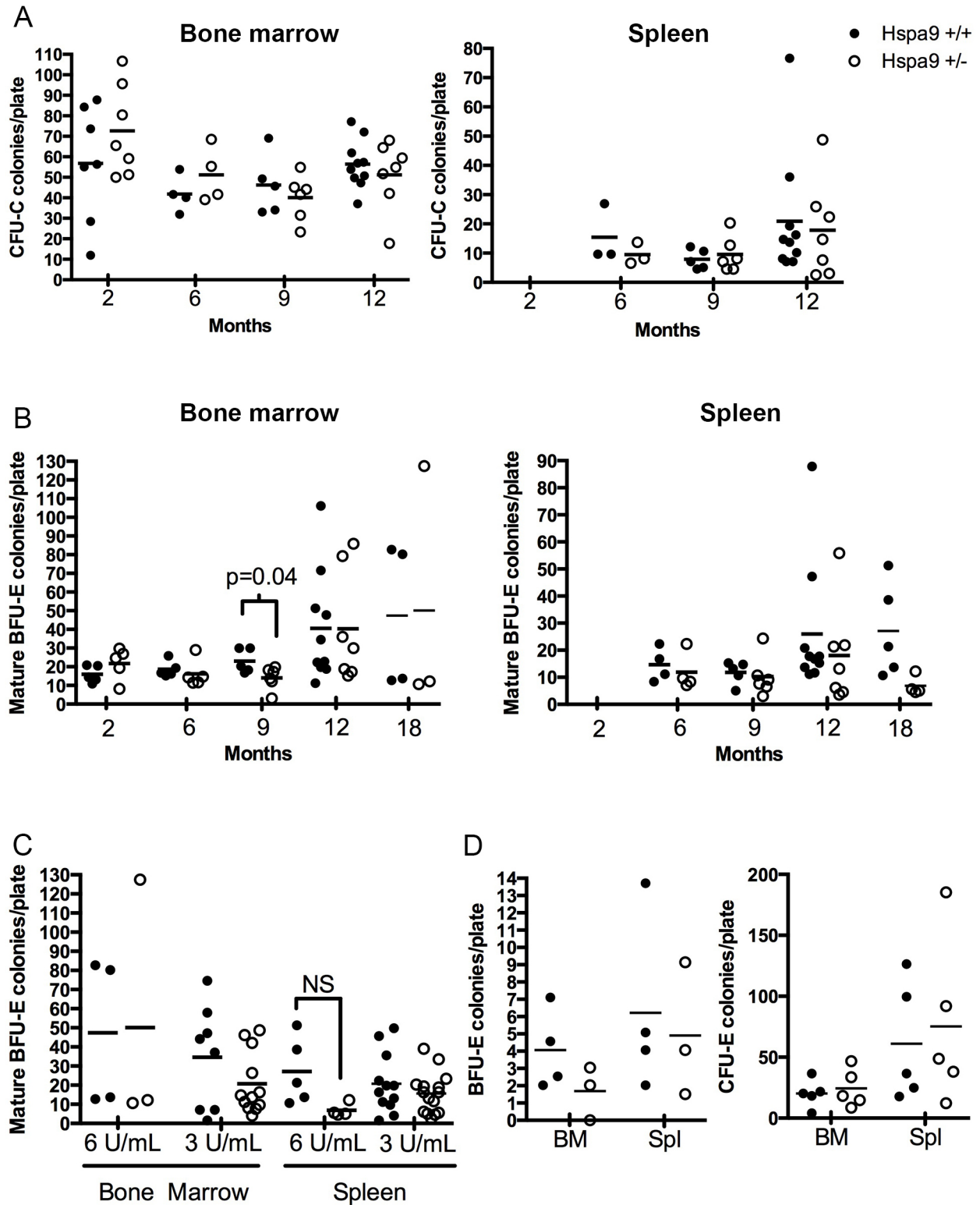


Figure 2.8: *Hspa9*^{+/-} and *Hspa9*^{+/+} littermate mice respond similarly to hematopoietic stress

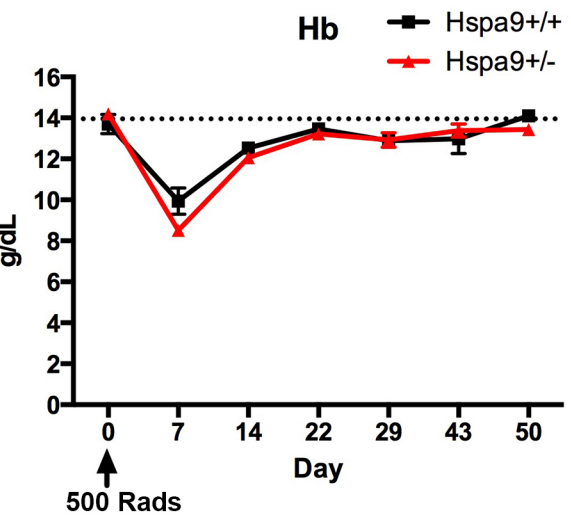
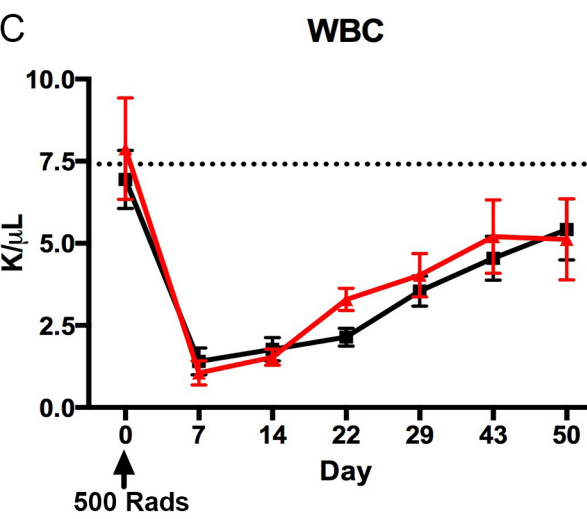
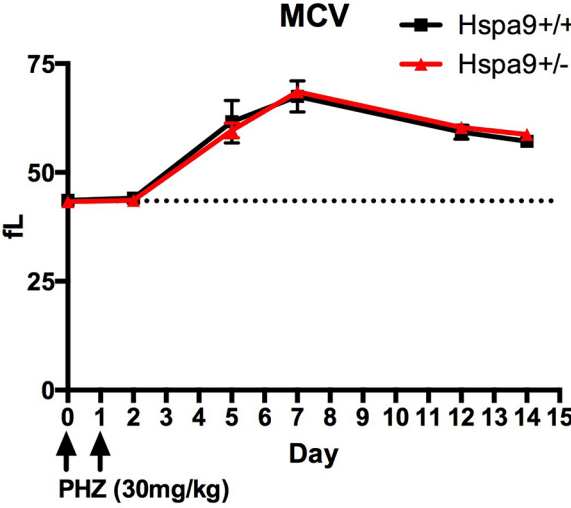
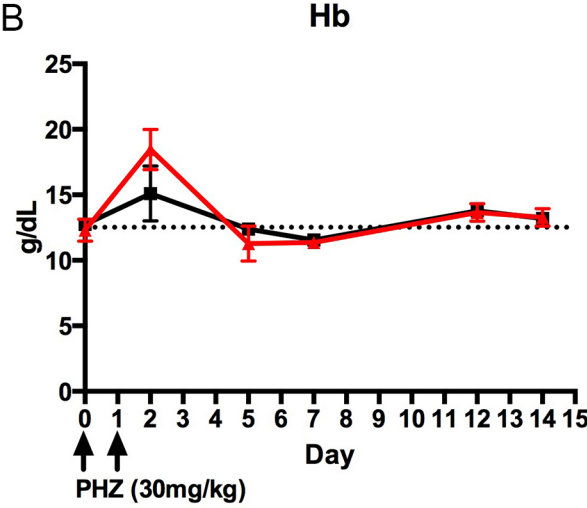
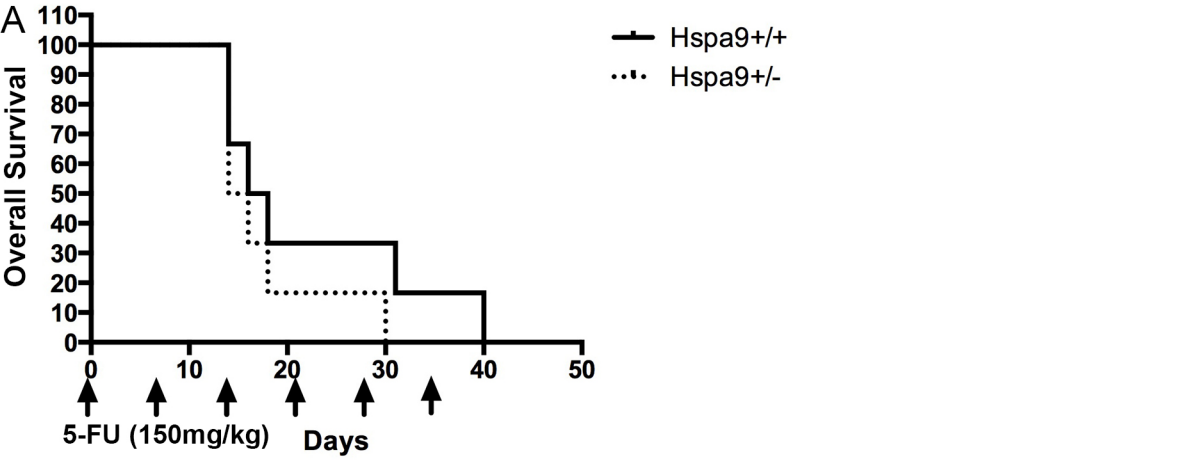


Figure 2.9: Colony forming ability of B-cell progenitors is significantly reduced in *Hspa9*^{+/-} compared to *Hspa9*^{+/+} mice

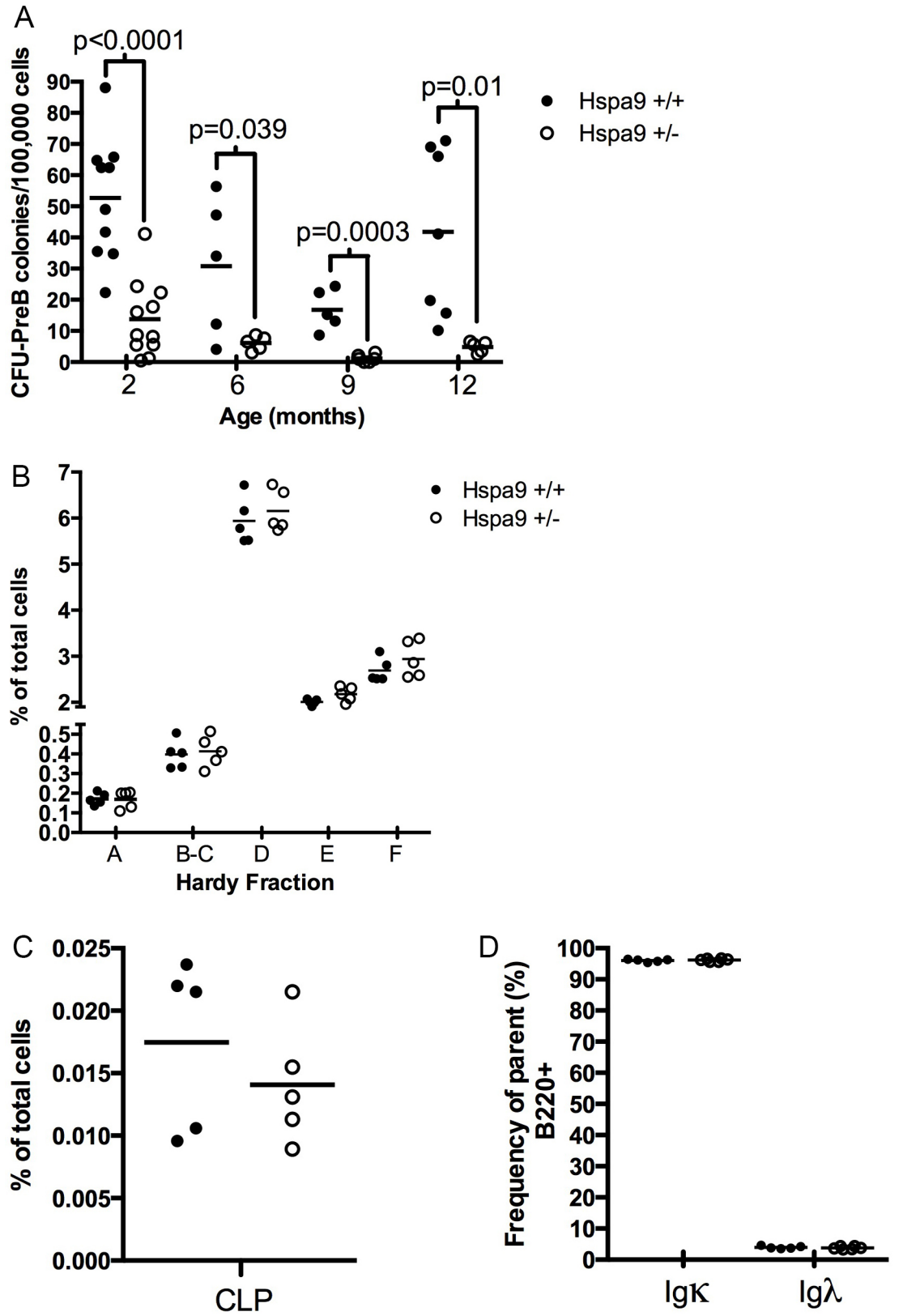


Figure 2.10: The gene trap insertion in *Hspa9* disrupts expression of both *Hspa9* and the snoRNA *Gm26109* located in intron 10 of *Hspa9*

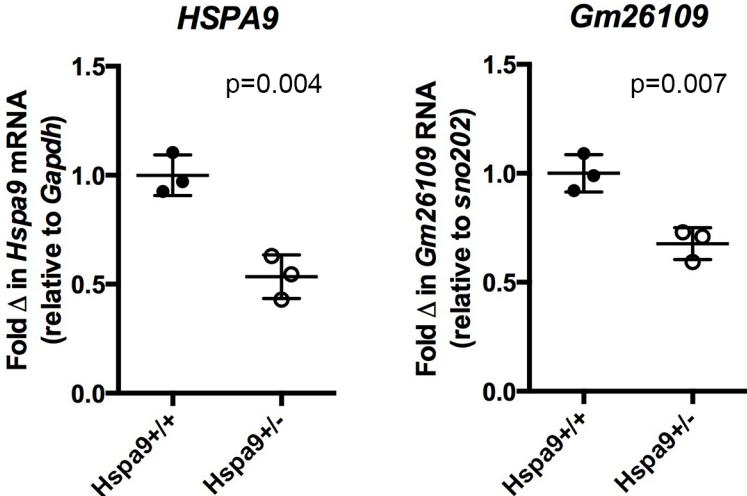


Figure 2.11: Overexpression of *HSPA9* in *Hspa9*^{+/-} bone marrow partially rescues the reduction in CFU-PreB colonies

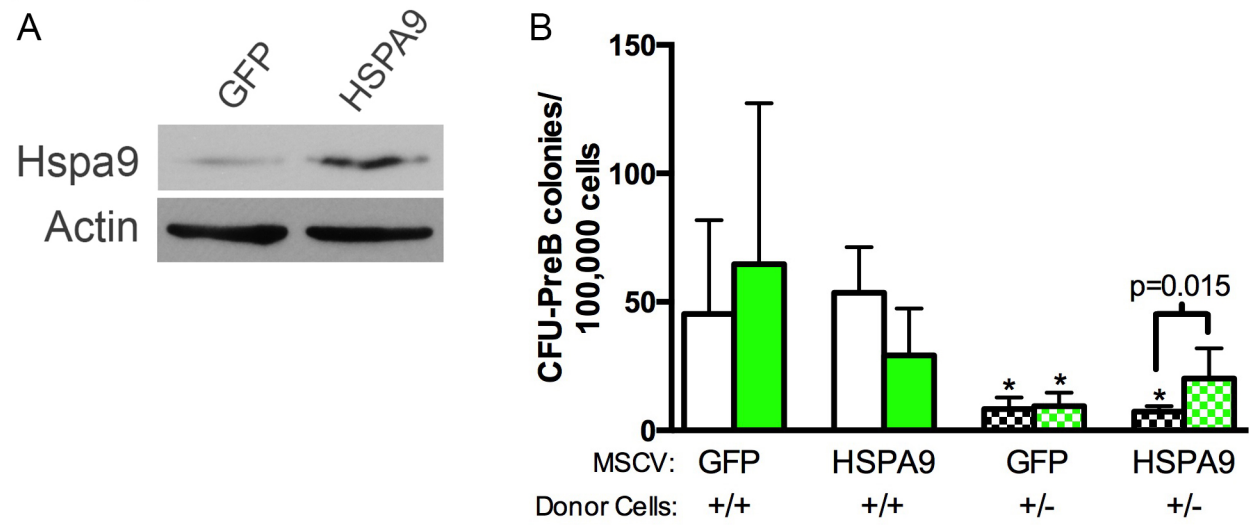


Figure 2.12: The reduction in CFU-PreB colony formation is hematopoietic cell-intrinsic

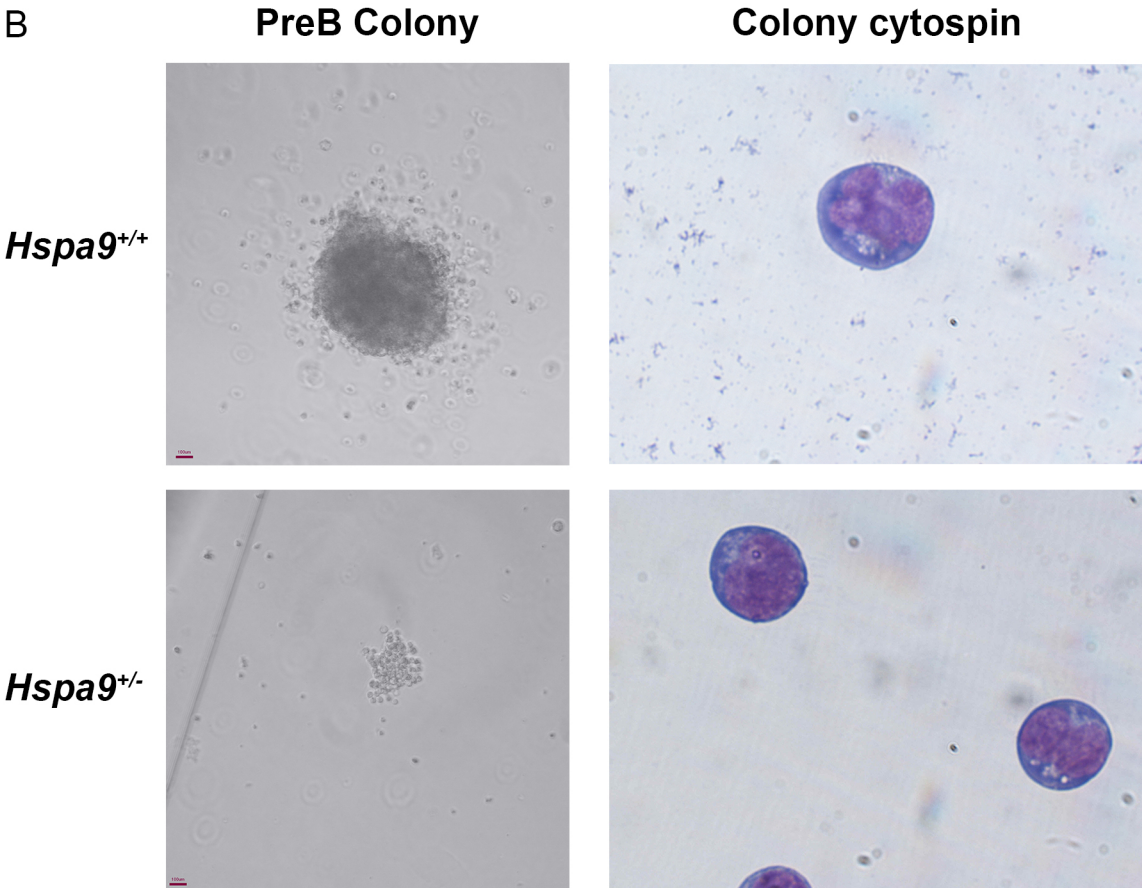
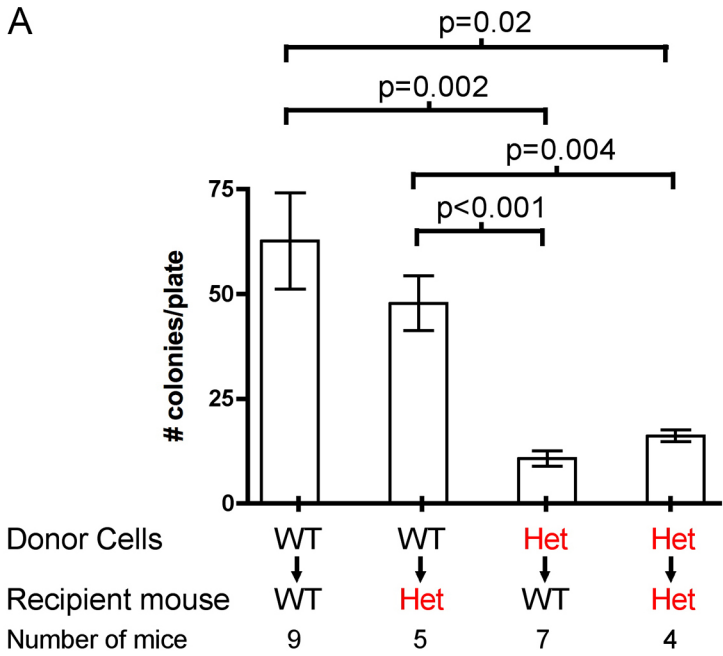


Figure 2.13: *Hspa9*^{+/-} bone marrow does not have a competitive advantage over control marrow in primary or secondary transplants

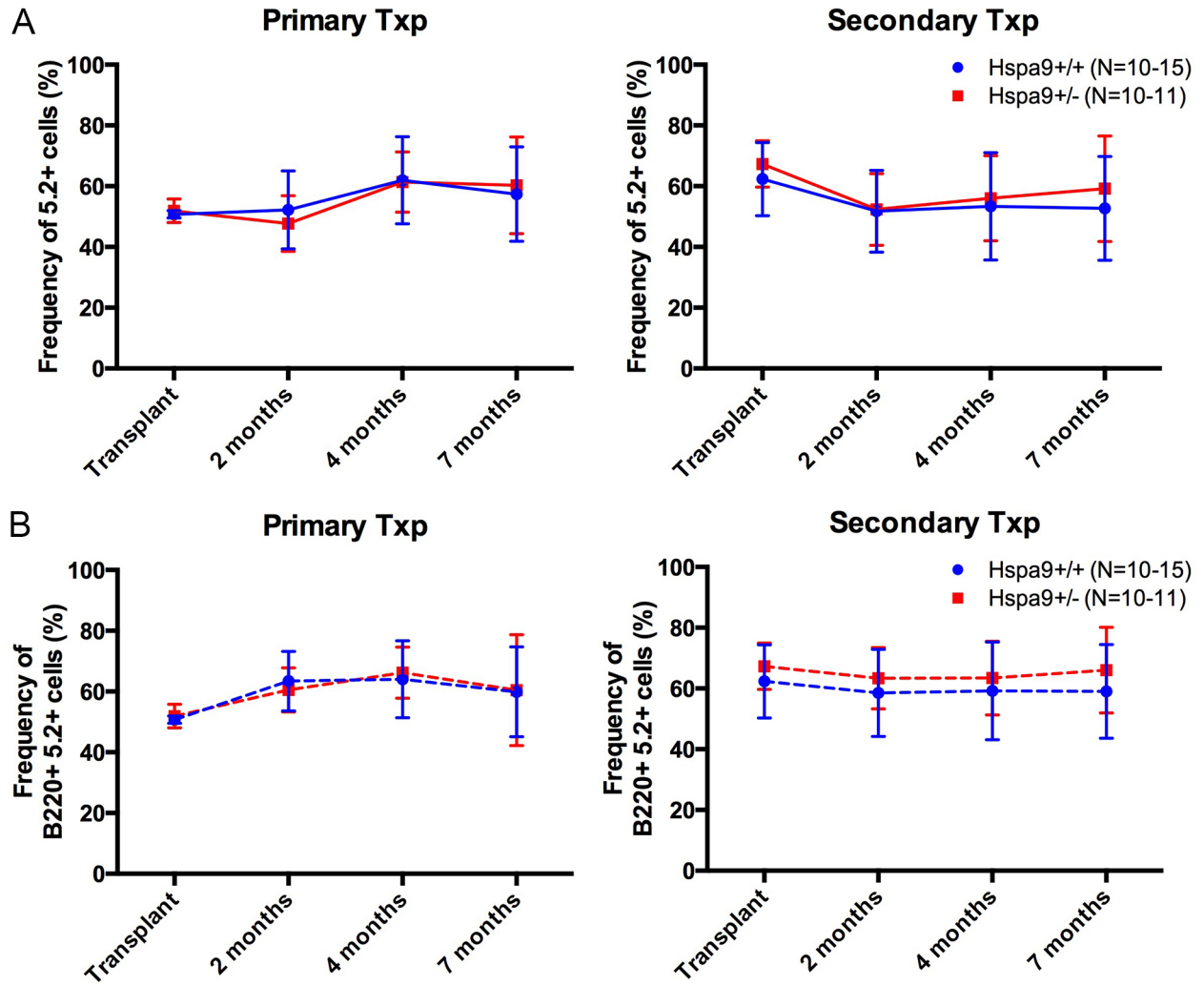


Figure 2.14: B-cell recovery is similar from *Hspa9*^{+/-} and *Hspa9*^{+/+} bone marrow following GCSF treatment

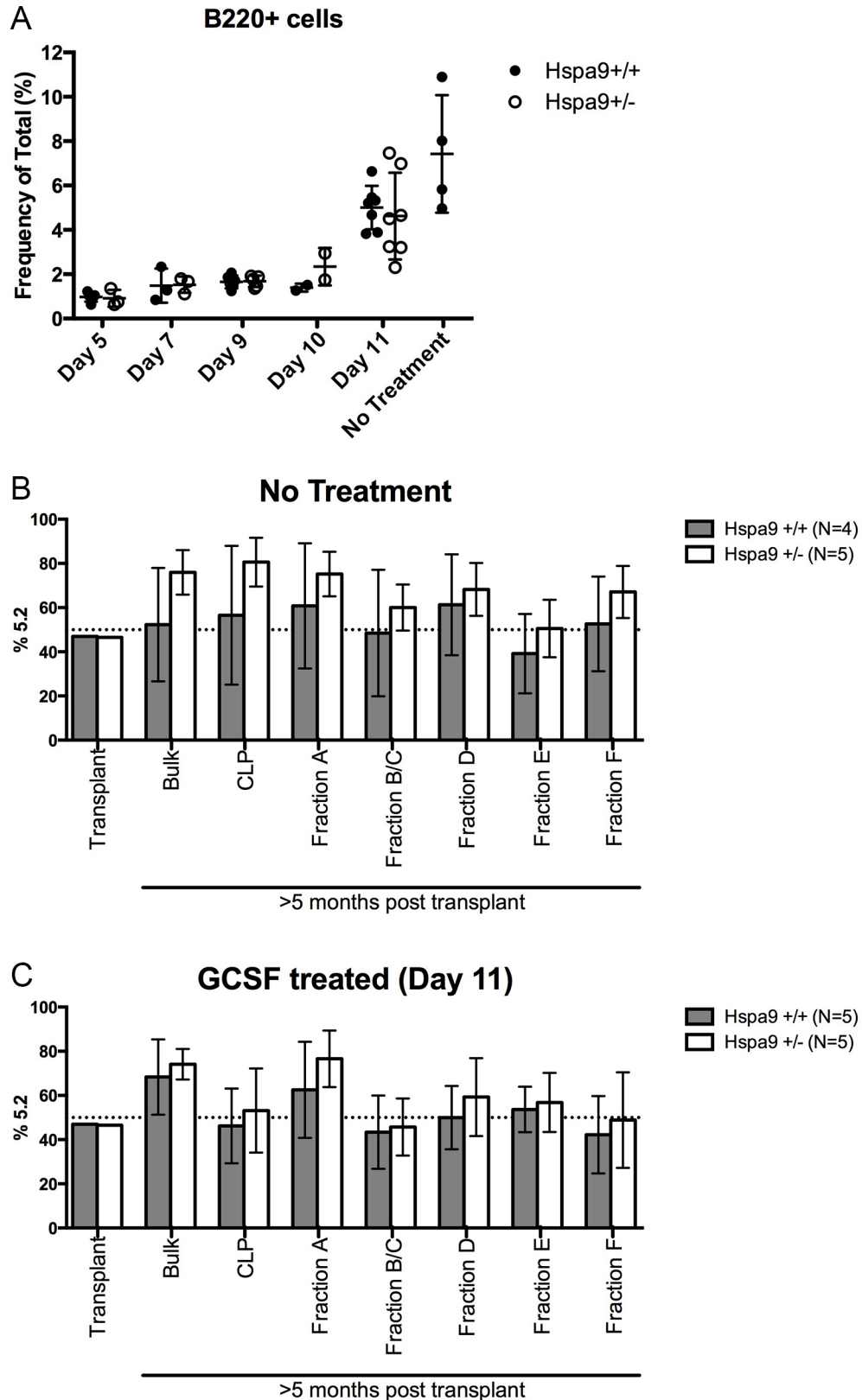


Figure 2.15: Overall and leukemia-free survival of *Hspa9*^{+/+} and *Hspa9*^{+/-} mice are not different

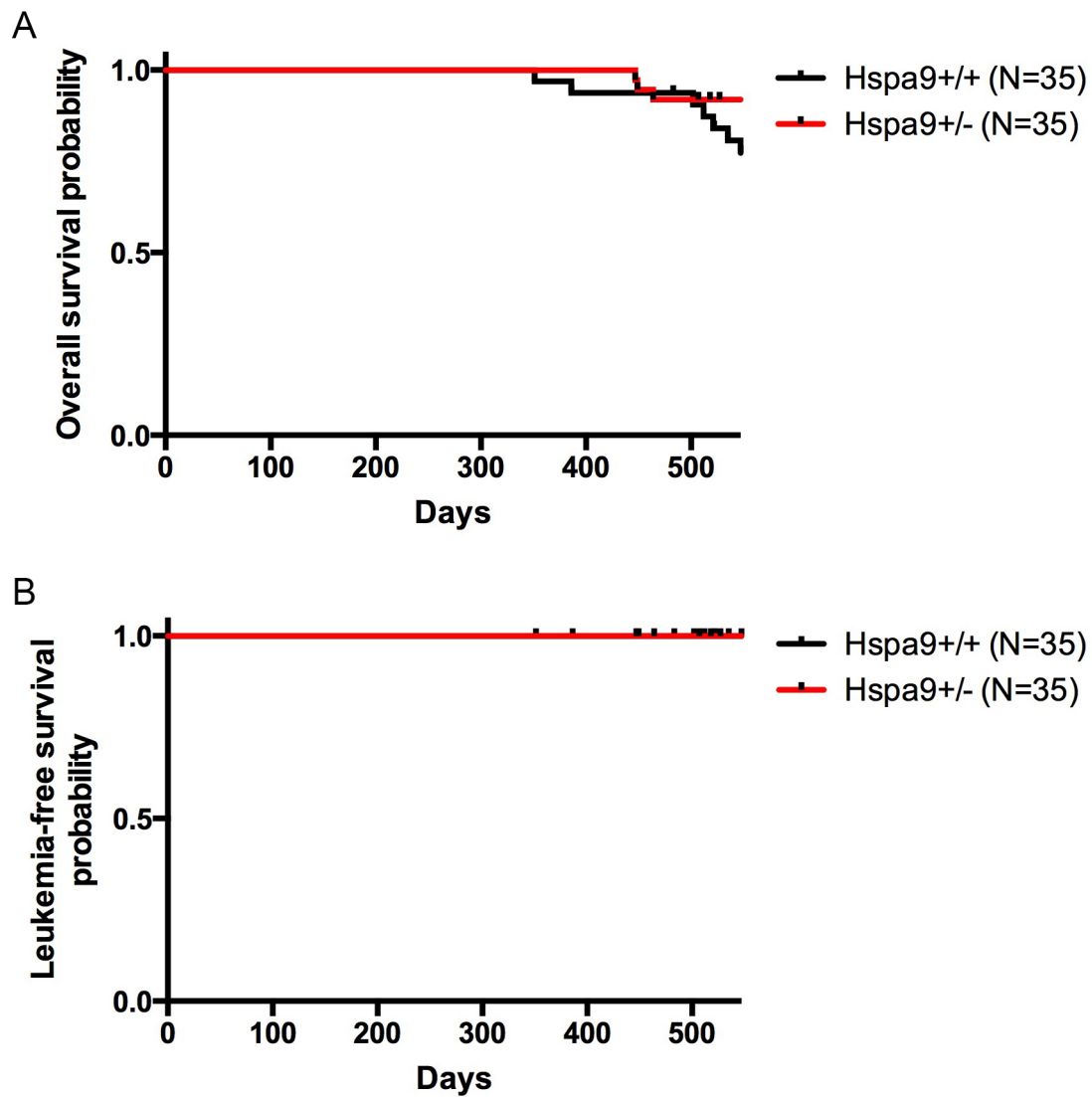


Figure 2.16: *Hspa9*^{+/-} mice are not more susceptible to leukemia induced by MOL4070LTR virus

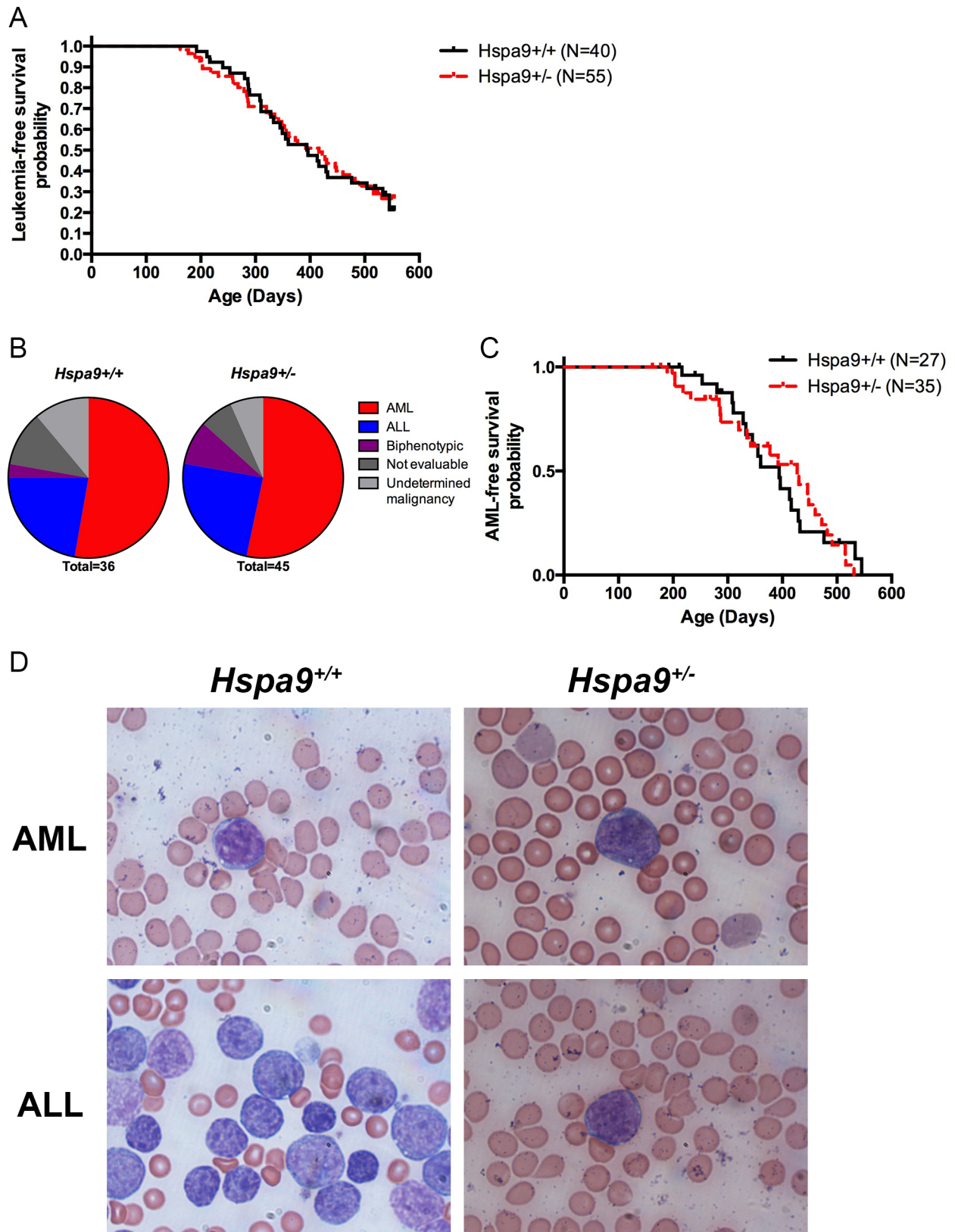


Table 2.1: Western blot antibodies

Antibody	Clone	Vendor	Catalog number
Actin	AC-15	Sigma	A5441
Hspa9	Polyclonal	Abcam	ab23854
Hspa9	JG-1	Pierce	MA3-028
Stat5	3H7	Cell Sig Tech	9358
pStat5	D47E7	Cell Sig Tech	4322

Table 2.2: Flow cytometry antibodies

Antigen	Fluorophore	Clone	Vendor	Catalog number
7AAD			Calbiochem	129935
B220 (CD45R)	APC	RA3-6B2	eBioscience	17-0452
B220 (CD45R)	APCe780	RA3-6B2	eBioscience	47-0452
B220 (CD45R)	eFluor450	RA3-6B2	eBioscience	48-0452
B220 (CD45R)	FITC	RA3-6B2	BD	533088
B220 (CD45R)	PE	RA3-6B2	eBioscience	12-0452
B220 (CD45R)	PE-Cy7	RA3-6B2	eBioscience	25-0452
B220 (CD45R)	PerCP-Cy5.5	RA3-6B2	eBioscience	45-0452
CD115 (c-fms)	PE	AF598	eBioscience	12-1152
CD117 (c-Kit)	APC	2B8	eBioscience	17-1171
CD117 (c-Kit)	APCe780	ACK2	eBioscience	47-1172
CD11b	APCe780	M1/70	eBioscience	27-0112
CD11c	PerCP-Cy5.5	N418	eBioscience	45-0114
CD135 (Flt3/Flk2)	APC	A2F10	eBioscience	17-1351
CD135 (Flt3/Flk2)	PE	A2F10	eBioscience	12-1351
CD150 (SLAM)	PE	TC15-12F12.2	Biologend	115903
CD16/32 (FcY)	eFluor450	93	eBioscience	48-0161
CD16/32 (purified)		93	eBioscience	16-0161
CD19	BV605	1D3	BD	563148
CD19	PE-Cy7	eBio1D3	eBioscience	25-0193
CD27	APC	LG.7F9	eBioscience	17-0271
CD34	PE	RAM34	eBioscience	12-0341
CD3e	APC	145-2C11	eBioscience	17-0031
CD3e	eFluor450	17A2	eBioscience	48-0032
CD3e	FITC	145-2C11	BD	553062
CD3e	PE	145-2C11	eBioscience	12-0031
CD3e	PE-Cy7	145-2C11	eBioscience	25-0031
CD3e	PerCP-Cy5.5	145-2C11	eBioscience	45-0031
CD4	FITC	RM4-5	eBioscience	11-0042
CD41	PE-Cy7	MWReg30	eBioscience	25-0411
CD43	Biotin	S7	BD	553269
CD43	PE	S7	BD	561857
CD45.1 (Ly5.1)	APC	A20	eBioscience	17-0453
CD45.1 (Ly5.1)	PE-Cy7	A20	eBioscience	25-0453
CD45.2 (Ly5.2)	FITC	104	BD	553772
CD45.2 (Ly5.2)	PerCP-Cy5.5	104	BD	552950
CD48	APC	HM48-1	eBioscience	17-0481
CD71	Alexa647	YTA74.4	ABD Serotec	MCA1033A647
CD8a (Ly-2)	APC	53-6.7	eBioscience	47-0081

DAPI			Invitrogen	D3571
Gr-1 (Ly-6G)	APC	RB6-8C5	Caltag	RM3005
Gr-1 (Ly-6G)	APCe780	RB6-8C5	eBioscience	47-5931
Gr-1 (Ly-6G)	FITC	RB6-8C5	eBioscience	11-5931
Gr-1 (Ly-6G)	PacBlue	RB6-8C5	Life Technologies	RM3028
Gr-1 (Ly-6G)	PE	RB6-8C5	eBioscience	12-5931
Gr-1 (Ly-6G)	PE-Cy7	RB6-8C5	eBioscience	25-5931
IgD	APC	11-26c	eBioscience	17-5993
IgD	eFluor450	11-26c	eBioscience	48-5993
IgD	PE	11-26c	eBioscience	12-5993
IgM	APC	II/41	BD	652032
IgM	eFluor450	eB121-15F9	eBioscience	48-5890
IgM	PE-Cy7	II/41	eBioscience	25-5790
Igk	PE-Cy7	187.1	BD	560667
Igλ	FITC	R26-46	BD	553434
IL7Rα	Biotin		**	
Ki67	FITC	B56	BD	556026
Ly6D	Alexa647	49-H4	BD	561147
Ly6D	FITC	49-H4	BD	561148
NK1.1	PerCP-Cy5.5	PK136	eBioscience	45-5941
Sca-1 (Ly-6A/E)	PE	D7	eBioscience	12-5981
Sca-1 (Ly-6A/E)	PerCP-Cy5.5	D7	eBioscience	45-5981
Stat5 (pY694)	Alexa647	47/Stat5pY694	BD	612599
Streptavidin	605NC		eBioscience	93-4317
Streptavidin	APCe780		eBioscience	47-4317
Streptavidin	eFluor450		eBioscience	48-4317
Ter119	APCe780	TER119	eBioscience	47-5921
Ter119	PE-Cy7	TER119	eBioscience	25-5921

**Kindly provided by Deepta Bhattacharya

Table 2.3: Results of *Hspa9*^{+/-} breeding indicate embryonic lethality

<i>Hspa9</i>^{+/-} x <i>Hspa9</i>^{+/+}			
	<i>Hspa9</i> ^{+/+}	<i>Hspa9</i> ^{+/-}	Total
Males	59	83	142
Females	62	57	119
Total	121	140	261

	<i>Hspa9</i> ^{+/+}	<i>Hspa9</i> ^{+/-}
Expected ratio	1	1
Observed ratio	1	1.16

<i>Hspa9</i>^{+/-} x <i>Hspa9</i>^{+/-}				
	<i>Hspa9</i> ^{+/+}	<i>Hspa9</i> ^{+/-}	<i>Hspa9</i> ^{-/-}	Total
Males	19	25	0	44
Females	11	18	0	29
Total	30	43	0**	73

	<i>Hspa9</i> ^{+/+}	<i>Hspa9</i> ^{+/-}	<i>Hspa9</i> ^{-/-}
Expected ratio	1	2	1
Observed ratio	1	1.43	0

<i>Hspa9</i>^{+/-} (B6129F1) x <i>Hspa9</i>^{+/-} (B6129F1)				
	<i>Hspa9</i> ^{+/+}	<i>Hspa9</i> ^{+/-}	<i>Hspa9</i> ^{-/-}	Total
Total	52	87	0**	139

	<i>Hspa9</i> ^{+/+}	<i>Hspa9</i> ^{+/-}	<i>Hspa9</i> ^{-/-}
Expected ratio	1	2	1
Observed ratio	1	1.67	0

**p<0.0001, Chi-squared test (two-tailed)

Table 2.4: No *Hspa9*^{-/-} embryos are found following fetal liver formation

Embryonic Day	<i>Hspa9</i>^{+/+}	<i>Hspa9</i>^{+/-}	<i>Hspa9</i>^{-/-}	total	# litters
Day 9.5	2	5	0	7	1
Day 11.5	3	2	0	5	1
Day 12.5	4	7	0	11	2
Day 13	3	4	0	7	1
Day 14	3	2	0	5	2
total	15	20	0	35	7

Expected ratio	1	2.00	1
Observed ratio	1	1.33	0

Expected #	8.75	17.50	8.75
Observed #	15	20	0*

*p=0.001, Chi-squared test (two-tailed)

Table 2.5: Immunophenotypic markers

Cell Type	Cell type by description in text	Flow cytometric markers
B-cell	B-cells	B220+
	Hardy Fraction A	B220+CD3e-CD11c-NK1.1-IgM-IgD-CD19-CD43+LY6D+
	Hardy Fraction BC	B220+CD3e-CD11c-NK1.1-IgM-IgD-CD19+CD43+
	Hardy Fraction D	B220+CD3e-CD11c-NK1.1-IgM-IgD-CD19+CD43-
	Hardy Fraction E	B220+CD3e-CD11c-NK1.1-IgM-IgD+
	Hardy Fraction F	B220+CD3e-CD11c-NK1.1-IgM+IgD+
Erythroid	proerythroblasts	Ter119 ^{med} CD71 ^{hi}
	polychromatic erythroblasts	Ter119 ^{hi} CD71 ^{hi} FSC ^{int}
	basophilic erythroblasts	Ter119 ^{hi} CD71 ^{hi} FSC ^{hi}
	reticulocytes	Ter119 ^{hi} CD71 ^{lo} FSC ^{lo}
T-cell	T-cells	CD3e+
Myeloid	Neutrophils	Gr1+CD115-
	Monocytes	Gr1+CD115+
Progenitor populations	Common lymphoid progenitor (CLP)	B220-CD3e-Gr1-Ter119-CD27+Flk2+IL7R α +Ly6D-
	Granulocyte-monocyte progenitor (GMP)	Lin-Sca-cKit+FcyR ^{hi} CD34+
	Common myeloid progenitor (CMP)	Lin-Sca-cKit+FcyR ^{lo} CD34+
	Megakaryocyte-erythrocyte progenitor (MEP)	Lin-Sca-cKit+FcyR ^{lo} CD34-
Stem-cell enriched populations	KLS	Lin-Sca+cKit+
	SLAM	Lin-Sca+cKit+CD150+CD48-

REFERENCES

1. Nolte, F. & Hofmann, W. K. Myelodysplastic syndromes: molecular pathogenesis and genomic changes. *Ann. Hematol.* (2008).
2. Haase, D. *et al.* New insights into the prognostic impact of the karyotype in MDS and correlation with subtypes: evidence from a core dataset of 2124 patients. *Blood* **110**, 4385–4395 (2007).
3. Rollison, D. E. *et al.* Epidemiology of myelodysplastic syndromes and chronic myeloproliferative disorders in the United States, 2001-2004, using data from the NAACCR and SEER programs. *Blood* **112**, 45–52 (2008).
4. Mauritzson, N. *et al.* Pooled analysis of clinical and cytogenetic features in treatment-related and de novo adult acute myeloid leukemia and myelodysplastic syndromes based on a consecutive series of 761 patients analyzed 1976-1993 and on 5098 unselected cases reported in the literature 1974-2001. *Leukemia* **16**, 2366–2378 (2002).
5. Walter, M. J. *et al.* Clonal diversity of recurrently mutated genes in myelodysplastic syndromes. *Leukemia* **27**, 1275–1282 (2013).
6. Jerez, A. *et al.* Topography, clinical, and genomic correlates of 5q myeloid malignancies revisited. *J. Clin. Oncol.* **30**, 1343–1349 (2012).
7. Boultonwood, J. *et al.* Narrowing and genomic annotation of the commonly deleted region of the 5q- syndrome. *Blood* **99**, 4638–4641 (2002).
8. Patnaik, M. M. *et al.* WHO-defined ‘myelodysplastic syndrome with isolated del (5q)’ in 88 consecutive patients: survival data, leukemic transformation rates and prevalence of JAK2, MPL and IDH mutations. *Leukemia* **24**, 1283–1289 (2010).
9. Ebert, B. L. *et al.* Identification of RPS14 as a 5q- syndrome gene by RNA interference screen. *Nature* **451**, 335–339 (2008).
10. Zhao, N. *et al.* Molecular delineation of the smallest commonly deleted region of chromosome 5 in malignant myeloid diseases to 1-1.5 Mb and preparation of a PAC-based physical map. *Proc. Natl. Acad. Sci. U.S.A.* **94**, 6948–6953 (1997).
11. Horrigan, S. K. *et al.* Delineation of a minimal interval and identification of 9 candidates for a tumor suppressor gene in malignant myeloid disorders on 5q31. *Blood* **95**, 2372–2377 (2000).
12. Graubert, T. A. *et al.* Integrated Genomic Analysis Implicates Haploinsufficiency of Multiple Chromosome 5q31.2 Genes in De Novo Myelodysplastic Syndromes Pathogenesis. *PLoS ONE* **4**, e4583 (2009).
13. Lai, F. *et al.* Transcript map and comparative analysis of the 1.5-Mb commonly deleted segment of human 5q31 in malignant myeloid diseases with a del(5q). *Genomics* **71**, 235–245 (2001).
14. Joslin, J. M. *et al.* Haploinsufficiency of EGR1, a candidate gene in the del(5q), leads to the development of myeloid disorders. *Blood* **110**, 719–726 (2007).
15. Dubourg, C. *et al.* Evaluation of ETF1/eRF1, mapping to 5q31, as a candidate myeloid tumor suppressor gene. *Cancer Genet. Cytogenet.* **134**, 33–37 (2002).
16. Craven, S. E., French, D., Ye, W., de Sauvage, F. & Rosenthal, A. Loss of Hspa9b in zebrafish recapitulates the ineffective hematopoiesis of the myelodysplastic syndrome. *Blood* **105**, 3528–3534 (2005).
17. Ohtsuka, R. *et al.* Mortalin is a novel mediator of erythropoietin signaling. *Eur. J. Haematol.* **79**, 114–125 (2007).
18. Tai-Nagara, I., Matsuoka, S., Ariga, H. & Suda, T. Mortalin and DJ-1 coordinately regulate hematopoietic stem cell function through the control of oxidative stress. *Blood* **123**, 41–50 (2014).
19. Ito, K. *et al.* Regulation of oxidative stress by ATM is required for self-renewal of haematopoietic stem cells. *Nature* **431**, 997–1002 (2004).
20. Miyamoto, K. *et al.* Foxo3a is essential for maintenance of the hematopoietic stem cell

- pool. *Cell Stem Cell* **1**, 101–112 (2007).
21. Chuikov, S., Levi, B. P., Smith, M. L. & Morrison, S. J. Prdm16 promotes stem cell maintenance in multiple tissues, partly by regulating oxidative stress. *Nat. Cell Biol.* **12**, 999–1006 (2010).
 22. Guo, F. *et al.* Mechanistic role of heat shock protein 70 in Bcr-Abl-mediated resistance to apoptosis in human acute leukemia cells. *Blood* **105**, 1246–1255 (2005).
 23. Ribeil, J.-A. *et al.* Hsp70 regulates erythropoiesis by preventing caspase-3-mediated cleavage of GATA-1. *Nature* **445**, 102–105 (2007).
 24. Zou, P. *et al.* p57(Kip2) and p27(Kip1) cooperate to maintain hematopoietic stem cell quiescence through interactions with Hsc70. *Cell Stem Cell* **9**, 247–261 (2011).
 25. Mihařada, K. *et al.* Cripto Regulates Hematopoietic Stem Cells as a Hypoxic-Niche-Related Factor through Cell Surface Receptor GRP78. *Cell Stem Cell* **9**, 330–344 (2011).
 26. Mjehed, H., Girodon, F., Fontenay, M. & Garrido, C. Heat shock proteins in hematopoietic malignancies. *Exp. Cell Res.* **318**, 1946–1958 (2012).
 27. Suzuki, T. *et al.* New genes involved in cancer identified by retroviral tagging. *Nat. Genet.* **32**, 166–174 (2002).
 28. Du, Y., Spence, S. E., Jenkins, N. A. & Copeland, N. G. Cooperating cancer-gene identification through oncogenic-retrovirus-induced insertional mutagenesis. *Blood* **106**, 2498–2505 (2005).
 29. Uren, A. G. *et al.* Large-scale mutagenesis in p19(ARF)- and p53-deficient mice identifies cancer genes and their collaborative networks. *Cell* **133**, 727–741 (2008).
 30. Chen, T. H.-P. *et al.* Knockdown of Hspa9, a del(5q31.2) gene, results in a decrease in hematopoietic progenitors in mice. *Blood* **117**, 1530–1539 (2011).
 31. Zambrowicz, B. P. *et al.* Wnk1 kinase deficiency lowers blood pressure in mice: a gene-trap screen to identify potential targets for therapeutic intervention. *Proc. Natl. Acad. Sci. U.S.A.* **100**, 14109–14114 (2003).
 32. Zambrowicz, B. P. *et al.* Disruption and sequence identification of 2,000 genes in mouse embryonic stem cells. *Nature* **392**, 608–611 (1998).
 33. Ryan, M. R. *et al.* An IL-7-dependent rebound in thymic T cell output contributes to the bone loss induced by estrogen deficiency. *Proc. Natl. Acad. Sci. U.S.A.* **102**, 16735–16740 (2005).
 34. Ma, Z. *et al.* Mortalin controls centrosome duplication via modulating centrosomal localization of p53. *Oncogene* **25**, 5377–5390 (2006).
 35. Wolff, L., Koller, R., Hu, X. & Anver, M. R. A Moloney murine leukemia virus-based retrovirus with 4070A long terminal repeat sequences induces a high incidence of myeloid as well as lymphoid neoplasms. *J. Virol.* **77**, 4965–4971 (2003).
 36. Morse, H. C. *et al.* Bethesda proposals for classification of lymphoid neoplasms in mice. *Blood* **100**, 246–258 (2002).
 37. Kogan, S. C. Bethesda proposals for classification of nonlymphoid hematopoietic neoplasms in mice. *Blood* **100**, 238–245 (2002).
 38. Thyagarajan, T., Totey, S., Danton, M. J. S. & Kulkarni, A. B. Genetically altered mouse models: the good, the bad, and the ugly. *Crit. Rev. Oral Biol. Med.* **14**, 154–174 (2003).
 39. Liu, Y., Liu, W., Song, X.-D. & Zuo, J. Effect of GRP75/mthsp70/PBP74/mortalin overexpression on intracellular ATP level, mitochondrial membrane potential and ROS accumulation following glucose deprivation in PC12 cells. *Mol. Cell. Biochem.* **268**, 45–51 (2005).
 40. Williamson, C. L., Dabkowski, E. R., Dillmann, W. H. & Hollander, J. M. Mitochondria protection from hypoxia/reoxygenation injury with mitochondria heat shock protein 70 overexpression. *Am. J. Physiol. Heart Circ. Physiol.* **294**, H249–56 (2008).
 41. Orsini, F. *et al.* The life span determinant p66Shc localizes to mitochondria where it associates with mitochondrial heat shock protein 70 and regulates trans-membrane

- potential. *J. Biol. Chem.* **279**, 25689–25695 (2004).
42. Grisendi, S. *et al.* Role of nucleophosmin in embryonic development and tumorigenesis. *Nature* **437**, 147–153 (2005).
 43. Buonamici, S. *et al.* EVI1 induces myelodysplastic syndrome in mice. *J. Clin. Invest.* **114**, 713–719 (2004).
 44. Lane, S. W. *et al.* The Apc(min) mouse has altered hematopoietic stem cell function and provides a model for MPD/MDS. *Blood* **115**, 3489–3497 (2010).
 45. Zhang, Y. *et al.* MLL5 contributes to hematopoietic stem cell fitness and homeostasis. *Blood* **113**, 1455–1463 (2009).
 46. Sadekova, S., Lehnert, S. & Chow, T. Y. Induction of PBP74/mortalin/Grp75, a member of the hsp70 family, by low doses of ionizing radiation: a possible role in induced radioresistance. *Int. J. Radiat. Biol.* **72**, 653–660 (1997).
 47. Inlay, M., Alt, F. W., Baltimore, D. & Xu, Y. Essential roles of the kappa light chain intronic enhancer and 3' enhancer in kappa rearrangement and demethylation. *Nat. Immunol.* **3**, 463–468 (2002).
 48. Beck, K., Peak, M. M., Ota, T., Nemazee, D. & Murre, C. Distinct roles for E12 and E47 in B cell specification and the sequential rearrangement of immunoglobulin light chain loci. *J. Exp. Med.* **206**, 2271–2284 (2009).
 49. Malin, S. *et al.* Role of STAT5 in controlling cell survival and immunoglobulin gene recombination during pro-B cell development. *Nat. Immunol.* **11**, 171–179 (2010).
 50. Calvi, L. M. *et al.* Osteoblastic cells regulate the haematopoietic stem cell niche. *Nature* **425**, 841–846 (2003).
 51. Omatsu, Y. *et al.* The essential functions of adipo-osteogenic progenitors as the hematopoietic stem and progenitor cell niche. *Immunity* **33**, 387–399 (2010).
 52. Greenbaum, A. *et al.* CXCL12 in early mesenchymal progenitors is required for haematopoietic stem-cell maintenance. *Nature* **495**, 227–230 (2013).
 53. Dail, M. *et al.* Mutant Ikzf1, KrasG12D, and Notch1 cooperate in T lineage leukemogenesis and modulate responses to targeted agents. *Proc. Natl. Acad. Sci. U.S.A.* **107**, 5106–5111 (2010).
 54. Bies, J. *et al.* Myeloid-specific inactivation of p15Ink4b results in monocytosis and predisposition to myeloid leukemia. *Blood* **116**, 979–987 (2010).
 55. Kallapur, S., Ormsby, I. & Doetschman, T. Strain dependency of TGF β 1 function during embryogenesis. *Mol. Reprod. Dev.* **52**, 341–349 (1999).
 56. Sternberg, A. *et al.* Evidence for reduced B-cell progenitors in early (low-risk) myelodysplastic syndrome. *Blood* **106**, 2982–2991 (2005).
 57. Amin, H. M. *et al.* Increased apoptosis in bone marrow B lymphocytes but not T lymphocytes in myelodysplastic syndrome. *Blood* **102**, 1866–1868 (2003).
 58. Tycowski, K. T., Smith, C. M., Shu, M. D. & Steitz, J. A. A small nucleolar RNA requirement for site-specific ribose methylation of rRNA in *Xenopus*. *Proc. Natl. Acad. Sci. U.S.A.* **93**, 14480–14485 (1996).
 59. Wadhwa, R. *et al.* Upregulation of mortalin/mthsp70/Grp75 contributes to human carcinogenesis. *Int. J. Cancer* **118**, 2973–2980 (2006).
 60. Sportoletti, P. *et al.* Npm1 is a haploinsufficient suppressor of myeloid and lymphoid malignancies in the mouse. *Blood* **111**, 3859–3862 (2008).
 61. Liu, T. X. *et al.* Chromosome 5q deletion and epigenetic suppression of the gene encoding α -catenin (CTNNA1) in myeloid cell transformation. *Nat. Med.* **13**, 78–83 (2006).
 62. Nilsson, L. *et al.* Isolation and characterization of hematopoietic progenitor/stem cells in 5q-deleted myelodysplastic syndromes: evidence for involvement at the hematopoietic stem cell level. *Blood* **96**, 2012–2021 (2000).

CHAPTER 3:
The Role of Hspa9 in IL-7 Receptor Signaling

1. Abstract

Heterozygous loss of *Hspa9* in mice causes a significant, hematopoietic-cell intrinsic reduction in CFU-PreB colony formation *in vitro*. Gene expression profiling of CFU-PreB colony cells revealed significant down-regulation of B-cell signaling and activation pathway genes in *Hspa9*^{+/-} compared to wild-type mice. Furthermore, knockdown of *Hspa9* levels below 50% caused a significant reduction in B-cell progenitors *in vivo* without disrupting myeloid or T-cell lineages, further implicating *Hspa9* in B-cell development. The addition of exogenous IL-7 to *Hspa9*^{+/-} CFU-PreB cultures could partially rescue the reduction in colonies, without affecting *Hspa9*^{+/+} colonies, implicating *Hspa9* in IL-7 receptor signaling. *Hspa9* knockdown in an IL-7 dependent mouse proB-cell line resulted in a significant growth defect similar to that observed by reducing IL-7 concentrations in the culture media. Consistent with blunted IL-7 receptor signaling in *Hspa9* knockdown cells, Stat5 phosphorylation was reduced in *Hspa9* knockdown compared to control cells following IL-7 stimulation. Collectively, these results suggest that loss of *Hspa9* alters B-cell function by reducing IL-7-dependent Stat5 activation.

2. Introduction

The mitochondrial heat shock 70kDa protein, *Hspa9*, has roles in a variety of cellular processes and cell types. Loss of *Hspa9* has been associated with reduced cellular proliferation and an increase in apoptosis in several genetic systems¹⁻⁵. Previous work has illustrated how these alterations affect hematopoietic progenitors and particularly erythropoiesis in zebrafish, mouse and human cells^{2-4,6}. A novel finding in an shRNA-mediated *Hspa9* knockdown mouse model identified a reduction in B-cells (B220+), as well as erythroid cells (Ter119^{hi}CD71⁺) in peripheral blood, bone marrow and spleen of mice³. This effect was erythroid and B-cell lineage specific as myeloid and T-cell lineages were unaffected. These results recapitulated phenotypes, such as anemia and other cytopenias resulting from ineffective hematopoiesis, observed in myelodysplastic syndrome (MDS), a clonal hematopoietic stem cell disorder. Up to 25% of

patients have an interstitial deletion or loss on the long arm of chromosome 5, where *HSPA9* is located⁷. *HSPA9* specifically lies within a 2.5 megabase commonly deleted region of 5q that is associated with poorer prognosis, implicating it in pathogenesis of this disease⁸⁻¹².

The previously described alterations in hematopoietic progenitors, erythropoiesis and mature B-cells in models of *Hspa9* loss support a role for *HSPA9* in the pathogenesis of MDS. Anemia and effects on stem and progenitor populations are well described in MDS; however, alterations in B-cell populations have also been observed in MDS patients. B-cell progenitors ($CD34^+CD19^{+/-}$) are significantly reduced in low-risk MDS patients, and increased levels of apoptosis occur in $CD19^+$ cells in MDS patients with RA, RARS and RAEB^{13,14}. Engraftment of hematopoietic stem cells (HSCs) from patients with low-risk MDS resulted in significantly fewer donor-derived B-cells than normal HSCs¹⁵. Additionally, two B-cell signaling pathways were among the top 5 significantly down-regulated gene expression pathways in $CD34^+$ cells from MDS patients (n=183) and del(5q) MDS patients (n=29) compared to 17 normal $CD34^+$ bone marrow cells¹⁶. However, whether this is due to the loss of specific cell populations or altered B-cell signaling is unclear. Another study showed that del(5q) also occurs in MDS patient bone marrow proB-cells ($CD34^+/CD19^+$), indicating B-cells can harbor del(5q) in MDS¹⁷. Although the literature on B-cells in MDS is limited, taken together, these results indicate that alterations in B-cell populations exist in MDS patients, and early mouse data indicates that loss of *HSPA9* may contribute to these alterations.

In Chapter 2, we described a novel heterozygous knockout mouse used to investigate the role of *Hspa9* in hematopoiesis. As early as 2 months of age, *Hspa9*^{+/-} mice have a significant, hematopoietic cell-intrinsic reduction in CFU-PreB colony formation compared to *Hspa9*^{+/+} littermates. However, *in vivo* frequencies of B-cell progenitors are normal in *Hspa9*^{+/-} mice when compared to *Hspa9*^{+/+} littermates at different ages, following a non-competitive or competitive

transplant. These results suggest that *in vivo* compensation may occur in mice to overcome the B-cell progenitor defect observed *in vitro*. *In vivo*, several cytokines are involved in B-cell proliferation and differentiation at different stages of B-cell development and may be involved in this compensation. However, IL-7 is the only exogenous cytokine added to CFU-PreB methylcellulose medium to promote colony formation suggesting it may be important in the phenotype. In order to investigate the role of Hspa9 on B-cell development and better understand the mechanism of *in vivo* compensation, we further investigated the role of Hspa9 in IL-7R signaling.

3. Materials and Methods

3.1. Colony forming assays

CFU-PreB colonies were grown in methylcellulose medium containing 10ng/mL IL-7 (Stem Cell Technologies: M3630). Bone marrow cells were added at a concentration of 100,000 cells/plate, in duplicate for each point reported. Exogenous IL-7 (Stem Cell Technologies: 02577, 10ug/mL stock concentration) or Flt3-ligand (Peprotech: 50ug/mL stock concentration) was added to the media at various concentrations. The final concentration of IL-7 includes the 10ng/mL already present in the media (i.e., 90ng/mL was added for the reported 100ng/mL concentration).

3.2. Microarray analysis

To generate enough material for gene expression analysis, bone marrow was plated at 250,000 cells/plate for *Hspa9*^{+/+} and 1x10⁶ cells/plate for *Hspa9*^{+/-} mice and replicate plates were pooled. Cells were isolated from CFU-PreB (Stem Cell Technologies: M3630) media on Day 7 by the addition of pre-warmed IMDM Media (Gibco: 12440046) with 20% FCS. Cells were washed with warmed media to remove remaining methylcellulose and cell surface stained. B220+ cells were sorted directly into TRIzol LS Reagent (Life Technologies: 10296-028) using a Beckman Coulter MoFlo at the Washington University Siteman Flow

Cytometry Core. The Washington University Tissue Procurement Core performed RNA preparation and quantification. RNA was extracted from TRIzol LS using standard protocols. Total RNA quality and quantity was evaluated using the Eukaryote Total RNA Nano Series II (Agilent) assay on a 2100 bioanalyzer (Agilent). cDNA was prepared using the PicoSL Ovation system (NuGen). Samples were hybridized to Mouse Gene 1.0 ST arrays by the Washington University Biomedical Informatics Core. Gene-level normalization and signal summarization was performed for all arrays using Affymetrix Expression Console. Unsupervised hierarchical clustering using Ward's, UPGMA, or WPGMA clustering algorithms with Euclidean distance were performed (Tibco Spotfire DecisionSite software). Differentially expressed individual genes were identified using Significance Analysis of Microarrays (SAM). Pathway analysis was performed on significantly altered genes using the Database for Annotation, Visualization, and Integrated Discovery (DAVID, <http://david.abcc.ncifcrf.gov/>).

3.3. Cell culture

B7 (Ba/F3 cells stably transduced with MSCV-mIL7R-IRES-GFP)¹⁸ cells were maintained at a density <2 million cells/mL in RPMI media with 10% FCS, 2mM L-glutamine, 100U/mL penicillin, 100ug/mL streptomycin and 10ng/mL mIL-7 (Peprotech: 217-17). HEK293T and NIH3T3 cells were maintained in DMEM with 10% FCS, 2mM L-glutamine, 100U/mL penicillin and 100ug/mL streptomycin. All cells were grown in a 37°C incubator with 5% atmospheric CO₂.

3.4. Flow Cytometry

3.4.1. Cell cycle analysis

Bone marrow cells were collected from 9-week old mice. 5 million cells/tube were incubated in 200µL FACS buffer (1mM EDTA, 2% FCS, PBS) for 10 minutes with purified anti-mouse CD16/32 to prevent non-specific binding. Cell surface staining (IgD, IgM, B220) was performed on ice, protected from light for 20 minutes. Cells were fixed

using BD Cytofix/Cytoperm solution (BD: 554714) for 15 minutes at room temperature. Cells were gently permeabilized with 2 washes in BD Fixation/Permeabilization solution before incubating with 5% goat serum (Sigma: G9023). Cells were stained with Ki67 for 30 minutes on ice, washed and resuspended in FACS buffer containing DAPI prior to analysis. Cells were analyzed using a Gallios cytometer (BD Biosciences) and FlowJo software.

3.4.2. Intracellular flow

B7 cells were counted and collected by centrifugation at 90xg for 10 minutes. Cells were resuspended at a concentration of 20 million cells/mL in Nucleofector solution from the Amaxa Kit V per manufacturer's instructions (Lonza: VCA-1003). Cells were electroporated with 1000nM *Hspa9*-targeting siRNAs (Thermo Scientific siGENOME *Hspa9* siRNA D-057872-03 [siRNA 1] and D-057872-04 [siRNA 2]) or non-targeting control siRNA (Thermo Scientific siGenome Non-Targeting siRNA pool #2: D-001206-14) using a Nucleofector Device (Lonza) program X-001. 500 μ L complete B7 media was immediately added to cells, which were transferred to culture plates containing B7 media for a final concentration of 1.3 million cells/mL. Cells were allowed to rest overnight in an incubator with 5% CO₂ at 37°C before being counted and added to fresh media. Three days following electroporation, cells were collected, washed once with media lacking IL-7, pelleted, and recultured in media without cytokines overnight. The next morning cells were stimulated with IL-7 at the described concentrations and collected. Media was removed and cells were resuspended in 500 μ L 2% paraformaldehyde. The time points indicated are from the addition of IL-7 to the resuspension in the 2% paraformaldehyde fixation solution. Cells were incubated at 37°C for 10 minutes and washed with 1mL PBS. Cells were pelleted and resuspended in 300 μ L ice-cold, 100% methanol and incubated on ice for 30 minutes for permeabilization. Cells were washed first with 1mL PBS, then with 1mL FACS buffer. pStat5 master mix was made by adding 10 μ L pStat5-

Alexa 647 (BD Bioscience: 612599) per 100uL FACS. Cells were resuspended in 100uL pStat5 master mix and incubated at room temperature for 30 minutes, then cells were washed with FACS buffer and analyzed by FACScan (BD biosciences) using FlowJo software.

3.5. Western blot analysis

3.5.1. Standard Western blots

Western blots were performed as previously described³. Cells were washed with PBS and pelleted before being resuspended in radioimmunoprecipitation (RIPA) buffer (150 mM NaCl, 50 mM Tris [pH 8], 1 mM EDTA, 0.1%SDS, 0.5% sodium deoxycholate, 1% NP-40, 1 mM PMSF) with proteinase and phosphatase inhibitors (10mM NaF, 20mM NaPP, 1.25mM Na₃VO₄). Protein lysates were quantified using a standard BCA Protein Assay Kit (Pierce). Equal amounts of protein were loaded onto 4-20% gradient or 10% Bis-Tris gels and transferred to PVDF membranes according to standard protocols. Antibody detection was performed using SuperSignal West Pico Substrate (Thermo Scientific: 34077).

3.5.2. Phosphorylated protein Western blots

Western blots for phosphorylated proteins were performed as previously described¹⁹. Briefly, cells were either sorted directly into trichloroacetic acid (TCA, Sigma: T0699) or suspended in water and the final concentration of TCA was adjusted to be 10% v/v. Extracts were centrifuged at 13,200 rpm for 10 minutes at 4°C. Pellets were washed twice with acetone and dried at room temperature. Pellets were solubilized in 1% dithiothreitol, 9M urea, and 2% Triton X-100 and 4X LDS sample buffer was added (Invitrogen: NP0008) before lysates were incubated for 10 minutes at 70°C. Samples were run on Novex 4-12% gradient Bis-Tris gels (Invitrogen: NP0321) and transferred to PVDF membranes (Millipore). Antibody detection was performed using SuperSignal West Femto Substrate (Thermo Scientific: 34095). Membranes were stripped by

incubation with a stripping buffer consisting of 25mM glycine, pH 2, and 1% sodium dodecyl sulfate for 30 minutes at room temperature, with agitation.

3.6. Hspa9 knockdown studies

3.6.1. Virus generation and titer

Previously described Fcy-si control (shLUC) or Hspa9 knockdown (shHspa9 #3) vector plasmids were co-transfected into HEK293T cells with the packaging plasmids pMD-LgpRRE (containing HIV gag/pol), pCMV-G (containing VSV-G), and RSV-Rev (containing Rev) by the Washington University HOPE Center viral vectors core³. Hspa9 shRNAs are composed of a 21 or 23bp sequence (shLUC: 5'-GGT AGC GAC TAA ACA CAT CAA-3'; shHspa9 #3: 5'-GGG AGG CGT CTT TAC CAA ACT TA-3') and a 9bp loop (ttcaagaga) followed by the reverse complement 21 or 23bp sequence. Viral titers were evaluated by transduction of NIH3T3 cells followed by flow cytometric measurement of the percentage of YFP+ cells on a FACScan flow cytometer (BD biosciences) with FlowJo software.

3.6.2. Bone marrow transduction and transplantation

Bone marrow was harvested from 10 C57Bl/6 (Ly5.2) mice and pooled. Cells were stained with biotinylated antibodies against CD3e, B220, Ter119 and Gr-1 (eBiosciences) for lineage-depletion by AutoMACS column (Milteny Biotech) using anti-Biotin beads (Milteny Biotech: 130-90-485). Lineage-depleted bone marrow was plated in 6-well plates at a density of 4 million cells/well in α -MEM media containing 15% FCS, 50ng/mL mFlt3, 100ng/mL mSCF, 10ng/mL mL-3, 10ng/mL mTPO (Peprotech) and penicillin/streptomycin. Cells were transduced once with an MOI of 20 by spinning for 90 minutes at 2500rpm in the presence of 4 μ g/mL polybrene (American Bioanalytical: AB01643-00001) and 25mM HEPES buffer (Gibco: 15630-106). The following day, cells were pooled, counted and 0.75-1x10⁶ cells were transplanted into the retro-orbital sinus of lethally irradiated (1100Rads) recipients (Ly5.1).

3.6.3. Colony formation

YFP+ cells were sorted from recipients that received control (shLUC) or Hspa9-knockdown (shHspa9 #3) transduced bone marrow using an iCyt Synergy flow sorter (Sony). 100,000 cells were plated in CFU-PreB methylcellulose media (Stem Cell Technologies, M3630), in duplicate.

3.6.4. Flow cytometry

Peripheral blood, bone marrow and spleen cells were isolated and red blood cells were lysed as described in **Chapter 2, Section 3.9**. Hardy fractions and other lineage markers were labeled and analyzed by immunophenotypic markers detailed in **TABLE 2.5** using a Gallios or FACScan flow cytometer (BD Biosciences) and FlowJo Software.

3.7. BCR/ABL transplantation

3.7.1. Virus production

HEK293T cells were transfected with 48µg MSCV-p210-BCR/ABL-IRES-GFP vector²⁰ and 24µg EcoPAC packaging vector by calcium phosphate transfection using the CalPhos Mammalian Transfection Kit (Clontech: 631312). Viral supernatant was collected 48 and 72 hours later. Viral titer was evaluated by calculating the percentage of GFP+ cells per volume of virus added by flow cytometry of NIH3T3 cells transduced with the virus using a FACScan (BD Biosciences) and FlowJo software.

3.7.2. Transplantation

C57Bl/6 *Hspa9*^{+/-} mice were crossed with wild-type FVB mice. F1 *Hspa9*^{+/-} or *Hspa9*^{+/+} progeny were used as donors and *Hspa9*^{+/+} F1 mice as recipients. Bone marrow from 3 *Hspa9*^{+/+} or 3 *Hspa9*^{+/-} mice was pooled and plated at 5 million cells/mL in RPMI with 10% FCS. Cells were transduced once with an MOI of 0.1 by spinning for 90 minutes at 1000xg in the presence of 8µg/mL polybrene (American Bioanalytical: AB01643-00001) and 10mM HEPES buffer (Gibco: 15630-106). Bone marrow was rested for 1 hour at 37°C. Lethally irradiated recipients (1100 Rads) were transplanted by tail vein injection

with 1×10^5 transduced cells and 1×10^6 untransduced wild-type helper total bone marrow cells in 200 μ L PBS. Mice were sacrificed when moribund and bone marrow and spleen cells were cryopreserved.

4. Results

4.1. The expression of B-cell proliferation and activation genes is reduced in *Hspa9*^{+/-}

CFU-PreB colonies

To investigate whether a functional defect in downstream IL-7R signaling contributes to the reduction in CFU-PreB colonies in *Hspa9*^{+/-} mice, we performed gene expression array profiling on colonies produced by *Hspa9*^{+/-} and compared them to wild-type colonies. Day 7 colonies were collected from methylcellulose and sorted for B220+ cells (N=5 mice/genotype) (**FIGURE 3.1**). Analysis of mRNA expression levels revealed no global alterations as illustrated by the arrays not segregating by genotype in unsupervised hierarchical clustering. However, we identified small changes between *Hspa9*^{+/-} and wild-type colonies. Of the ~15,000 genes analyzed, 242 were significantly down-regulated and 169 were significantly up-regulated in *Hspa9*^{+/-} compared to controls. *Hspa9* expression was reduced by 50% in *Hspa9*^{+/-} versus *Hspa9*^{+/+} mice, as expected (**FIGURE 3.1**). When pathway analysis was performed on these genes using DAVID, we identified high enrichment scores (>3 fold enrichment) in pathways that promote lymphocyte proliferation and activation but no pathway enrichment in up-regulated genes (>1.5 fold enrichment) (**TABLE 3.1**). These results suggest that the reduction in CFU-PreB colonies may be due to blunted signaling *in vitro*. Nonetheless, it suggests that *in vivo* compensation may overcome the alterations seen *in vitro*, perhaps by increased cytokine production. Results of this assay were limited because it queried only the small number of cells that survived to Day 7 in CFU-PreB culture. Day 7 colonies consist of cells that have proliferated and differentiated from B-cell progenitors. Therefore, critical and potentially larger gene expression changes

may have been missed in populations that were more immature or died prior to this time point.

To further investigate B-cell proliferation *in vivo* we stained whole bone marrow for B-cell and proliferation markers. Bone marrow from 9-week old mice showed no significant difference in cell cycle distribution by Ki67 and DAPI staining in Hardy Fractions E, F or combined early fractions A-D (N=5 mice/genotype) (**FIGURE 3.2**).

4.2. IL-7, but not Flt3-ligand, partially rescues the CFU-PreB phenotype

IL-7, Flt3-ligand, and SCF cytokine signaling drive early B-cell maturation *in vivo*²¹⁻²³. To test whether increasing levels of cytokines *in vitro* could rescue the CFU-PreB phenotype, we added increasing concentrations of IL-7 in the media and observed a dose-dependent increase in *Hspa9*^{+/-} colonies compared to no increase in *Hspa9*^{+/+} colony numbers (fold change in colony formation from 10ng/mL to 50ng/mL IL-7 was 1.80 for *Hspa9*^{+/-} vs. 0.80 for *Hspa9*^{+/+}, p=0.01 by one-way ANOVA, N=6 mice/genotype) (**FIGURE 3.3**). Supplementation of the media with Flt3 ligand did not alter *Hspa9*^{+/-} or *Hspa9*^{+/+} CFU-preB colony formation, further implicating altered IL-7R signaling in the reduced CFU-PreB colonies (**FIGURE 3.3**).

To ensure that this dose-dependent increase was not due to differences in IL-7 receptor expression, we evaluated IL-7R α cell surface expression by flow cytometry. No significant difference in frequency or geometric mean was identified in Hardy fractions A-D in *Hspa9*^{+/-} vs *Hspa9*^{+/+} mice (N=5/genotype)(data not shown).

We also investigated IL-7 expression in the bone marrow of *Hspa9*^{+/-} vs *Hspa9*^{+/+} mice to determine if heterozygous mice overexpressed B-cell promoting cytokines as a mechanism of compensation. Femurs were flushed with Trizol and evaluated for mRNA expression

levels of *IL-7* and *Flt3-ligand* by qRT-PCR. *IL-6* mRNA levels were also measured as a negative control since we did not anticipate *IL-6* levels would be different. No significant difference was observed in mRNA levels of *IL-7*, *IL-6* or *Flt3-ligand* in young mice (3 months old, N=3/genotype) as well as *IL-6* or *IL-7* levels in old mice (18 months old, 3-6/genotype) (**FIGURE 3.4**). However, these results queried total bone marrow levels and do not exclude the possibility of smaller, local niche differences.

In summary, exogenous IL-7 could partially rescue the reduction of CFU-PreB colonies observed in *Hspa9*^{-/-} compared to *Hspa9*^{+/+} littermates *in vitro*. This response does not appear to be due to a difference in IL-7R α cell surface expression and evaluation of bone marrow *IL-7* expression revealed no large changes *in vivo*. However, this does not exclude the possibility of smaller, local niche changes in IL-7 concentration.

4.3. Analysis of B-cell progenitors in *Hspa9* knockdown mice

As described in **Chapter 2**, homozygous knockout of *Hspa9* was lethal prior to fetal liver formation, preventing analysis of *Hspa9*^{-/-} B-cell progenitors. In order to evaluate the effect of >50% reduction of *Hspa9*, we utilized a previously described shRNA knockdown model. We previously reported 2 shRNA's that reduce *Hspa9* levels 50-70% *in vivo* (levels are 30-50% of control expression). The more severe knockdown vector yielded few YFP⁺ cells available for analysis at 1 month. Therefore, we chose to use the less severe shRNA vector for further studies (shRNA #3). Previously, knockdown of *Hspa9* by this shRNA in a bone marrow transduction/transplantation model significantly reduced mature erythroid cells, erythroid progenitors and mature B-cells³. However, B-cell progenitors and precursors were not evaluated in this initial investigation.

We utilized this model to acutely reduce *Hspa9* levels more than 50% in order to study B-cell progenitors and precursors. Bone marrow was transduced with a control vector (shLUC) or a vector containing *Hspa9*-targeting shRNA (shHspa9) and transplanted into lethally irradiated recipient mice. Cells transduced with virus (YFP+) were sorted and the mRNA level of *Hspa9* was confirmed to be 37% of control cells (i.e., 63% knockdown)(**FIGURE 3.5**). YFP+ bone marrow cells with knockdown of *Hspa9* (shHspa9) had significantly reduced CFU-PreB colony formation compared to control (shLUC) cells (p=0.017, N=5-6 mice/genotype) (**FIGURE 3.6**).

In addition to colony forming ability, this model allowed us to interrogate stage-specific defects in B-cell maturation. Our results show a significant reduction in all Hardy fractions in YFP+ shHspa9 bone marrow (1.5-5.75 fold reduction), with the most notable difference in Hardy fraction D compared to control bone marrow (N=9 mice/group, p<0.05). YFP+ Hardy fractions B-F in the spleen of shHspa9 mice were also significantly reduced (1.7-3.5 fold, N=8 mice/group, p<0.05); however, fraction A was not significantly different when compared to control spleen cells (**FIGURE 3.7**). Fraction A cells are extremely rare in the spleen which may account for why we observe no difference. As previously described, the frequency of mature myeloid (Gr1+) and T-cell (CD3e+) populations were not significantly different following knockdown of *Hspa9* (data not shown).

Acute reduction of *Hspa9* levels (37% of control levels) in a bone marrow transduction/transplantation model resulted in a significant reduction in all Hardy Fractions of the bone marrow and a significant reduction in CFU-PreB colony formation, supporting a role for *Hspa9* in B-cell progenitor development.

4.4. Signaling downstream of the IL-7 receptor is altered in B-cells following *Hspa9* knockdown

Exogenous addition of the early B-cell promoting cytokine IL-7, but not Flt3-Ligand, is able to partially overcome the reduction in CFU-PreB colonies observed in *Hspa9*^{+/-} mice, indicating loss of *Hspa9* may alter downstream IL-7R signaling. In order to further investigate the role of *Hspa9* in IL-7 receptor signaling, we utilized the IL-7 dependent cell line known as B7 cells and *Hspa9*-targeting siRNAs¹⁸. The B7 cell line was made IL-7 dependent through stable integration of MSCV-mIL7R-IRES-GFP in the IL-3-dependent Ba/F3 cell line. We used a combination of flow cytometry and Western blot analysis to query downstream effectors of the IL-7R pathway.

4.4.1. Loss of *Hspa9* reduces B7 cell growth

We first tested the effects of IL-7 withdrawal on B7 cells. B7 cells are usually maintained in media containing 10ng/mL mIL-7. At lower concentrations of IL-7, B7 cells stop proliferating, allowing us to define the minimum dose of IL-7 required for normal B7 growth (**FIGURE 3.8**). B7 cells were electroporated with *Hspa9*-targeting siRNAs. Knockdown of *Hspa9* in B7 cells grown in sufficient amounts of IL-7 causes a reduction in cell numbers over time compared to B7 cells electroporated with non-targeting siRNA control. This result is similar to the reduction observed when cells are grown in low concentrations of IL-7 (**FIGURE 3.8**).

4.4.2. Rapid Stat5 phosphorylation can be measured by flow cytometry of B7 cells

IL-7 stimulation rapidly induces tyrosine phosphorylation of the IL-7 receptor and several downstream targets²⁴. We used B7 cells to query downstream targets of IL-7 by starving them of IL-7, which reduced phosphorylation of downstream targets, and spiking the

media with IL-7 to induce signaling through the IL-7 receptor. Stat5 is indispensable for B-cell development and is rapidly activated by phosphorylation by IL-7 stimulation of the IL-7 receptor²⁵. We used flow cytometry to evaluate phospho-Stat5 levels to optimize starvation and stimulation periods. Overnight starvation resulted in the largest shift in pStat5 levels by flow cytometry and almost undetectable levels by Western blot. Spiking cultures with 10ng/mL IL-7 rapidly induced phosphorylation of Stat5 with maximal detection 30 minutes following stimulation and high pStat5 levels at later time points (**FIGURE 3.9**).

4.4.3. Activation of Stat5, a major IL-7R downstream signaling molecule, is reduced by loss of Hspa9

B7 cells were electroporated with *Hspa9*-targeting siRNAs and allowed to rest for three days to ensure recovery from electroporation. At this time, Hspa9 protein levels were reduced more than 50% (**FIGURE 3.8**). B7 cells were then starved of IL-7 overnight and stimulated with different concentrations of IL-7 (0.1, 1 or 10ng/mL). Cells were collected at 4 time points following stimulation (5, 10, 15 and 30 minutes) for flow cytometry or 2 time points (10 and 30 minutes) for Western blot to evaluate phosphorylation of downstream targets. Phosphorylation of Stat5 was reduced at all time points and concentrations when evaluated by flow cytometry in B7 cells treated with siRNA against *Hspa9* (**FIGURE 3.9**). These results were confirmed by Western blot of cells following stimulation with 1ng/mL IL-7 (**FIGURE 3.9**).

Collectively, these results suggest that Stat5 phosphorylation is reduced following IL-7R stimulation in cells with reduced levels of *Hspa9*, *in vitro*. We next tested whether this occurred *in vivo*.

4.5. Loss of *Hspa9* prolongs survival of mice in a BCR-ABL induced leukemia model

Isolation and measurement of rare B-cell progenitor populations *in vivo* limited our ability to test Stat5 activation in *Hspa9*^{+/-} mice. Therefore, we used a model system that is dependent on B-cell Stat5 activation. IL-7R signaling is a key mediator of B-cell differentiation and proliferation. During basal rates of lymphopoiesis *in vivo*, B-cells may be able to compensate for delayed or reduced IL-7R signaling through cross talk with other cytokines or increased levels of IL-7 in the local niche. However, when B-cell progenitors are pressed to rapidly proliferate by the introduction of an oncogene (BCR-ABL), this defect may reduce the rate of proliferation and therefore delay the onset of oncogene-induced leukemia.

To investigate whether *Hspa9*^{+/-} B-cell progenitors were able to rapidly proliferate in response to stress *in vivo*, we utilized an MSCV-p210-BCR/ABL-IRES-GFP system. When F1 mice generated from an FVB x C57Bl/6 cross are transplanted with bone marrow transduced with MSCV-p210-BCR/ABL-GFP, they rapidly develop and succumb to B-ALL²⁶. This leukemia development requires rapid expansion of B-cell progenitors and BCR-ABL leukemias are known to be Stat5 dependent²⁷⁻³⁰. Survival is prolonged in mice that received *Hspa9*^{+/-} compared to mice that received *Hspa9*^{+/+} bone marrow transduced with BCR/ABL, suggesting Stat5 activation may be reduced *in vivo* in *Hspa9*^{+/-} mice (N=20/genotype, p=0.045, representative of 3 independent cohorts)(**FIGURE 3.10**).

5. Discussion

We have shown that *Hspa9*^{+/-} mice have a hematopoietic cell-intrinsic reduction in CFU-PreB colony numbers that is not due to a difference in B-cell progenitor frequency. In order to investigate how loss of *Hspa9* can affect B-cell progenitor function, we first investigated gene expression changes in CFU-PreB colonies from *Hspa9*^{+/-} and *Hspa9*^{+/+} controls. Although we did not observe large unsupervised differences in gene expression between genotypes, supervised

analysis identified that genes with significantly reduced expression were enriched in pathways associated with proliferation and B-cell activation. With this analysis, we may have missed larger changes in gene expression that occurred in the cultures at earlier time points due to cell death induced by loss of Hspa9. This discovery did, however, lead us to further pursue signaling pathways key to B-cell progenitor proliferation (e.g., IL-7 receptor signaling).

IL-7 is the only cytokine added to CFU-PreB methylcellulose culture media. Therefore, we first focused on IL-7R signaling. Although relative levels of IL-7 expression in whole bone marrow was not altered in *Hspa9*^{+/-} mice compared to *Hspa9*^{+/+} littermates, *in vitro* responses to IL-7 differed. The addition of higher concentrations of exogenous IL-7 to CFU-PreB cultures was able to partially rescue the number of CFU-PreB colonies from *Hspa9*^{+/-} mice, but had no effect on colonies from wild-type littermates, indicative of blunted IL-7R signaling in *Hspa9*^{+/-} B-cells. Several possible explanations exist for the lack of increased IL-7 expression in bulk bone marrow from *Hspa9*^{+/-} versus *Hspa9*^{+/+} mice. First, local (i.e., niche specific) concentrations of IL-7 may be different in *Hspa9*^{+/-} mice, which could account for the observed *in vivo* compensation. However, if this were the case, B-cell progenitors would likely be outcompeted in a competitive transplant setting, which was not observed at steady state or following B-cell stress. Second, local IL-7 concentrations may be high enough *in vivo* that *Hspa9*^{+/-} B-cell progenitors are not significantly affected. Third, CFU-PreB media contains only IL-7, while *in vivo* B-cell differentiation and proliferation are regulated by multiple cytokines that may contribute to *in vivo* compensation^{23,31-33}. Flt3-ligand acts synergistically with IL-7 to promote expansion of hematopoietic progenitors³². However, the addition of Flt3-ligand to CFU-PreB media was unable to restore CFU-PreB colony formation by *Hspa9*^{+/-}. Although this was not mediated by Flt3-ligand, cross talk between multiple signaling pathways may allow *Hspa9*^{+/-} cells to be less IL-7 dependent *in vivo*. For example, Stat proteins can compensate for the loss of each other. Like many cytokine signaling pathways, IL-7R utilizes the Jak/Stat pathway, primarily activating

Stat3 and Stat5a/b^{24,25}. In one example, loss of Stat5 in hepatocytes led to inappropriate activation of Stat1 and Stat3 through reduced expression of negative regulators of Stat signaling, resulting in compensation for the loss of Stat5 signaling in these cells³⁴.

In order to test whether loss of *Hspa9* altered IL-7R signaling, we analyzed downstream targets in an IL-7 dependent murine B-cell line. We first focused on Stat5 for the following reasons. Stat5 is a critical target of IL-7R signaling and is responsible for inducing expression of pro-survival and pro-proliferation genes^{24,35,36}. B-lymphopoiesis in Stat5a^{-/-}/b^{-/-} mice is arrested at the pre-pro B stage^{25,34,37}. Overexpression of Stat5 can restore B-cell development in IL-7^{-/-} mice, indicating it is the primary target of IL-7R signaling^{38,39}. Indeed, we show by flow cytometry and Western blot that Stat5 phosphorylation following IL-7R stimulation is impaired by knockdown of *Hspa9*. Total levels of Stat5 do not appear to change by Western blot following knockdown of *Hspa9*, indicating that activation, not expression, of Stat5 may be regulated by *Hspa9*.

One possible mechanism for how *Hspa9* could regulate Stat5 is through its J-protein Dnaja3, which has been shown to be a negative regulator of Stat5b⁴⁰. Dnaja3 is the J protein associated with *Hspa9*'s non-mitochondrial import functions and recruits substrates to *Hspa9*⁴¹.

Phosphorylation of Stat5 by cytokine stimulation resulted in disassociation of Dnaja3 from Stat5b in two IL-7 responsive B-cell lines (697 pre-B cells and Ba/F3, the B7 parental pro-B cell line)⁴⁰. Conversely, increasing amounts of Dnaja3 resulted in dose-dependent inhibition of Stat5 phosphorylation, cell growth, and expression of the Stat5 target Bcl-xl. Therefore, reduced levels of the highly expressed *Hspa9* may increase the cellular availability of its J protein, Dnaja3. Increased Dnaja3 availability, in turn, may bind Stat5b, inhibiting its phosphorylation and reducing the expression of Stat5 target genes.

In a similar fashion, Hspa9 and Dnaja3 proteins have been implicated in opposing regulation of another transcription factor, p53⁴²⁻⁴⁴. Dnaja3 overexpression promotes p53 mitochondrial translocation and apoptosis while a reduction in Hspa9, which binds p53 in the cytoplasm, results in translocation of p53 into the nucleus. Hspa9 and Dnaja3 may regulate Stat5 translocation in a similar way through protein interactions. In addition to nuclear translocation, Stat5, but not Stat3 or Stat1, was shown to translocate to the mitochondria following cytokine stimulation in Ba/F3 cells and to stimulate mitochondrial DNA transcription⁴⁵. Like its pro-apoptotic role in p53 regulation, Dnaja3 may promote apoptosis by preventing the translocation of Stat5 and thus prevent up-regulation of pro-survival signals. Meanwhile, Hspa9 may act antagonistically to this process by binding Dnaja3. Future studies of Stat5 regulation by Dnaja3 and Hspa9 could be informed by prior studies of p53 regulation by Dnaja3 and Hspa9.

Dnaja3 was also shown to reduce levels of Stat5b, but not Stat5a, following overexpression of Dnaja3; however, the mechanism of this inhibition is unknown. Although we do not see changes in total Stat5 levels following Hspa9 knockdown, we utilized an antibody that recognizes both Stat5a and Stat5b. Therefore, our use of a pan Stat5 antibody may have masked an effect on Stat5b levels. Future studies utilizing Stat5a and Stat5b specific antibodies will be required to determine if Stat5b levels are altered by Hspa9 knockdown.

While our B-cell progenitor signaling studies have focused on IL-7R signaling, signaling of the pre-B cell receptor (pre-BCR) is another important receptor for B-lymphopoiesis. As B-cells differentiate and migrate away from the HSC niche, IL-7 becomes less available and B-cells become more IL-7 sensitive^{46,47}. During this transition, B-cells undergo selection for appropriate pre-BCR rearrangement and expression. Effective rearrangement and expression of the pre-BCR makes pro-B cells more sensitive to lower doses of IL-7 through cross talk of pathways downstream of both the IL-7R and the pre-BCR such as the PI3K and MAPK/Erk pathways⁴⁸⁻⁵².

Both Erk1/2 and PI3K signaling promote B-cell proliferation and differentiation^{51,52}. Conditional knockout of Erk1/2 in mice (Erk1^{-/-}/2^{-/-}) have a block in B-cell differentiation at the pro-B to pre-B transition, and conditional knockout of two PI3K isoforms in mice (p110α^{-/-}δ^{-/-}) resulted in a block at the pre-B stage^{49,53}. Using our system, we identified no differences in total levels of Erk1/2 or Akt, a key downstream target of PI3K (data not shown). Our investigation of Erk1/2 activation is ongoing and will be discussed further in **Chapter 4**, and although we could readily detect Akt in B7 cells, we were unable to detect phosphorylation of Akt in B7 cells stimulated with IL-7. These results are consistent with another report using IL-7R expressing Ba/F3 cells derived independently of the B7 cells we have used, suggesting pAkt is not a dominant downstream target of IL-7R signaling in B7 cells³². However, whether Hspa9 is involved in the activation of Akt by the Pi3K pathway in pre-B cells should be addressed in future studies and will be discussed further in **Chapter 4**.

Although our novel *Hspa9*^{+/-} mouse models the heterozygous loss of human HSPA9 in MDS, possible differences exist and may indicate that >50% knockdown of Hspa9 is required for hematopoietic dysfunction in mice. Previous studies have demonstrated that *HSPA9* mRNA is 50% reduced in patients with MDS¹⁰. However, HSPA9 has not been measured at the protein level, which could be lower. Post-translational modifications of unknown function have been identified for HSPA9^{54,55}. Such modifications may affect its stability or localization. Additionally, the threshold for dysfunction due to loss of Hspa9 may be different in mice, requiring >50% knockdown to recapitulate dysfunction observed in humans. Homozygous loss of *Hspa9* is lethal prior to fetal liver formation, so they could not be used for further hematopoietic studies. To investigate the effects of >50% loss of Hspa9, we transduced bone marrow cells with virus carrying an shRNA that targets *Hspa9* and transplanted these cells into lethally irradiated recipients. Achieving 63% knockdown of *Hspa9* mRNA, we first set out to determine the colony forming ability of bone marrow following *Hspa9* knockdown and observed a reduction in CFU-

PreB colony formation similar to what is seen in *Hspa9*^{+/-} mice. *In vivo*, >50% knockdown of *Hspa9* resulted in a significant reduction in B-cell progenitors and precursors (CLPs and Hardy fractions) when compared to control mice. Collectively, these studies strongly imply appropriate HSPA9 expression levels may be needed in normal human B-cell lymphopoiesis.

These results led us to further investigate the effects of Hspa9 loss on B-cells *in vivo*. We utilized a Stat5-dependent system to induce B-ALL in *Hspa9*^{+/-} and *Hspa9*^{+/+} littermates. Stat5 is constitutively activated and required for transformation and leukemic development by Abelson oncogenes, including the BCR-ABL fusion^{24,27-30,56}. The rapid onset of BCR-ABL-induced leukemia requires rapid proliferation of the very small percentage of cells transduced with BCR-ABL in order to become the dominant clone. We hypothesized that cells with impaired Stat5 signaling would be unable to rapidly proliferate, resulting in longer leukemic latency. Although mild, the prolonged survival of mice that received *Hspa9*^{+/-} bone marrow versus *Hspa9*^{+/+} bone marrow following BCR-ABL transduction was consistent across three cohorts of transplanted mice. Further investigation of the distribution of leukemic subtypes is ongoing and may reveal additional differences in B-cell phenotypes (i.e., Hardy fractions) between leukemias induced in *Hspa9*^{+/-} and *Hspa9*^{+/+} mice.

Collectively, we have demonstrated Hspa9 is involved IL-7R signaling. Gene expression pathways associated with B-cell signaling and activation are significantly reduced in CFU-PreB colonies from *Hspa9*^{+/-} mice. Further analysis of IL-7R signaling revealed impaired Stat5 activation following IL-7 stimulation of B7 cells treated with siRNA against *Hspa9*. Future experiments will reveal whether Stat5 activation is altered in B-cells of MDS patients with del(5q), contributing to the observed reduction in B-cell progenitors.

Figure 3.1: *Hspa9*^{+/-} B-cells isolated from CFU-PreB culture have an ~50% reduction in *Hspa9* mRNA expression

Bone marrow from *Hspa9*^{+/-} or *Hspa9*^{+/+} mice was plated in CFU-PreB culture media. On day 7, colonies were counted and cells were isolated from methylcellulose. RNA from B220+ cells was hybridized to Mouse Gene 1.0 ST arrays (Affymetrix) and analyzed for mRNA expression. Levels of *Hspa9* mRNA were ~50% reduced in *Hspa9*^{+/-} samples compared to *Hspa9*^{+/+} samples (N=5/genotype). Statistical analysis by two tailed Student's t-test. Error bars represent mean ± SD.

Figure 3.2: The cell cycle distributions of *Hspa9*^{+/-} bone marrow and spleen B-cell fractions are not different than *Hspa9*^{+/+} B-cell fractions

Bone marrow (*black circles*) and spleen cells (*blue circles*) from 2 month old *Hspa9*^{+/-} and *Hspa9*^{+/+} littermates were isolated and stained for cell surface markers prior to fixation and permeabilization for intracellular staining. Cells were stained for Ki67 and DAPI for cell cycle analysis (*top panel*, cells in G₀/G₁ of cell cycle; *bottom panel*, cells in G₂/M/S of cell cycle). Hardy fractions are divided as follows: A-D (B220+, IgM-, IgD-), E (B220+, IgM-, IgD+) and F (B220+, IgM+, IgD+). (BM, bone marrow; Spl, Spleen)

Figure 3.3: Exogenous IL-7, but not Flt3-ligand, partially rescues the reduction in *Hspa9*^{+/-} CFU-PreB colony formation

Bone marrow from *Hspa9*^{+/-} (*red bars*) or *Hspa9*^{+/+} mice (*white bars*) was harvested and grown in methylcellulose containing 10ng/mL IL-7 (M3630 media) supplemented with additional **A**) IL-7 (N=6/genotype) or **B**) Flt-3 ligand (N=3/genotype). *Hspa9*^{+/-} colony numbers were significantly increased following the addition of exogenous IL-7 (one-way ANOVA, p=0.01) while *Hspa9*^{+/-} colony numbers were significantly decreased with increasing IL-7 (one-way ANOVA, p<0.01).

No change was seen in either genotype after addition of Flt3-Ligand. Error bars represent mean \pm SD.

Figure 3.4: Total bone marrow expression of *IL-7*, *IL-6* and *Flt3-ligand* are not different in *Hspa9*^{+/-} mice

Femurs from *Hspa9*^{+/-} (grey bars) and *Hspa9*^{+/+} littermates (white bars) at 3 months (solid bars) and 18 months of age (checkered bars) were flushed with Trizol. Expression of **A) *IL-7***, **B) *Flt3-ligand*** and **C) *IL-6*** were measured by qRT-PCR (N=3-6/genotype). Error bars represent mean \pm SD.

Figure 3.5: *Hspa9* expression levels are reduced more than 50% by shRNA-mediated knockdown

A) Expression of *Hspa9* analyzed by qRT-PCR in bone marrow cells from *Hspa9*^{+/+} (open circles) and *Hspa9*^{+/-} mice (filled circles) (N=3mice/genotype) compared to YFP+ bone marrow cells sorted from mice that received Fcysi-shLUC (open squares) and Fcysi-sh*Hspa9* (filled squares) transduced bone marrow (N=7-8mice/group). Reduction of *Hspa9* at the mRNA level is greater in shRNA-mediated knockdown (63%) than observed in heterozygous knockout mice (*Hspa9*^{+/-}, 47%). **B)** Expression of *Gm26109* in the same bone marrow populations showing shRNA-mediated knockdown does not alter *Gm26109* expression. Error bars represent mean \pm SD.

Figure 3.6: CFU-PreB colony numbers are significantly reduced in mice that received Fcysi-sh*Hspa9*-transduced bone marrow

YFP+ sorted bone marrow cells from Fcysi-shLUC or Fcysi-sh*Hspa9* mice 10-12 weeks post-transplant were plated in CFU-PreB methylcellulose medium. CFU-PreB colonies were counted

on day 7 and significantly reduced in Fc γ si-shHspa9 mice (p=0.017). Statistical analysis by two tailed Student's t-test. Error bars represent mean \pm SD.

Figure 3.7: Significant reduction in B-cell progenitors in mice following lentiviral-mediated knockdown of *Hspa9*

Frequency of bone marrow and spleen cells from mice 8-12 weeks following transplantation with bone marrow transduced with lentivirus containing control (shLUC) or *Hspa9*-targeting shRNA (shHspa9). **A)** The frequency of YFP⁺ cells is significantly reduced in the bone marrow and spleens of mice that received shHspa9-transduced bone marrow (*red circles*) compared to shLUC-transduced control (*blue circles*), as previously described³. The frequency of CLP's (**B**) and Hardy fractions A-F from the bone marrow (**C**) and spleen (**D**) within the YFP⁺ population of recipient mice is significantly reduced. Statistical analysis by two tailed Student's t-test. Error bars represent mean \pm SD. *p<0.05, **p<0.01, ***p<0.001

Figure 3.8: Reduction in IL-7 levels and knockdown of *Hspa9* in IL-7 dependent cells (B7) reduces cell counts in culture

B7 cells were electroporated with a non-targeting siRNA or siRNA targeting *Hspa9*. The following day (Day 1), cells were counted and replated at the same cell concentration. Cells were maintained at <1 million cells/mL and counted each day. **A)** Hspa9 levels were evaluated by Western blot on day 2. **B)** Growth of B7 cells maintained in 10ng/mL IL-7 is significantly inhibited by knockdown of *Hspa9* by two independent *Hspa9*-targeting siRNAs (Day 4 siRNA 1 vs Control, N=3/group, p=0.004, *Students t-test*). **C)** Lowering the concentration of IL-7 in the media also reduces cell counts (N=2). Error bars represent mean \pm SD.

Figure 3.9: Stat5 activation by IL-7 receptor signaling is reduced in B7 cells following knockdown of *Hspa9*

B7 cells were starved of cytokine overnight and spiked with various concentrations of IL-7 to stimulate phosphorylation of Stat5. Lysates were collected at designated times. **A)** Representative histogram of flow cytometry results showing activation of pStat5 in B7 cells starved overnight (*grey line*) and following IL-7 stimulation at different time points (*colored histograms*). **B)** Geometric mean of pStat5 fluorescence measured by flow cytometry over time showing maximal signaling 30 minutes after IL-7 stimulation. **C) Left panel:** Representative flow cytometry histogram showing reduced pStat5 levels in *Hspa9* knockdown cells 5 minutes after B7 cells were stimulated with 1ng/mL IL-7 (*Grey*, IL-7 starved cells; *Blue*, *Hspa9*-targeting siRNA; *Red*, non-targeting siRNA). *Right panel:* The geometric mean of pStat5 fluorescence is depicted for cells treated with non-targeting control (*solid lines*) or *Hspa9*-targeting siRNA (*dashed lines*) following IL-7 stimulation with 0.1ng/mL (*green lines*) or 1ng/mL (*red lines*). Similar results were noted with 10ng/mL IL-7 stimulation (data not shown). Geometric mean of pStat5 in B7 cells starved of IL-7 is shown (*dotted black line*). Representative data is shown from 3 biological replicates. **D)** Western blot of lysates from B7 cells treated with *Hspa9*-targeting siRNA or non-targeting control were analyzed for Stat5 phosphorylation. Cells were grown in 10ng/mL IL-7 for 4 days (*Lane 1 and 2*). Cells were starved overnight starting on day 3 (*Lane 3 and 4*). Cells were starved overnight and stimulated on day 4 with 1ng/mL IL-7 and lysates were collected after 10 minutes (*Lane 5 and 6*) and 30 minutes (*Lane 7 and 8*). Levels of Stat5 phosphorylation, but not total Stat5, were reduced in cells treated with *Hspa9*-targeting siRNA. Representative data is shown from 4 biological replicates.

Figure 3.10: Prolonged survival of BCR-ABL induced leukemia in *Hspa9*^{+/-} mice

Induction of leukemia by BCR-ABL was previously shown to be Stat5-dependent. Survival of recipients that received MSCV-p210-IRES-GFP transduced *Hspa9*^{+/-} bone marrow was extended compared to *Hspa9*^{+/+} recipients (p=0.045, Log-rank test). Data includes 3 independently transduced and transplanted cohorts of mice (N=20 mice/genotype).

Figure 3.1: *Hspa9*^{+/-} B-cells isolated from CFU-PreB culture have an ~50% reduction in *Hspa9* mRNA expression

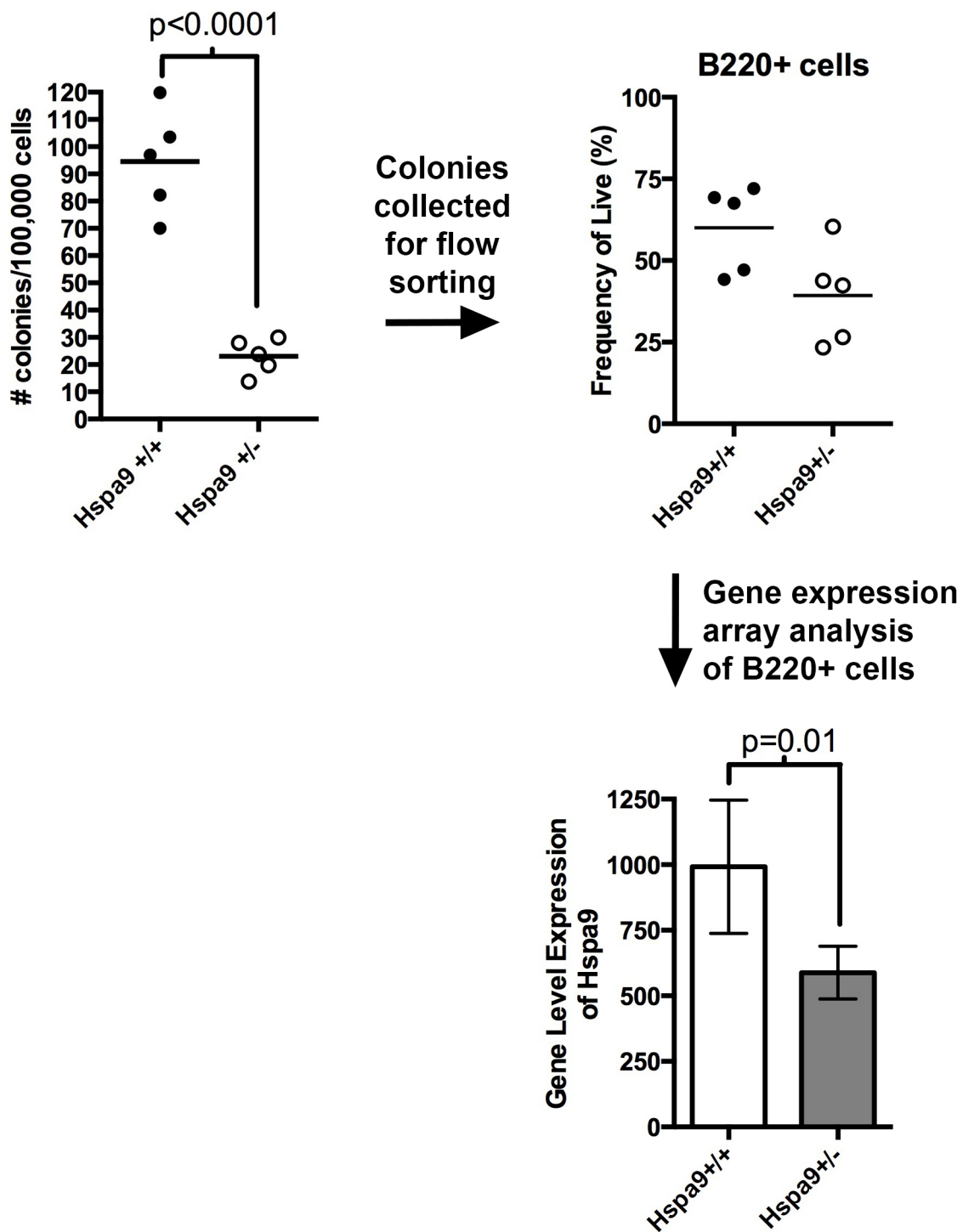


Figure 3.2: The cell cycle distributions of *Hspa9*^{+/-} bone marrow and spleen B-cell fractions are not different than *Hspa9*^{+/+} B-cell fractions

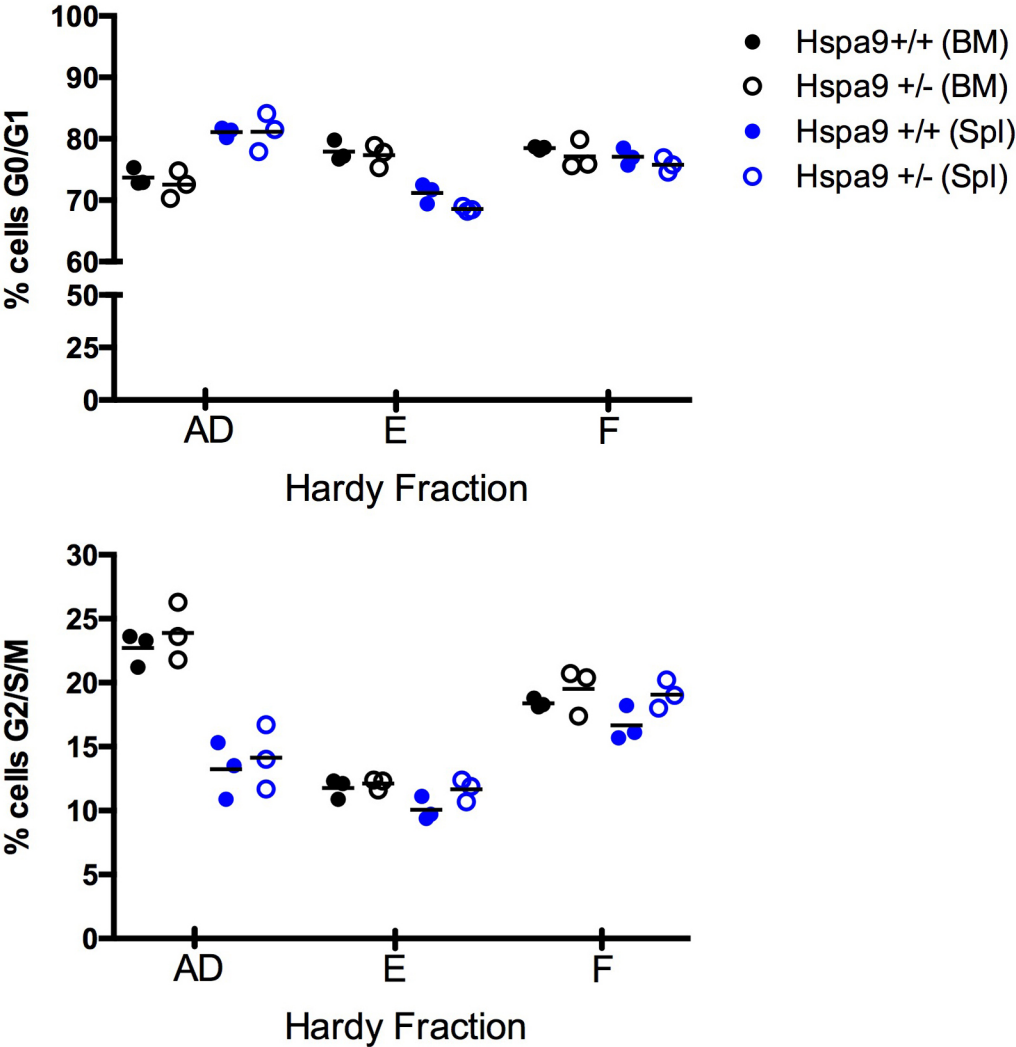


Figure 3.3: Exogenous IL-7, but not Flt3-ligand, partially rescues the reduction in *Hspa9*^{+/-} CFU-PreB colony formation

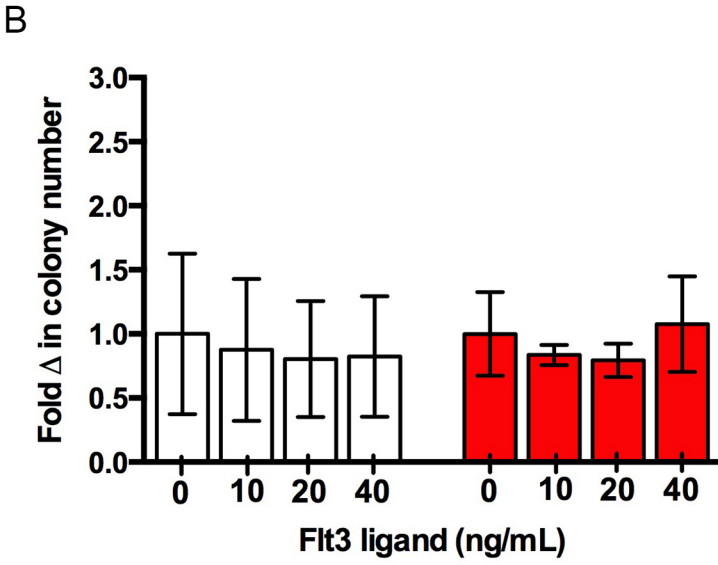
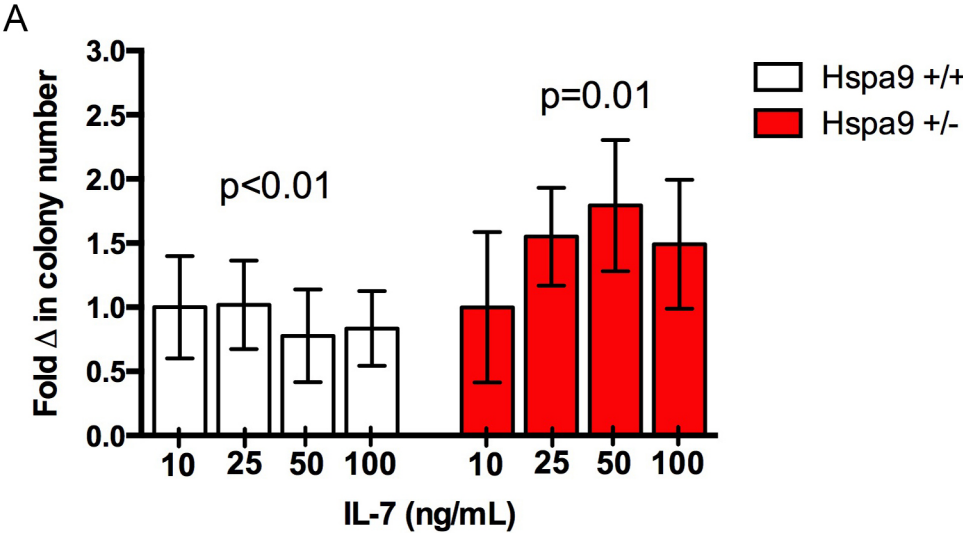


Figure 3.4: Total bone marrow expression of *IL-7*, *IL-6* and *Flt3-ligand* are not different in bone marrow of *Hspa9^{+/-}* mice

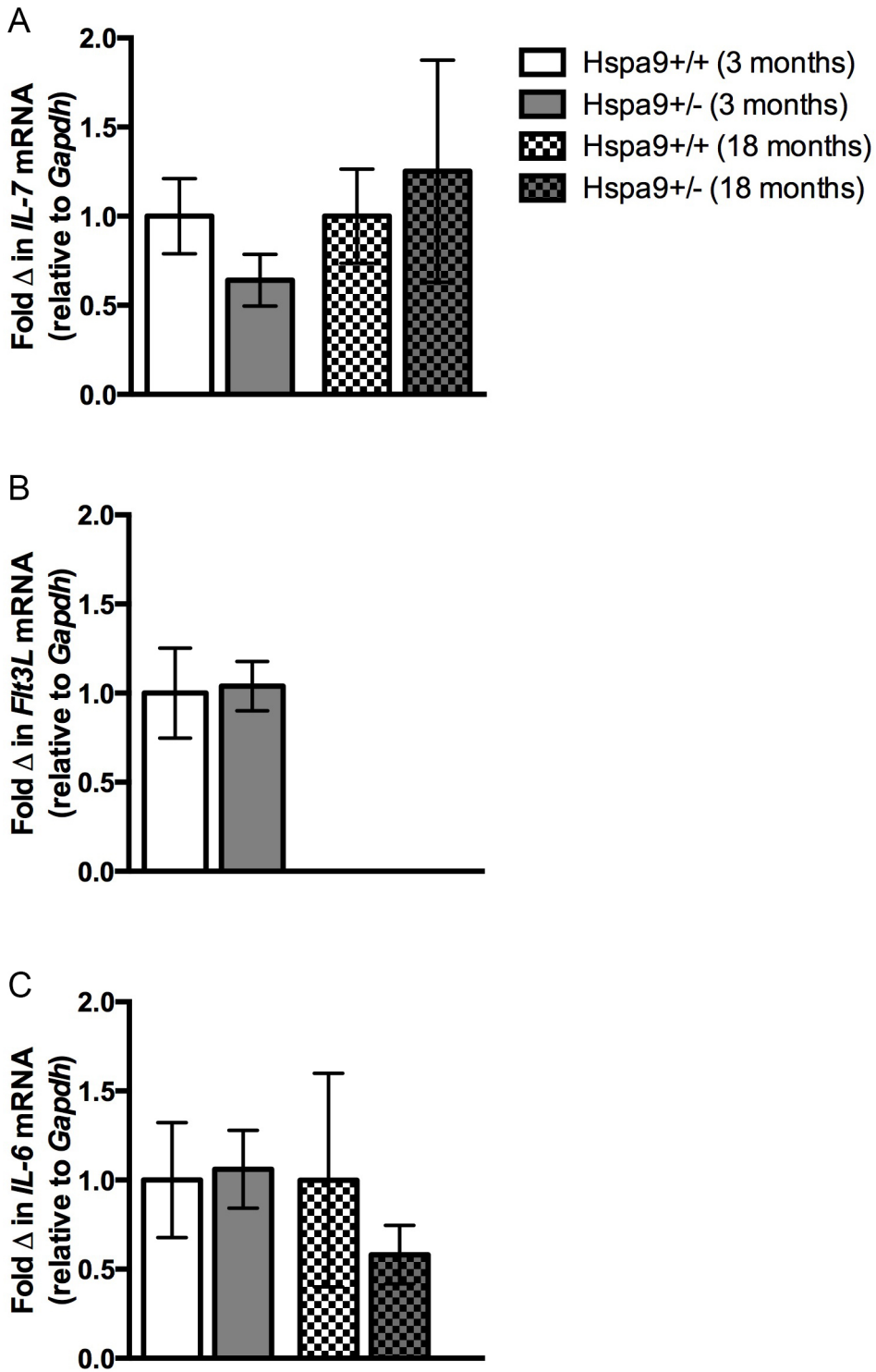


Figure 3.5: *Hspa9* expression levels are reduced more than 50% by shRNA-mediated knockdown

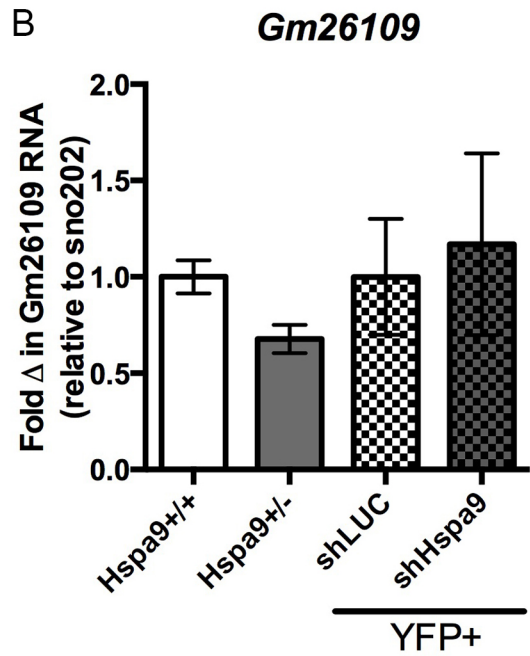
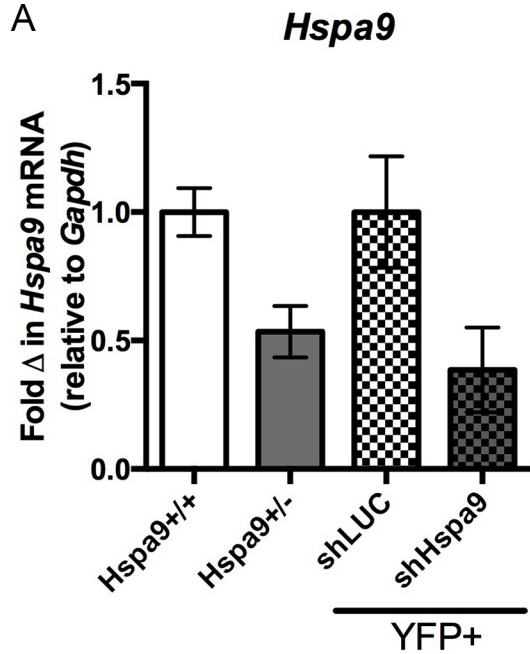


Figure 3.6: CFU-PreB colony numbers are significantly reduced in mice that received Fc γ si-shHspa9-transduced bone marrow

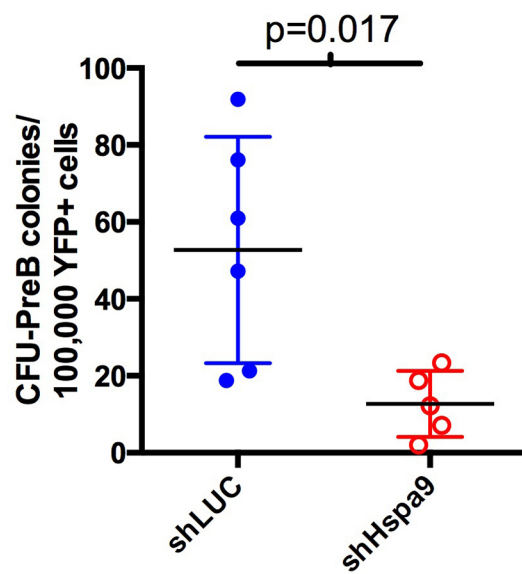


Figure 3.7: Significant reduction in B-cell progenitors in mice following lentviral-mediated knockdown of *Hspa9*

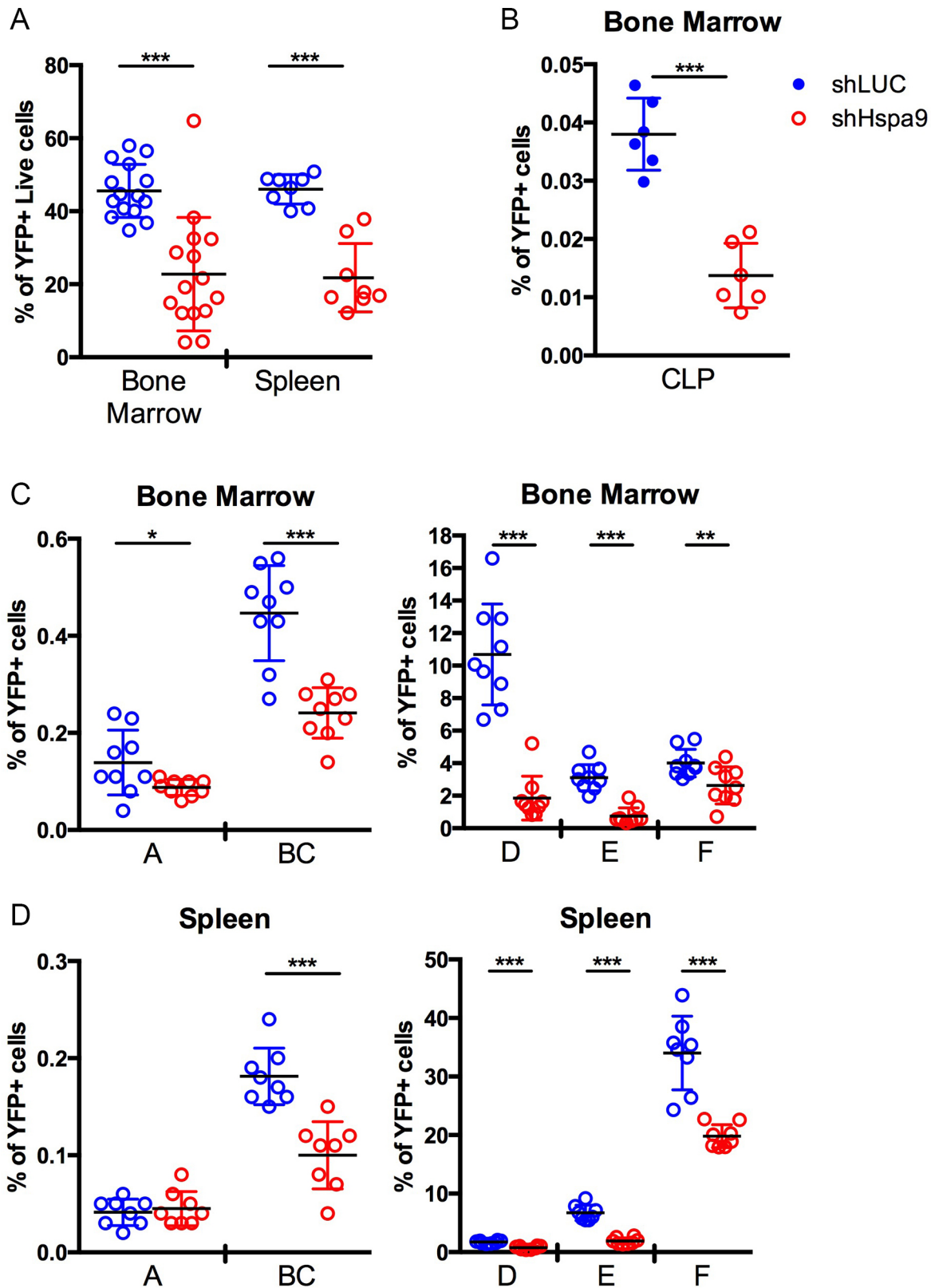


Figure 3.8: Reduction in IL-7 levels and knockdown of *Hspa9* in IL-7 dependent cells (B7) reduces cell counts in culture

A

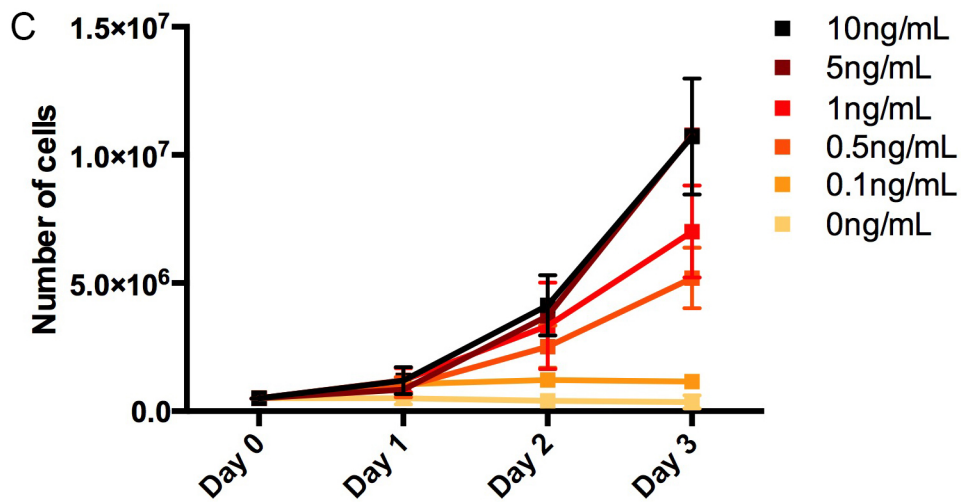
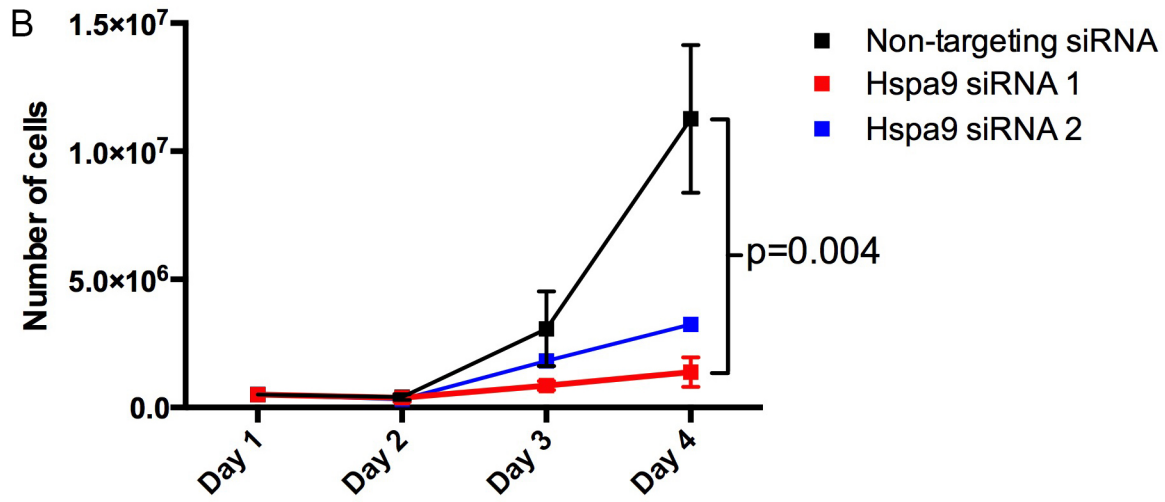
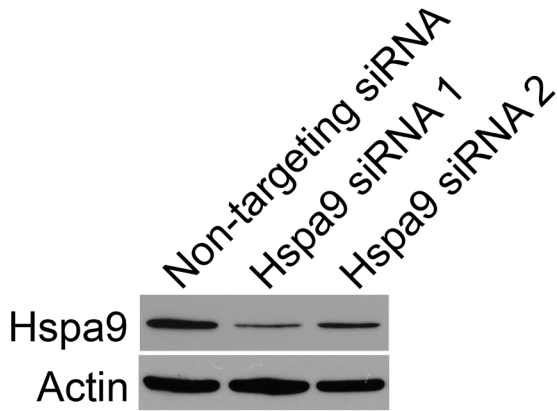


Figure 3.9: Stat5 activation by IL-7 receptor signaling is reduced in B7 cells following knockdown of *Hspa9*

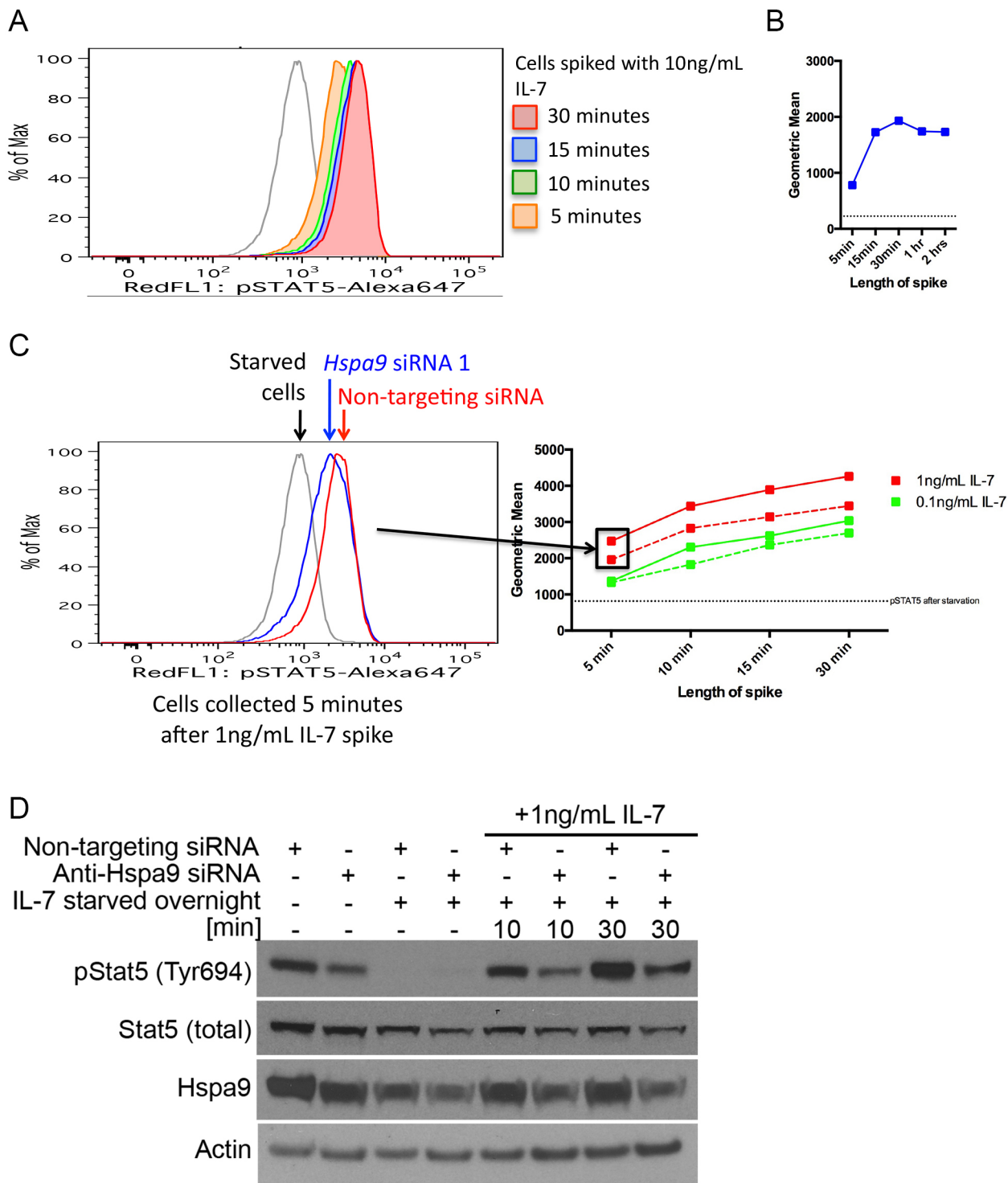


Figure 3.10: Prolonged survival of BCR-ABL induced leukemia in *Hspa9*^{+/-} mice

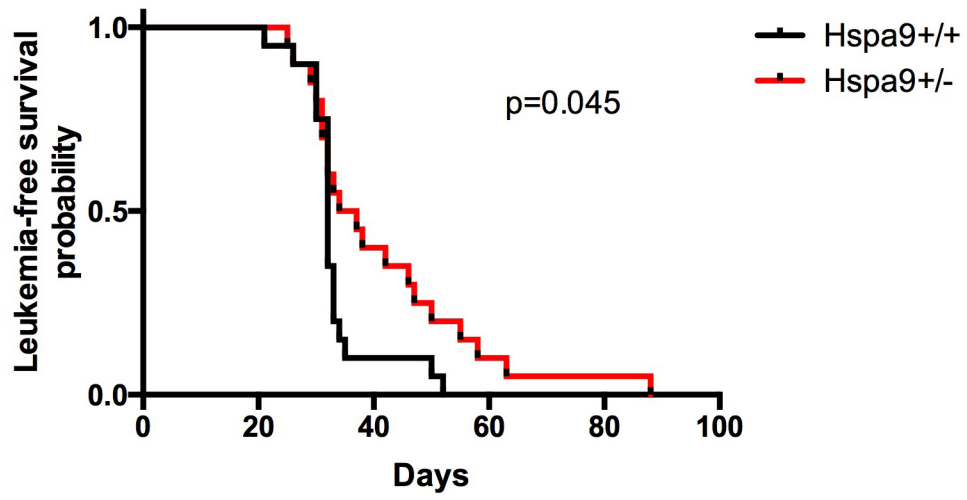


Table 3.1: Enriched pathways in genes significantly down-regulated in *Hspa9*^{+/-} CFU-PreB colonies

Annotation Cluster 1: Enrichment Score 5.02				
Term		# genes	PValue	Benjamini
GO:0045321	leukocyte activation	13	5.56E-06	6.28E-03
GO:0046649	lymphocyte activation	12	8.65E-06	4.89E-03
GO:0001775	cell activation	13	1.80E-05	6.77E-03
Annotation Cluster 2: Enrichment Score 3.48				
GO:0051249	regulation of lymphocyte activation	9	1.94E-04	5.36E-02
GO:0032944	regulation of mononuclear cell proliferation	7	2.51E-04	5.53E-02
GO:0050670	regulation of lymphocyte proliferation	7	2.51E-04	5.53E-02
GO:0070663	regulation of leukocyte proliferation	7	2.87E-04	5.28E-02
GO:0002694	regulation of leukocyte activation	9	3.07E-04	4.85E-02
GO:0050865	regulation of cell activation	9	3.35E-04	4.64E-02
GO:0050863	regulation of T cell activation	7	1.24E-03	1.31E-01

REFERENCES

1. Yoshinari, N., Ishida, T., Kudo, A. & Kawakami, A. Gene expression and functional analysis of zebrafish larval fin fold regeneration. *Dev. Biol.* (2009).
2. Craven, S. E., French, D., Ye, W., de Sauvage, F. & Rosenthal, A. Loss of Hspa9b in zebrafish recapitulates the ineffective hematopoiesis of the myelodysplastic syndrome. *Blood* **105**, 3528–3534 (2005).
3. Chen, T. H.-P. *et al.* Knockdown of Hspa9, a del(5q31.2) gene, results in a decrease in hematopoietic progenitors in mice. *Blood* **117**, 1530–1539 (2011).
4. Tai-Nagara, I., Matsuoka, S., Ariga, H. & Suda, T. Mortalin and DJ-1 coordinately regulate hematopoietic stem cell function through the control of oxidative stress. *Blood* **123**, 41–50 (2014).
5. Wu, P. K. *et al.* A Mortalin/HSPA9-Mediated Switch in Tumor-Suppressive Signaling of Raf/MEK/Extracellular Signal-Regulated Kinase. *Mol. Cell. Biol.* **33**, 4051–4067 (2013).
6. Ohtsuka, R. *et al.* Mortalin is a novel mediator of erythropoietin signaling. *Eur. J. Haematol.* **79**, 114–125 (2007).
7. Haase, D. *et al.* New insights into the prognostic impact of the karyotype in MDS and correlation with subtypes: evidence from a core dataset of 2124 patients. *Blood* **110**, 4385–4395 (2007).
8. Zhao, N. *et al.* Molecular delineation of the smallest commonly deleted region of chromosome 5 in malignant myeloid diseases to 1-1.5 Mb and preparation of a PAC-based physical map. *Proc. Natl. Acad. Sci. U.S.A.* **94**, 6948–6953 (1997).
9. Horrigan, S. K. *et al.* Delineation of a minimal interval and identification of 9 candidates for a tumor suppressor gene in malignant myeloid disorders on 5q31. *Blood* **95**, 2372–2377 (2000).
10. Graubert, T. A. *et al.* Integrated Genomic Analysis Implicates Haploinsufficiency of Multiple Chromosome 5q31.2 Genes in De Novo Myelodysplastic Syndromes Pathogenesis. *PLoS ONE* **4**, e4583 (2009).
11. Lai, F. *et al.* Transcript map and comparative analysis of the 1.5-Mb commonly deleted segment of human 5q31 in malignant myeloid diseases with a del(5q). *Genomics* **71**, 235–245 (2001).
12. Jerez, A. *et al.* Topography, clinical, and genomic correlates of 5q myeloid malignancies revisited. *J. Clin. Oncol.* **30**, 1343–1349 (2012).
13. Sternberg, A. *et al.* Evidence for reduced B-cell progenitors in early (low-risk) myelodysplastic syndrome. *Blood* **106**, 2982–2991 (2005).
14. Amin, H. M. *et al.* Increased apoptosis in bone marrow B lymphocytes but not T lymphocytes in myelodysplastic syndrome. *Blood* **102**, 1866–1868 (2003).
15. Pang, W. W. *et al.* Hematopoietic stem cell and progenitor cell mechanisms in myelodysplastic syndromes. *Proc. Natl. Acad. Sci. U.S.A.* **110**, 3011–3016 (2013).
16. Pellagatti, A. *et al.* Deregulated gene expression pathways in myelodysplastic syndrome hematopoietic stem cells. *Leukemia* **24**, 756–764 (2010).
17. Nilsson, L. *et al.* Isolation and characterization of hematopoietic progenitor/stem cells in 5q-deleted myelodysplastic syndromes: evidence for involvement at the hematopoietic stem cell level. *Blood* **96**, 2012–2021 (2000).
18. Mullighan, C. G. *et al.* Rearrangement of CRLF2 in B-progenitor- and Down syndrome-associated acute lymphoblastic leukemia. *Nat. Genet.* **41**, 1243–1246 (2009).
19. Magee, J. A. *et al.* Temporal Changes in PTEN and mTORC2 Regulation of Hematopoietic Stem Cell Self-Renewal and Leukemia Suppression. *Stem Cell* **11**, 415–428 (2012).
20. Zhang, X. & Ren, R. Bcr-Abl Efficiently Induces a Myeloproliferative Disease and Production of Excess Interleukin-3 and Granulocyte-Macrophage Colony-Stimulating Factor in Mice: A Novel Model for Chronic Myelogenous Leukemia. (1998).

21. Hardy, R. R. B-cell commitment: deciding on the players. *Curr. Opin. Immunol.* **15**, 158–165 (2003).
22. Mackarehtschian, K. *et al.* Targeted disruption of the *flk2/flt3* gene leads to deficiencies in primitive hematopoietic progenitors. *Immunity* **3**, 147–161 (1995).
23. Dolence, J. J., Gwin, K., Frank, E. & Medina, K. L. Threshold levels of Flt3-ligand are required for the generation and survival of lymphoid progenitors and B-cell precursors. *Eur. J. Immunol.* **41**, 324–334 (2011).
24. Baker, S. J., Rane, S. G. & Reddy, E. P. Hematopoietic cytokine receptor signaling. *Oncogene* **26**, 6724–6737 (2007).
25. Goetz, C. A., Harmon, I. R., O'Neil, J. J., Burchill, M. A. & Farrar, M. A. STAT5 activation underlies IL7 receptor-dependent B cell development. *J. Immunol.* **172**, 4770–4778 (2004).
26. Lane, A. A. *et al.* Triplication of a 21q22 region contributes to B cell transformation through HMGN1 overexpression and loss of histone H3 Lys27 trimethylation. *Nat. Genet.* **46**, 618–623 (2014).
27. Hoelbl, A. *et al.* Clarifying the role of Stat5 in lymphoid development and Abelson-induced transformation. *Blood* **107**, 4898–4906 (2006).
28. Huettner, C. S., Zhang, P., Van Etten, R. A. & Tenen, D. G. Reversibility of acute B-cell leukaemia induced by BCR-ABL1. *Nat. Genet.* **24**, 57–60 (2000).
29. Ye, D., Wolff, N., Li, L., Zhang, S. & Ilaria, R. L. STAT5 signaling is required for the efficient induction and maintenance of CML in mice. *Blood* **107**, 4917–4925 (2006).
30. Carlesso, N., Frank, D. A. & Griffin, J. D. Tyrosyl phosphorylation and DNA binding activity of signal transducers and activators of transcription (STAT) proteins in hematopoietic cell lines transformed by Bcr/Abl. *J. Exp. Med.* **183**, 811–820 (1996).
31. Funk, P. E., Varas, A. & Witte, P. L. Activity of stem cell factor and IL-7 in combination on normal bone marrow B lineage cells. *J. Immunol.* **150**, 748–752 (1993).
32. Åhsberg, J. *et al.* Interleukin-7-induced Stat-5 acts in synergy with Flt-3 signaling to stimulate expansion of hematopoietic progenitor cells. *J. Biol. Chem.* **285**, 36275–36284 (2010).
33. Egawa, T. *et al.* The earliest stages of B cell development require a chemokine stromal cell-derived factor/pre-B cell growth-stimulating factor. *Immunity* **15**, 323–334 (2001).
34. Cui, Y. *et al.* Loss of signal transducer and activator of transcription 5 leads to hepatosteatosis and impaired liver regeneration. *Hepatology* **46**, 504–513 (2007).
35. Socolovsky, M. Ineffective erythropoiesis in Stat5a-/-5b-/- mice due to decreased survival of early erythroblasts. *Blood* **98**, 3261–3273 (2001).
36. Murray, P. J. The JAK-STAT signaling pathway: input and output integration. *J. Immunol.* **178**, 2623–2629 (2007).
37. Yao, Z. *et al.* Stat5a/b are essential for normal lymphoid development and differentiation. *Proc. Natl. Acad. Sci. U.S.A.* **103**, 1000–1005 (2006).
38. Kikuchi, K., Lai, A. Y., Hsu, C.-L. & Kondo, M. IL-7 receptor signaling is necessary for stage transition in adult B cell development through up-regulation of EBF. *J. Exp. Med.* **201**, 1197–1203 (2005).
39. Dias, S., Silva, H., Cumano, A. & Vieira, P. Interleukin-7 is necessary to maintain the B cell potential in common lymphoid progenitors. *J. Exp. Med.* **201**, 971–979 (2005).
40. Dhennin-Duthille, I. *et al.* The tumor suppressor hTid1 inhibits STAT5b activity via functional interaction. *J. Biol. Chem.* **286**, 5034–5042 (2011).
41. Goswami, A. V., Chittoor, B. & D'Silva, P. Understanding the Functional Interplay between Mammalian Mitochondrial Hsp70 Chaperone Machine Components. *J. Biol. Chem.* **285**, 19472–19482 (2010).
42. Ahn, B. Y. *et al.* Tid1 is a new regulator of p53 mitochondrial translocation and apoptosis in cancer. *Oncogene* **29**, 1155–1166 (2010).

43. Kaul, S., Reddel, R. R., Mitsui, Y. & Wadhwa, R. An N-terminal region of mot-2 binds to p53 in vitro. *Neoplasia* **3**, 110–114 (2001).
44. Kanai, M. *et al.* Physical and functional interaction between mortalin and Mps1 kinase. *Genes Cells* **12**, 797–810 (2007).
45. Chueh, F.-Y., Leong, K.-F. & Yu, C.-L. Mitochondrial translocation of signal transducer and activator of transcription 5 (STAT5) in leukemic T cells and cytokine-stimulated cells. *Biochem. Biophys. Res. Commun.* **402**, 778–783 (2010).
46. Fleming, H. E. & Paige, C. J. Cooperation between IL-7 and the pre-B cell receptor: a key to B cell selection. *Semin. Immunol.* **14**, 423–430 (2002).
47. Espeli, M. *et al.* Initiation of pre-B cell receptor signaling: common and distinctive features in human and mouse. *Semin. Immunol.* **18**, 56–66 (2006).
48. Marshall, A. J., Fleming, H. E., Wu, G. E. & Paige, C. J. Modulation of the IL-7 dose-response threshold during pro-B cell differentiation is dependent on pre-B cell receptor expression. *J. Immunol.* **161**, 6038–6045 (1998).
49. Fleming, H. E. & Paige, C. J. Pre-B cell receptor signaling mediates selective response to IL-7 at the pro-B to pre-B cell transition via an ERK/MAP kinase-dependent pathway. *Immunity* **15**, 521–531 (2001).
50. Yasuda, T. *et al.* Erk Kinases Link Pre-B Cell Receptor Signaling to Transcriptional Events Required for Early B Cell Expansion. *Immunity* **28**, 499–508 (2008).
51. Hofmeister, R. *et al.* Interleukin-7: physiological roles and mechanisms of action. *Cytokine Growth Factor Rev.* **10**, 41–60 (1999).
52. Calamito, M. *et al.* Akt1 and Akt2 promote peripheral B-cell maturation and survival. *Blood* **115**, 4043–4050 (2010).
53. Ramadani, F. *et al.* The PI3K isoforms p110 {alpha} and p110 {delta} are essential for Pre-B cell receptor signaling and B cell development. *Sci. Signal.* **3**, ra60–ra60 (2010).
54. Hadari, Y. R., Haring, H. U. & Zick, Y. p75, a member of the heat shock protein family, undergoes tyrosine phosphorylation in response to oxidative stress. *J. Biol. Chem.* **272**, 657–662 (1997).
55. Osorio, C. *et al.* Mortalin is regulated by APOE in hippocampus of AD patients and by human APOE in TR mice. *Neurobiol. Aging* **28**, 1853–1862 (2007).
56. Nieborowska-Skorska, M. *et al.* Signal transducer and activator of transcription (STAT)5 activation by BCR/ABL is dependent on intact Src homology (SH)3 and SH2 domains of BCR/ABL and is required for leukemogenesis. *J. Exp. Med.* **189**, 1229–1242 (1999).

CHAPTER 4:
Ongoing Work and Future Directions

1. Ongoing work

1.1. Does Hspa9 knockdown alter activation of Jak1 or Jak3 downstream of the IL-7R?

In **Chapter 3** we showed Stat5 activation/phosphorylation was reduced following knockdown of Hspa9 in B7 cells. Binding of IL-7 to the IL-7R α chain induces recruitment of the common γ -chain. Heterodimerization brings together the Jak proteins associated with each chain, resulting in trans-phosphorylation of γ -chain-associated Jak3 and IL-7R α -associated Jak1^{1,2}. For proper activation of Stat5, phosphorylation of Jak1 and Jak3 must occur². We are using the same system described in **Section 4.3 of Chapter 3** in B7 cells to evaluate Jak1 and Jak3 activation. Briefly, B7 cells are electroporated with siRNA against Hspa9 or non-targeting control and 3 days later starved of IL-7 overnight followed by stimulation with 1ng/mL IL-7. Whole cell lysates are collected at 10 and 30 minutes after stimulation. Our initial results show that Jak1 and Jak3 total levels are unchanged following IL-7 stimulation with or without Hspa9 knockdown, indicating that Hspa9 does not effect Jak1 or Jak3 stability or expression. These experiments are being repeated and activation of Jak1 and Jak3 by phosphorylation is being evaluated.

1.2. Does Hspa9 knockdown reduce Erk1/2 activation following IL-7R stimulation?

As mentioned in **Chapter 3**, we have evaluated total Erk1/2 levels in B7 cells following IL-7 stimulation and observed no difference between cells that received anti-Hspa9 siRNA or control siRNA. These experiments have been repeated more than 3 times utilizing biological replicates with the same result. Evaluation of Erk1/2 phosphorylation is ongoing; however, starving B7 cells of IL-7 overnight causes only a mild reduction in the levels of activated Erk1/2 present. In comparison, pStat5 levels are reduced to an almost undetectable level following overnight starvation. This mild reduction in pErk1/2 levels limits the dynamic range of the assay and indicates Erk1/2 phosphorylation also occurs in B7 cells independently of the IL-7R pathway.

1.3. Is the subtype of BCR-ABL induced leukemia different in *Hspa9*^{+/-} mice compared to *Hspa9*^{+/+} mice?

In **Chapter 3, Section 4.5** we showed that mice that receive *Hspa9*^{+/-} bone marrow have prolonged survival following BCR-ABL induced leukemia compared to mice that receive *Hspa9*^{+/+} bone marrow. BCR-ABL has been shown to induce different subtypes of B-ALL, specifically pro-B and pre-B. We will also determine the frequency of B-ALL in this cohort since BCR-ABL is able to induce a variety of hematopoietic malignancies, including chronic myeloid leukemia, myeloproliferative disorder, and T-ALL, depending on the strain of mice used, viral titer and the treatment of cells prior to transplant (i.e., 5-fluorouracil treatment)^{3,4}. Our method has been reported to produce almost all B-ALLs from C57Bl/6 x FVB F1 mice⁵. Cryopreserved bone marrow and spleen cells will be analyzed by flow cytometry using the Bethesda criteria and more stringent markers for pro-B and pre-B cells⁶. Control samples will be stained and analyzed alongside all leukemic samples. For subtyping of B-ALLs, we will use B220, CD43, CD24 and BP.1 to identify GFP+ leukemic populations as pro-B (GFP+, B220^{int}, CD43+, CD24+, BP.1-) or pre-B (GFP+, B220^{int}, CD43+, CD24+, BP1+) subtypes. In addition to prolonged survival of BCR-ABL induced leukemia, we may observe differences in the subtypes of leukemia in mice that received *Hspa9*^{+/-} bone marrow.

1.4. Are there recurrent cooperating mutations induced by MOL4070LTR virus in *Hspa9*^{+/-} mice?

In **Chapter 2, Section 4.9** we show that *Hspa9*^{+/-} mice are not more susceptible than *Hspa9*^{+/+} mice to myeloid or lymphoid leukemia as a result of retroviral insertional mutagenesis. However, the common insertion sites identified from *Hspa9*^{+/-} may be different than those identified in wild-type mice. We will identify common insertion sites in tumors banked from *Hspa9*^{+/-} and *Hspa9*^{+/+} mice described in **Chapter 2**. *HSPA9* is located in a

commonly deleted region associated with transformation to acute myeloid leukemia. In mice, *Hspa9* was identified as a common insertion site (CIS) in retroviral insertional mutagenesis screens in association with AML^{7,8}. *Hspa9* was also identified as a CIS in a large screen of genes that cooperate with the p19^{ARF}-MDM2-p53 signaling pathway in acceleration of lymphomagenesis⁹. Common insertion sites unique to *Hspa9*^{+/-} mice would identify genes that cooperate with *Hspa9* loss to produce leukemia in mice and could be strong candidate genes for future studies. Future studies could include crossing *Hspa9*^{+/-} mice with other appropriate mouse models (e.g., overexpression, knockout) for recurrently mutated genes and evaluate them for disease development.

2. Future Directions

2.1. Further analysis of *Hspa9*^{+/-} mice

2.1.1. Does the snoRNA *Gm26109* contribute to alterations observed in B-cells?

In **Chapter 2, Section 4.5**, we describe partial rescue of the CFU-PreB colony reduction by mild overexpression of HSPA9 in *Hspa9*^{+/-} mice. We also describe a reduction in the expression of *Gm26109*, the snoRNA contained in intron 10 of *Hspa9*, in *Hspa9*^{+/-} mice. In order to study the contribution of reduced expression of *Gm26109* to this phenotype, overexpression of *Gm26109* in mouse bone marrow can be used to assess whether it rescues the reduction in CFU-PreB colony number observed in *Hspa9*^{+/-} mice. For this experiment, lineage depleted *Hspa9*^{+/-} or *Hspa9*^{+/+} bone marrow are transduced with a lentivirus overexpressing *Gm26109*. The Fcy-si lentiviral vector (the same lentivirus used in **Chapter 3, Section 4.3**) has previously been used to overexpress snoRNAs in murine bone marrow¹⁰. The coding region of *Gm26109* is cloned from murine genomic DNA into the Fcy-si vector. Overexpression will be evaluated by qRT-PCR as described in **Chapter 2, Section 3.7.3**. Transduced bone marrow is transplanted into lethally irradiated recipients. 8 weeks following transplant, mice are sacrificed and YFP+ cells

are sorted for CFU-PreB methylcellulose assay, as described in **Chapter 2, Section 4.5**. The number of CFU-PreB colonies from both *Hspa9*^{+/-} and *Hspa9*^{+/+} bone marrow transduced with either Fcy-siLUC-YFP control or Fcy-Gm26109-YFP virus are evaluated and compared.

Alternatively, analysis of CFU-PreB colony formation in a conditional heterozygous knockout mouse that does not alter expression of *Gm26109* could definitively answer this question. Creation of a conditional *Hspa9* knockout mouse is an important future direction of this work and is an ongoing effort in the Walter lab.

2.1.2. Is T-cell differentiation affected by loss of *Hspa9* *in vitro*?

IL-7R signaling is important for both B- and T-cell development. Therefore, T-cell potential from *Hspa9*^{+/-} mice should be evaluated. Currently, no methylcellulose assay exists to analyze T-cell progenitors. However, T-cell differentiation can be evaluated by co-culture of hematopoietic progenitor cells with stromal cells that express the notch ligand delta-1 (OP9-DL1). For this experiment, 150 HSCs or 500 LMPPs from c-Kit-enriched (autoMACS) cells are sorted directly into 24-well plates containing OP9-DL1 stroma plated the previous day¹¹. Opti-MEM media containing 10% FBS, 50µM β-mercaptoethanol and 10µg/mL L-glutamine is supplemented with 10 ng/mL SCF, 10 ng/mL FLT3L, and 10 ng/mL IL-7 to promote T-cell development, as previously described¹¹. Cultures are evaluated on Day 20 for expression of T-cell immunophenotypic markers, as previously described. (CD44/CD25 to define DN1-DN4, CD4/CD8 for DP/SP stages)^{12,13}. An inhibition, reduction or delay in T-cell development from *Hspa9*^{+/-} stem and progenitor cells would indicate *Hspa9* also plays a role in IL-7R signaling in T-cells.

2.1.3. Does loss of *Hspa9* effect Stat5 activation in primary B-cell progenitors?

In Chapter 3 we showed that knockdown of *Hspa9* in an IL-7 dependent B-cell line led to reduced Stat5 activation. Future studies should include analysis of primary B-cell progenitors comparing *Hspa9*^{+/-} and *Hspa9*^{+/+} mice. Using immunophenotypic markers defined in **TABLE 2.5**, CLPs and Hardy fractions A-D are sorted directly into IMDM media supplemented with 20% FBS lacking cytokines (pooling mice if necessary). Following a 1-hour rest period, 50,000-500,000 cells are resuspended in 0.5-1mL volume and stimulated with 10ng/mL IL-7. Cell lysates should be collected at 10 minutes (and 30 minutes if sample allows) following stimulation per our B7 protocol detailed in **Chapter 3**. Total and pStat5 levels are analyzed by Western blot. A reduction in pStat5 levels is predicted to occur in *Hspa9*^{+/-} mice compared to *Hspa9*^{+/+} littermates if *in vivo* compensation occurs via local IL-7 concentrations.

Alternatively, pStat5 levels in a CLP-enriched population can be evaluated by flow cytometry as previously described¹⁴. Briefly, whole bone marrow cells from *Hspa9*^{+/-} and *Hspa9*^{+/+} mice are collected, starved of IL-7 for 30 minutes and stimulated prior to collection. Cells are stained for cell surface markers, fixed with paraformaldehyde and permeabilized with methanol. Fixed and permeabilized cells are then stained with pStat5 prior to flow cytometric analysis. Cells expressing lineage markers (B220, DX5, Gr1, CD11b, CD3e, CD8, Ter119) are excluded and pStat5 levels are measured in AA4.1+ cells.

Finally, Stat5 activation could be investigated in primary MDS samples with and without del(5q). B-cell progenitors (CD34+CD10+CD19+/- cells) from MDS samples can be isolated by FACS and analyzed following IL-7 starvation and stimulation in culture.

2.2. How does Hspa9 regulate Stat5?

2.2.1. Does Hspa9 interact directly with Stat5?

Our results indicate Hspa9 inhibits activation of Stat5 following IL-7 stimulation of IL-7R. To investigate the mechanism through which this occurs, co-immunoprecipitation experiments should be performed in order to determine if Hspa9 directly interacts with Stat5. Both endogenous and overexpression of tagged Hspa9 have been successfully co-immunoprecipitated with other proteins¹⁵⁻¹⁷. Since Hspa9 is a chaperone protein, it is important to determine whether this interaction occurs within the substrate binding domain which lacks protein specificity or in a region that is more likely to have functional significance. This could be achieved by expressing tagged Hspa9 deletion mutants, as previously described¹⁶.

2.2.2. Does Hspa9 inhibit Stat5 activation by increasing availability of its J protein, Dnaja3?

In **Chapter 3** we proposed a model explaining how Hspa9 could regulate activation of Stat5. In the proposed model, reduction of the ubiquitously expressed Hspa9 leads to increased cellular availability of its J protein Dnaja3. Previously, Dnaja3 overexpression was shown to inhibit phosphorylation of Stat5, inhibit activation of Stat5 downstream targets and reduce expression of Stat5b, but not Stat5a. To test this hypothesis, Stat5 activation could be evaluated following knockdown of both Hspa9 and Dnaja3. Additionally, total levels of Stat5a and Stat5b should be evaluated separately to see if Stat5b total levels are reduced following knockdown of Hspa9 and restored by simultaneous knockdown of Dnaja3 in B7 cells.

If loss of Hspa9 inhibits Stat5b function, we would predict that loss of Stat5a, which performs a largely redundant role with Stat5b during lymphopoiesis, would further impair

B-cell development in *Hspa9*^{+/-} mice. CFU-PreB colony formation is normal in *Stat5a*^{-/-} and *Stat5b*^{-/-} mice but significantly reduced in *Stat5a*^{-/-}*b*^{-/-} mice¹⁸. These results indicate *Stat5a* and *Stat5b* can compensate for each other in B-lymphopoiesis. *Stat5a* may be responsible for *in vivo* compensation in *Hspa9*^{+/-} mice if loss of *Hspa9* inhibits *Stat5b*. In order to test whether *Stat5a* is responsible for *in vivo* compensation in *Hspa9*^{+/-} mice, *in vivo* frequencies of *Stat5a*^{-/-}*Hspa9*^{+/-} versus *Hspa9*^{+/-} B-cell progenitors could be evaluated by CFU-PreB methylcellulose assay and flow cytometry measurements of CLPs, Hardy fractions and mature B-cell populations.

2.3. Does *Hspa9* alter B-cell signaling pathways in human cells?

The IL-7 dependent cell line utilized in **Chapter 3** is a murine pro-B cell line. Additional studies utilizing the IL-7 responsive human pre-B cell line, 697 cells, may provide additional insights into other downstream signaling pathways such as the PI3K pathway^{19,20}. Normal B-cell development occurs in humans with severe combined immunodeficiency that have inactivating IL-7R mutations²¹. This data indicates that IL-7 is dispensable in humans. However, another key B-cell specific receptor, the pre-BCR, is required. Patients with mutations in components of the pre-BCR have a block in B-cell development at the pro-B stage^{3,4,22}. Significant cross talk occurs between these receptors, resulting in signaling through Erk1/2 and PI3K by both^{6,23-25}. Future studies should address these downstream signaling targets. Investigation of the impact of *Hspa9* loss on signaling in 697 cells will allow analysis of both human cells and pre-BCR signaling.

2.4. Does acute loss of *Hspa9* result in hematopoietic defects?

Hspa9^{+/-} mice do not recapitulate the reduction in erythroid and B-cell progenitor frequencies observed with >50% knockdown of *Hspa9*^{7,8,26}. However, it is not clear whether this difference is due to the level of *Hspa9* reduction or whether acute, shRNA-mediated

knockdown escapes compensation. *Hspa9*^{+/-} mice have a reduction in Hspa9 levels in every cell of the body throughout development, providing ample time for compensation to develop. Del(5q) is an acquired cytogenetic abnormality within a subset of hematopoietic cells in humans. It remains to be seen whether acute loss of Hspa9 in an adult mouse, as occurs in del(5q) MDS patients, will escape compensation and recapitulate the more severe hematopoietic defects observed in the knockdown model. A conditional knockout model would provide acute heterozygous or homozygous loss of Hspa9, as well as the ability to target loss to specific cellular subsets. For future investigations of lymphoid lineages, *CD2-Cre* mice provide the expression of Cre at the earliest B- and T-cell stages and could be used to specifically study B- and T-cell development^{9,27}.

3. Conclusion

Although *Hspa9*^{+/-} mice show minimal hematopoietic abnormalities, ample evidence exists to support further investigation of its role in hematopoiesis and MDS. Here we present several outstanding questions to be addressed by future studies of Hspa9 in hematopoiesis.

REFERENCES

1. Milne, C. D. & Paige, C. J. IL-7: a key regulator of B lymphopoiesis. *Semin. Immunol.* **18**, 20–30 (2006).
2. Corfe, S. A. & Paige, C. J. The many roles of IL-7 in B cell development; mediator of survival, proliferation and differentiation. *Semin. Immunol.* **24**, 198–208 (2012).
3. Wong, S. & Witte, O. N. Modeling Philadelphia chromosome positive leukemias. *Oncogene* **20**, 5644–5659 (2001).
4. Hoelbl, A. *et al.* Clarifying the role of Stat5 in lymphoid development and Abelson-induced transformation. *Blood* **107**, 4898–4906 (2006).
5. Lane, A. A. *et al.* Triplication of a 21q22 region contributes to B cell transformation through HMGN1 overexpression and loss of histone H3 Lys27 trimethylation. *Nat. Genet.* **46**, 618–623 (2014).
6. Morse, H. C. *et al.* Bethesda proposals for classification of lymphoid neoplasms in mice. *Blood* **100**, 246–258 (2002).
7. Suzuki, T. *et al.* New genes involved in cancer identified by retroviral tagging. *Nat. Genet.* **32**, 166–174 (2002).
8. Du, Y., Spence, S. E., Jenkins, N. A. & Copeland, N. G. Cooperating cancer-gene identification through oncogenic-retrovirus-induced insertional mutagenesis. *Blood* **106**, 2498–2505 (2005).
9. Uren, A. G. *et al.* Large-scale mutagenesis in p19(ARF)- and p53-deficient mice identifies cancer genes and their collaborative networks. *Cell* **133**, 727–741 (2008).
10. Chu, L. *et al.* Multiple myeloma-associated chromosomal translocation activates orphan snoRNA ACA11 to suppress oxidative stress. *J. Clin. Invest.* **122**, 2793–2806 (2012).
11. Mansson, R. *et al.* Single-cell analysis of the common lymphoid progenitor compartment reveals functional and molecular heterogeneity. *Blood* **115**, 2601–2609 (2010).
12. Wang, H., Pierce, L. J. & Spangrude, G. J. Distinct roles of IL-7 and stem cell factor in the OP9-DL1 T-cell differentiation culture system. *Exp. Hematol.* **34**, 1730–1740 (2006).
13. Rothenberg, E. V. Transcriptional Control of Early T and B Cell Developmental Choices. *Annu. Rev. Immunol.* (2014). doi:10.1146/annurev-immunol-032712-100024
14. Li, L. X., Goetz, C. A., Katerndahl, C. D. S., Sakaguchi, N. & Farrar, M. A. A Flt3- and Ras-Dependent Pathway Primes B Cell Development by Inducing a State of IL-7 Responsiveness. *J. Immunol.* **184**, 1728–1736 (2010).
15. Orsini, F. *et al.* The life span determinant p66Shc localizes to mitochondria where it associates with mitochondrial heat shock protein 70 and regulates trans-membrane potential. *J. Biol. Chem.* **279**, 25689–25695 (2004).
16. Kaul, S., Reddel, R. R., Mitsui, Y. & Wadhwa, R. An N-terminal region of mot-2 binds to p53 in vitro. *Neoplasia* **3**, 110–114 (2001).
17. Ma, Z. *et al.* Mortalin controls centrosome duplication via modulating centrosomal localization of p53. *Oncogene* **25**, 5377–5390 (2006).
18. Teglund, S. *et al.* Stat5a and Stat5b Proteins Have Essential and Nonessential, or Redundant, Roles in Cytokine Responses. *Cell* **93**, 841–850 (1998).
19. Lanvin, O. *et al.* Interleukin-7 induces apoptosis of 697 pre-B cells expressing dominant-negative forms of STAT5: evidence for caspase-dependent and -independent mechanisms. *Oncogene* **23**, 3040–3047 (2004).
20. Dhennin-Duthille, I. *et al.* The tumor suppressor hTid1 inhibits STAT5b activity via functional interaction. *J. Biol. Chem.* **286**, 5034–5042 (2011).
21. Leonard, W. J., Puel, A., Ziegler, S. F. & Buckley, R. H. Defective IL7R expression in T-B+NK + severe combined immunodeficiency - Nature Genetics. *Nat. Genet.* **20**, 394–397 (1998).
22. Espeli, M. *et al.* Initiation of pre-B cell receptor signaling: common and distinctive features in human and mouse. *Semin. Immunol.* **18**, 56–66 (2006).

23. Fleming, H. E. & Paige, C. J. Pre-B cell receptor signaling mediates selective response to IL-7 at the pro-B to pre-B cell transition via an ERK/MAP kinase-dependent pathway. *Immunity* **15**, 521–531 (2001).
24. Yasuda, T. *et al.* Erk Kinases Link Pre-B Cell Receptor Signaling to Transcriptional Events Required for Early B Cell Expansion. *Immunity* **28**, 499–508 (2008).
25. Hofmeister, R. *et al.* Interleukin-7: physiological roles and mechanisms of action. *Cytokine Growth Factor Rev.* **10**, 41–60 (1999).
26. Chen, T. H.-P. *et al.* Knockdown of Hspa9, a del(5q31.2) gene, results in a decrease in hematopoietic progenitors in mice. *Blood* **117**, 1530–1539 (2011).
27. de Boer, J. *et al.* Transgenic mice with hematopoietic and lymphoid specific expression of Cre. *Eur. J. Immunol.* **33**, 314–325 (2003).

Kilannin Cathleen Krysiak

April 1, 2014

660 South Euclid Ave, Box 8007
Saint Louis, MO 63110
Citizenship: USA

kkrysiak@wustl.edu
(314) 362-9405

EDUCATION:

2002-2006 B.S., Molecular and Cellular Biology
University of Illinois Urbana-Champaign

ACADEMIC POSITIONS:

- 2008-Present **Pre-doctoral candidate**, Matthew Walter Laboratory, Department of Medicine
Washington University in Saint Louis
- Investigated the contribution of genes on del(5q) for the development of MDS and subsequent transformation to AML.
 - Focused on characterizing the hematopoietic consequences of haploinsufficiency of *HSPA9*, a gene located in del(5q), using a novel mouse model. Using a variety of techniques, including flow cytometry, morphology, *in vitro* culture, and gene expression profiling, we identified that *Hspa9* haploinsufficiency alters B-cell progenitors in mice, similar to observations made in MDS patients.
 - Performed a large retroviral insertional mutagenesis screen in *Hspa9* haploinsufficient mice to identify genes that cooperate to cause AML.
- 2008-2011 **Cancer Pathway Fellow**, Siteman Cancer Center
Washington University in Saint Louis
- Shadowed oncologists from various departments in clinical and surgical settings.
 - Discussed patient care, diagnosis, standard treatment, clinical trials and the gaps between research and clinical practice.
- 2010 **Teaching Assistant**, BIO192: Phage Bioinformatics
Washington University in Saint Louis
- Worked with Freshman biology majors in a highly interactive course involving novel research using bioinformatic methods (i.e. BLAST, Apollo, ClustalW, Phamerator) to analyze and annotate bacteriophage whole genome sequences.
- 2006-2008 **Visiting Research Specialist**, Eric Oldfield Laboratory, Department of Chemistry
University of Illinois Urbana-Champaign
- Worked with an interdisciplinary team to develop bisphosphonates as more potent anti-cancer drugs and understand their mode of action within the mevalonate pathway.
- 2004-2005 **Undergraduate Researcher**, Lei Liu Laboratory, Bioinformatics Center
University of Illinois Urbana-Champaign
- Analyzed gene expression data to identify clusters of genes that were similarly regulated and evolutionarily conserved.

RESEARCH SUPPORT:

- 2012-Present Principal Investigator, *The Impact of Hspa9 Haploinsufficiency on Murine Hematopoiesis and Leukemogenesis* 1F31CA165702, NCI/NIH Ruth L. Kirschstein National Research Service Award 09/01/2012-08/31/2015, \$105,500.
- **Grant application received a 4th percentile score**
- 2009-2011 Special Emphasis Pathway in Cancer Biology Predoctoral Fellowship, Siteman Cancer Center, \$55,000.

OTHER HONORS AND AWARDS:

- 2012 Molecular Genetics Program Annual Retreat Poster Award
2002-2004 Hill Climbers Scholarship
2002-2003 General Assembly Public Affairs Scholarship
2002-2003 Merit Recognition Scholarship
Dean's List (Fall 2004, Spring 2005, Spring 2006)

PROFESSIONAL SOCIETIES:

Association for Women in Science
American Society of Hematology

PEER-REVIEWED PUBLICATIONS:

TA. Graubert, D. Shen, L. Ding, T. Okeyo-Owuor, CL. Lunn, J. Shao, **K. Krysiak**, CC. Harris, DC. Koboldt, DE. Larson, MD. McLellan, DJ. Dooling, RM. Abbott, RS. Fulton, H. Schmidt, J. Kalicki-Veizer, M. O'Laughlin, M. Grillo, J. Baty, S. Heath, JL. Frater, T. Nasim, DC. Link, MH. Tomasson, P. Westervelt, JF. DiPersio, ER. Mardis, TJ. Ley, RK. Wilson, and MJ. Walter. "Recurrent mutations in the *U2AF1* splicing factor in myelodysplastic syndromes." *Nat Gen*. 2011 Dec 11;44(1):53-7.

TH. Chen, A. Kambal, **K. Krysiak**, MA. Walshauer, G. Raju, JF. Tibbitts, MJ. Walter. "Knockdown of Hspa9, a del(5q31.2) gene, results in a decrease in hematopoietic progenitors in mice." *Blood*. 2011;117(5):1530-1539.

Y. Zhang, R. Cao, F. Yin, FY. Lin, H. Wang, **K. Krysiak**, JH. No, D. Mukkamala, K. Houlihan, J. Li, CT. Morita, E. Oldfield. "Lipophilic pyridinium bisphosphonates: potent gammadelta T cell stimulators." *Angew Chem Int Ed Engl*. 2010 Feb 1;49(6):1136-8. PMID: PMC2819003.

Y. Zhang, R. Cao, F. Yin, MP. Hudock, RT. Guo, **K. Krysiak**, S. Mukherjee, YG. Gao, H. Robinson, Y. Song, JH. No, K. Bergan, A. Leon, L. Cass, A. Goddard, TK. Chang, FY. Lin, E. Van Beek, S. Papapoulos, AH. Wang, T. Kubo, M. Ochi, D. Mukkamala, E. Oldfield, "Lipophilic bisphosphonates as dual farnesyl/geranylgeranyl diphosphate synthase inhibitors: an X-ray and NMR investigation." *J Am Chem Soc*. 2009 Apr 15;131(14):5153-62. PMID: PMC2753403.

Y. Song, JM. Chan, Z. Tovian, A. Secrest, E. Nagy, **K. Krysiak**, K. Bergan, MA. Parniak, E. Oldfield. "Bisphosphonate inhibitors of ATP-mediated HIV-1 reverse transcriptase catalyzed excision of chain-terminating 3'-azido,3'-deoxythymidine: A QSAR investigation." *Bioorg Med Chem*. 2008 Oct 1;16(19):8959-67. PMID: PMC2586422

Y. Zhang, M. Hudock, **K. Krysiak**, R. Cao, K. Bergan, F. Yin, A. Leon, E. Oldfield. "Activity of Sulfonium Bisphosphonates on Tumor Cell Lines." *J Med Chem*. 2007 Nov 29;50(24):6067-79.

ABSTRACTS AND PRESENTATIONS:

K. Krysiak, J. Tibbitts, MJ. Walter. "Reduced *Hspa9* Expression Alters IL-7 Signaling in B-cells." Poster presentation at the American Society of Hematology Annual Meeting. New Orleans, LA. December 7-10th, 2013.

K. Krysiak, J. Tibbitts, TH. Chen, MJ. Walter. "*Hspa9* Haploinsufficiency Induces a Cell-Intrinsic Defect in Mouse B-cell Progenitors". Poster presentation at the American Society of Hematology Annual Meeting. Atlanta, GA. December 8-11th, 2012.

K. Krysiak, TH. Chen, J. Tibbitts, MG. Martin, MJ. Walter. "The reduction in *Hspa9* haploinsufficient B-cell progenitors is partially rescued by exogenous IL-7." Poster presentation at Molecular Genetics Program Annual Retreat. New Haven, MO. September 28-29th, 2012.

K. Krysiak, TH. Chen, J. Tibbitts, MG. Martin, MJ. Walter. "B-cell Progenitors are Reduced in *Hspa9* Haploinsufficient Mice." Poster presentation at the American Society of Hematology Annual Meeting. San Diego, CA. December 10-13th, 2011.

K. Krysiak, TH. Chen, JF. Tibbitts, MJ. Walter. "B-cell Progenitors are Reduced in *Hspa9* Haploinsufficient Mice." Oral presentation at Molecular Genetics Program Annual Retreat. New Haven, MO. September 23-24th, 2011.

K. Krysiak, TH. Chen, JF. Tibbitts, MJ. Walter. "B-cell Progenitors are Reduced in *Hspa9* Haploinsufficient Mice." Poster presented at Hematopoietic Development and Malignancy Program Annual Retreat. St. Louis, MO. June 15th, 2011.

K. Krysiak, TH. Chen, JF. Tibbitts, MJ. Walter. "Genetics of Myelodysplastic Syndromes." Poster presented at Molecular Genetics Program Annual Retreat. New Haven, MO. September 24-25th, 2010.

K. Krysiak, TH. Chen, A. Kambal, MA. Walshauer, G. Raju, MJ. Walter. "*Hspa9* Haploinsufficiency Recapitulates Features of Ineffective Hematopoiesis Observed in MDS." Poster presented at Molecular Genetics Program Annual Retreat. New Haven, MO. October 2-3rd, 2009.

A. Ramani, **K. Krysiak**, C. Zhai, L. Liu. "A Multi-species Study of Chromosomal Domains of Co-expression." International Conference on Intelligent Systems in Molecular Biology. Fortaleza, Brazil. August 6-10th, 2006.